Chapter One

Introduction

Pterosaurs took to the air long before birds and from the hideous and ferocious pterodactyls of Arthur Conan-Doyle's fictional Lost World to the "leather-winged harpies" of Mark Witton's recent biography of the Pterosauria, these flying reptiles have long been a source of fascination. Many have asked questions about how well they flew, how they compared with birds and how large they became. Yet such questions are difficult to answer: from an engineering perspective in particular, the pterosaur literature contains precious little information on the shape of the wings, the aerodynamic performance of the wing airfoils, the structural characteristics of the wing bone "spar" that supported the membrane or indeed the properties of the membrane itself.

This study sets out to redress some of these deficiencies and produce new models of pterosaur flight, with particular reference to the large species (with wingspans of 6m or more) and the role that structural flexibility may have played in their flight dynamics.

1.1 The Pterosauria

Pterosaurs were the dominant flying animals of the early Mesozoic (Figure 1.1). Their origin is debated and since intermediary fossils are absent, they appear to have sprung, flight-ready, into the fossil record, perhaps as early as at the Triassic Carnian/Norian boundary (*Faxinalipterus minima* Bonaparte *et al.* 2010) or most certainly by the middle/late Norian (*Preondactylus bufarinii* Wild 1984) (Figure 1.2). The phylogenetic position of the pterosaurs has long been debated, but the current prevailing view is that they evolved from an as yet unknown archosaurian common ancestor in the mid Triassic (for example Lu *et al.* 2010, Andres 2007, Wang *et al.* 2012). These earliest representatives of the lineage were small animals (wingspan less than 0.5m) with large, toothed skulls and long bony tails (Figure 1.4).

By the early Jurassic the diversity was increasing, but overall size remained modest, with the largest being *Dimorphodon* with a 1.3m wingspan. By the mid-late Jurassic (about the time when feathered dinosaurs were starting to take to the air), short tailed pterodactyloid species started to appear and by the mid Cretaceous this had become the prevailing body plan (although it is unclear why this was so (Prentice *et al.* 2011) (Figure 1.3 and 1.4). With the transition from tailed to more or less tailless, there was an increase in size. The largest tailed (non-pterodactyloid) pterosaurs were around 2.5m wing span (Carpenter *et al.* 2003), but even some of the earliest pterodactyloids, for example *Istiodactylus latidens* had a wingspan approaching 4.5m (Hooley 1913, Howse *et al.* 2001), larger than any extant bird. An excellent

and comprehensive review of the Pterosauria can be found in Middleton & English (2014) and up-to-date species by species descriptions in Witton (2013) so a high level of detail will not be duplicated here.

During the Cretaceous, pterosaur diversity and disparity initially increased dramatically, but while the possibility of sampling bias should not be dismissed (Kellner 2003, Butler *et al.* 2009, Prentice *et al.* 2011) it appears that by the end of the Cretaceous the diversity had collapsed and the dominant species were azhdarchids. With the "great flowering" of the Cretaceous came diversity in the ecological niches occupied and diversity in size (Figure 1.5). Certain species exhibited trends towards gigantism, with ornithocheirids such as *Ornithocheirus*, *Anhanguera* and *Coloborhynchus* commonly reaching 4m to 5m, sometimes as much as 6m to 7m wing span (Wilkinson 2008) and in the case of *Tropeoghnathus* as much as 8.3m (Kellner *et al.* 2013). *Pteranodon*, the film star pterosaur, regularly attained wing spans in excess of 6m (Bennett 2001), with the largest individuals reaching 7.25m. This is larger than any birds extant or fossil and should be compared to the largest bird ever, the proposed 6.4m span of *Pelagornis sandersi* (Ksepka 2014) and the 6.5-7.0m *Argentavis* (Palmqvist & Viscaino 2003). By the late Cretaceous, some pterosaurs had become the largest animals ever to fly, and even larger were to come.

Towards the end of the Cretaceous, although pterosaur diversity decreased, the size of the dominant azhdarchids increased greatly. The smallest of these, for example *Montanazhdarcho*, had a wing span of 2.5m, but most were in the 4-6m size range (Company *et al.*1999 for example). However, there is evidence of some that were much larger still, with early estimates of the wing span of *Quetzalcoatlus northropi* of up to 15m (Lawson 1975), subsequently clipped to 11-12m (Langston 1981). Most recently, Witton & Habib (2010) have suggested that a further reduction better fits the fossil evidence, but still estimate the wing span to have been 10-11m. In addition to *Q. northropi* (which has yet to be formally described in the literature) very fragmentary remains of two other species of giant azhdarchid have been described: *Arambourgiania* (Frey & Martill 1996) and *Haztegopteryx* (Buffetaut *et al.* 2002, 2003) with the authors making wing span estimates of 12-13m and 12m respectively. Witton & Habib (2010) reassessed the material and concluded that there is no convincing evidence for wing span in excess of 10-11m for any azhdarchid.

1.2 Wing Morphology

In all pterosaurs the wing is comprised of a thin soft tissue membrane attached proximally to the body and hind limbs (extending most likely as far as the ankle) and supported anteriorly/distally by the bones of the forelimb. Between the glenoid and the wrist the membrane (generally, the patagium) extends from both the anterior and posterior sides of the wing bones, anteriorly forming a narrow, triangular propatagium. Beyond the wrist the patagium is only present on the posterior side of the wing bones, and is attached distally to the metacarpal and four hyper-elongated wing phalanges. It has no other bony tissue support, unlike bats where the wing fingers extend posteriorly (Figures 1.6 & 1.7).

While the dimensions of the wing bones are known from the fossil record (see Chapter 4 for more detail), the composition of the wing membrane is rather more of a mystery. Very few fossils preserve this soft tissue and in all those that do the remains are incomplete. However, it is now generally accepted (see Witton 2013:51-55 for the most up to date overview) that the membrane was thin (perhaps less than 1mm thick) and made from soft tissue layers containing blood vessels, muscle fibres and, unique to pterosaurs, higher tensile fibres, known as aktinofibrils, described in more detail in Chapter 6.

1.3 Mass estimation

The flight performance of any animal or indeed aircraft is intimately linked not only to its wingspan (and wing area) but also to its mass. In general terms, the heavier the animal for any given wing area the faster it will fly, although weight alone does not necessarily affect flight efficiency as measured by lift to drag ratio. The total mass also has important implications for takeoff and landing and is most likely a more significant consideration for these flight behaviours than for the steady flight.

Until quite recently the majority of mass estimates for pterosaurs have pointed to animals with a very low mass in relation to their size (Brower & Venius 1981, Hazlehurst & Rayner 1992b, Chatterjee & Templin 2004) as well as some dissenters to these "low weight" views, for example Paul (1990) and Marden (1994), who proposed a 250kg mass for *Quetzalcoatlus*. Bramwell & Whitfield (1974) estimated the mass of *Pteranodon* using a slicing method and proposed a mass of 16.6kg for an animal of almost 7m wingspan and noted that an extrapolation of bird data would have predicted a mass of 100kg. Typically these low weight estimates have a scaling exponent (based on data from birds) of about 2.4 on span (exhibiting negative allometry) and a proportionality constant of 0.2. This scaling then results in a mass of around 80kg for one of the largest known pterosaurs, the 10m to 11m wingspan *Quetzalcoatlus*, which implies an improbably low average specific gravity of 0.2 (Witton 2009). In this context it should be noted that recent work on the scaling for birds (Taylor and Thomas 2014) has shown that when corrected for phylogeny, the scaling exponent is close to isometry, in other word an exponent of 3.0. If this figure is applicable to pterosaurs, then it would result in increased mass estimates for the larger animals.

Recently these higher mass estimates have received new support. Witton (2009) used a dry skeletal mass estimation approach that gave an exponent of 2.4 but a much larger proportionality constant. Using Witton's (2009) methodology, the mass of a 7m *Pteranodon* is predicted to be around 50kg and that of *Quetzalcoatlus* nearer to 250kg. This matter is far from resolved amongst pterosaur workers, but the higher range of mass estimates has recently received further support (Prondvai *et al.* 2008, Henderson 2009). In fact Henderson (2009) used a volumetric approach to predict a mass for *Quetzalcoatlus* of more than 500kg, but this has been strongly criticised (Witton and Habib 2010) and it is perhaps fair to say that the current consensus view is for a mass of around 250kg for a 10m wingspan individual.

Whatever the minutiae of the debates about their maximum size, at the extreme end of the spectrum and based on very fragmentary remains, it does appear that by the end of the Cretaceous the

largest azhdarchids grew to have a wing span of at least 10m and a mass of 250kg, three times the span of the largest extant bird and almost twice that of the largest fossil birds (Figure 1.7). Earlier in the period, very robust fossil evidence shows that *Pteranodon* and various ornithocheirids were commonly 6-7m in wing span, so for many millions of years pterosaurs were certainly larger than any birds that ever roamed the skies.

1.4 Biomechanical studies of flight

At first sight the flight of pterosaurs appears to be well described. As early as 1914, Hankin & Watson (1914) and Short (1914) provided wide ranging initial assessments and identified that these animals would have flown at relatively low speeds when compared to birds. They were also aware of the fragility of pterosaur bones and how this might limit landing speed.

Wellnhofer's pterosaur encyclopaedia (Wellnhofer 1991a) and Unwin's more recent *Pterosaurs from Deep Time* (Unwin 2005) contain numerous illustrations depicting pterosaurs as masters of the air, a trend ably maintained by Witton (2013). In the intervening period a substantial literature has grown up examining the aerodynamics of pterosaurs.

1.4.1 Historical studies

In the early 70s, Bramwell and Whitfield produced what are arguably the classic biomechanical studies of large pterosaurs (Bramwell 1971, Bramwell & Whitfield 1970, Bramwell & Whitfield 1974, Bramwell *et al.* 1974). These were very comprehensive, landmark studies of the biomechanics and aerodynamics of *Pteranodon,* combining excellent understandings of both morphology and aerodynamics and remain to this day the only truly multidisciplinary papers on the subject. They contained pioneering work on aspects such as mass and centre of mass estimation and the authors recognised that under the flight regime appropriate to pterosaurs, a thin membrane wing was not necessarily as inefficient as might be supposed when compared to a 'proper' airfoil of the type familiar from aircraft. They also recognised that the wing bones were not sufficiently strong to support a membrane tensioned by a tendon along its posterior margin and based on their assessment of the static balance reconstructed an animal with forward (anterior) sweep to the wings (Figure 1.9). To understand their likely wing flight strokes and mode of land based locomotion they built mechanical, articulated models, fore-runners to the computer based 3D modelling so widespread today. With hindsight, there are some aspects of these papers which no longer ring true, for example the proposed locking of the shoulder joint inspired by reference to albatrosses and the use of the crest as an aerodynamic stabiliser, but otherwise they have more than stood the test of time.

Stein (1975) sought to build on this work and reported the results of wind tunnel tests on wing models. Unfortunately, the results cannot be reconciled with any other published aerodynamic results as they contain impossibly high values of maximum lift coefficient (C_{Lmax}) of up to 3.8 for a single surface

wing section (McMasters & Henderson 1979, Hoerner 1985:Chapter 4, Smith & Shyy 1996) and minimum drag coefficients that range from <0.01 to 0.7 for similar wing forms. (See Glossary for definitions of these terms and more explanation as to their aerodynamic significance.) The important point for now is that unfortunately the absence of detailed descriptions of the experiments coupled with the use of flexible, three dimensional models subject to uncontrolled distortion means that the anomalous results cast grave doubts over the validity of the conclusions. Stein (1975) also speculated that there was a membrane between the crest and the neck of the animal that might have been used for steering, a notion that has received no further support. However one point that Stein (1975) did make, which had until then attracted little attention, is that under aerodynamic load the wing would be subject to span-wise (mediolateral) twisting (raising the caudal edge of the wing relative to the wing spar) (Figure 1.10). This would have significant aerodynamic effects by changing the lift distribution along the wing and possibly providing pitch stability (Jones 1941, Dowlan 1944) - but see Chapters 3 and 4 for a discussion of this point. Like Bramwell & Whitfield (1974) he drew the wing with substantial forward sweep.

In 1982 Sneyd and others (Sneyd *et al.* 1982) made perhaps the first attempt to study the effects of wing membrane flexibility on the aerodynamics of *Pteranodon*. Unfortunately they had to make so many simplifying assumptions that the paper is in reality little more than a mathematical exercise with limited practical application. In particular, whilst they agree with Bramwell & Whitfield (1974) that spanwise membrane tension was the most likely, they modelled a wing with chordwise tension since it was the only way to obtain "*...a tractable mathematical problem…"* (Sneyd *et al.* 1982:463). Despite these limitations, the discussion of pitch stability is revealing, in which Sneyd *et al.* (1982) and in more detail in Sneyd (1984) show theoretically that flexible wing sections have flight stability characteristics that are different from a rigid wing - they are neutrally stable in pitch. This has more recently been confirmed experimentally (Bleischwitz *et al.* 2015)

Static stability will be discussed in more detail in Chapter 7, but briefly, a planar wing with rigid, cambered wing sections (typical of the great majority of aeroplanes) is what is termed statically unstable in pitch. This means that if the wing is flying steadily and is subject to a change in the airflow, from a gust for example, the resulting change in the aerodynamic forces is such as to induce instability (Figure 1.11). In conventional aeroplanes this tendency is counteracted by the tail, and in flying wings by the use of either special, statically stable "reflex" wing sections or by a combination of wing sweep and wing twist. The more stable the airplane configuration, the less manoeuvrable it becomes. Because of this, Maynard-Smith (1952) argued that birds and pterosaurs would tend to evolve towards being statically unstable, and in the absence of any experimental or other direct evidence, speculated as follows: *"There is, in fact, good evidence that birds do not need to be stable in order to fly. In some birds there is no tail in an aerodynamic sense at all. Other birds, which normally possess a tail, can fly without it; this can often be observed in the case of sparrows which have completely lost their tails. In fact, in most birds the tail does not seem to act as a stabiliser, but as an accessory lifting surface when flying slowly. This can be observed, for example, in the case of gulls. These birds open their tails only when turning*

sharply or flying slowly. It can then be seen that the slower the bird flies the more tail is lowered; as mentioned above, this is characteristic of the unstable state." (Maynard-Smith 1952:2)

Bramwell & Whitfield (1974) relied on Maynard Smith's (1952) view and speculated that *Pteranodon* was statically unstable in pitch but had sufficient neurological control to maintain stability by active means. In fact, for birds, others Hoey (1992), Krus (1992), Taylor & Thomas (2001) disagree with Maynard Smith (1952), based on rather more extensive experimental, theoretical and observational evidence and Sneyd *et al.* (1982) argue from a calculation of the likely pitch rate that *Pteranodon's* neurological reaction time would be inadequate. To this, I would add the observation that however fast the animal's brain may be able to react, the control surfaces are flexible structures, which would greatly compromise the possibility of making the fast, precise control responses required to limit the pitch excursions. Add to this the prediction that flexible wing sections are neutrally stable in pitch and it seems very unlikely that pterosaurs were statically unstable about this axis.

Brower (1983) produced an extensive aerodynamic study of *Pteranodon* and *Nyctosaurus* but did not really offer any additional insights over and above those that had already been made by Bramwell and Whitfield. In part, this was because all these authors had to rely on the pre-50's aerodynamic literature to obtain wing section data, necessarily unrepresentative of actual pterosaur wing profiles.

Padian (1985) was rather critical of what he saw as the aerodynamic bias in these earlier papers. He argued that such work needed to be better informed by knowledge of the animals' biology, which is curious in the case of Bramwell and Whitfield's papers in view of Bramwell's thoughtful and comprehensive anatomical contributions. Whilst there may be some validity to his views, Padian (1985) voiced the surprising opinion that the aktinofibrils were orientated at right angles to the tension in the wing membrane, paralleling the feather shafts of birds and the fingers of bats. This is a very perplexing conclusion given that Padian was a co-author of an earlier paper that showed from detailed observations of fossil specimens that the aktinofibrils ran more or less sub-parallel to the wing spar in the distal regions of the wing (Padian & Rayner 1993, Figure 1.12), precisely the expected direction of tension in the membrane predicted by Bramwell & Whitfield (1974). Padian (1985) used his conclusion to argue that pterosaurs could change the shape of the wing membrane in flight because as the wing spar flexed these fibres would contract to take up the slack. As a result he argued that the animal might be capable of achieving an extended range of flight speeds as compared to a wing lacking this "morphing" capability.

Further, Padian (1985) took the view that the posterior margin of the wing was anchored to the body and that the hind limbs were free. From this conclusion, Padian (1985) argued for a narrow chord wing, resulting in less wing area and thus higher wing loadings and higher flight speeds (an inevitable aerodynamic consequence) than estimated by others. This membrane attachment morphology is now considered extremely unlikely (Unwin 2005, Elgin *et al.* 2009), and it is anyway possible to envisage a narrow wing associated with an attachment to the ankle (Figure 1.13). Padian (1985) also argued that the

forward sweep of the wings proposed by Bramwell & Whitfield (1974) was unlikely but did not indicate the implications of this difference in interpretation or the reason for his view.

His paper concluded by arguing that if only engineers took proper account of the biology then they might come up with a *Pteranodon* with *"….higher speeds more manoeuvrability and better takeoff and landing performance."* (Padian 1985:429). This speculative (and possibly wishful) view of pterosaurs as exceptional fliers prevails and can be found to this day in, for example, Hone's pterosaur blog (http://archosaurmusings.wordpress.com) which contains the following *"These were no clumsy fliers with big, ungainly, leathery wings but had highly derived wings with multiple layers of specialised tissues providing an integrated ability to control the shape and camber of the wing during flight. It would make them exceptionally competent aeronauts and easily the equal of birds and bats, and quite possibly, in the case of pterodactyloids at least, their superior."* To support this view he states, without any justification, that pterosaurs can change the shape (camber) of their wings by contracting or relaxing the muscle fibres and that the aktinofibrils are "stiffening rods". There is no direct evidence of the former and simple mechanical analysis demonstrates that the small diameter aktinofibrils were not "rod-like" to the extent that the term suggests they can provide out-of-plane stiffness. (See Section Chapter 6 for more detail.)

In the late 80s and early 90s a number of people who had previously worked on birds made contributions to understanding pterosaur flight (Pennycuick 1988; 1990, Padian & Rayner 1991; 1993, Hazlehurst & Rayner 1992a; 1992b). Pennycuick (1988) went so far as to question the very existence of the aktinofibrils, suggesting instead that what was seen in the fossils were wrinkles caused by contraction of the membrane material, analogous to the highly extensible tissue around the jaws of some whales.

1.4.2 Revival of interest

Since the mid 1990s there has been a revival of interest in the flight characteristics of pterosaurs, starting with Bennett (2000) who looked at the role of the aktinofibrils. This study was clearly based on an exceptional knowledge of the fossils and anatomy, but the engineering conclusions were less convincing. He appeared to suggest (Figure 1.14) that these very fine fibres (around the same cross section as a human hair (Martill & Unwin 1989, Padian & Rayner 1991, Unwin *et al.* 1993) were capable of resisting compression and thus enabled the posterior margin of the wing membrane to be convex, somewhat in the manner of modern yacht sails that are supported by battens in compression. As a result of this "cable and strut" model of the structural role of the aktinofibrils, Bennet (2000) was also of the view (like Padian 1985) that the membrane tension was directed more or less normal to the aktinofibril orientation, with these fibres acting as "spreading elements" somewhat like the struts in a paper hand held fan. Bennett (2000) maintained this was required to stop the membrane contracting chordwise as it was tensioned spanwise. However, Bennett (2000) made no estimates of the likely chordwise contraction, nor did he state why it was necessarily a functional problem. This model of aktinofibril behaviour requires that they are capable of resisting compressive forces, but it is mechanically impossible for fibres as thin as the

aktinofibrils and embedded in a soft tissue matrix to perform in this way, in other words to be the "stiffening rods" that Hone describes or the "spreading elements" that Bennett (2000) describes (see Chapter 7 for more detail of the reasons for this view).

In 2003, Frey and co-workers (Frey *et al.* 2003) speculated on the possible aerodynamic effects of the different wing attachment locations in Cretaceous pterosaurs, noting that the vertical location of the glenoid varies from high to mid-level to low in ornithocheirid, azhdarchid and tapejaroids respectively. They coined the terms "top-decker", "middle-decker" and "bottom-decker" for these wing locations and saw the varied positions as a response to differing lateral stability requirements, using an analysis based on the aerodynamics of fixed wing aircraft which has doubtful relevance to an animal with wings that are flexible and can be articled relative to the body. The paper over-interprets the possible aerodynamic influences of morphological features, finding an engineering or biomechanical explanation for them with precious little experimental or even theoretical justification.

In the same year, Wilkinson completed his Ph.D. thesis on the flight of ornithocheirid pterosaurs (Wilkinson 2003) and from that flowed a number of papers that taken together probably represent the most thoughtful approach so far to understanding the flight of these animals, summarised in Wilkinson (2008). Wilkinson combined a deep understanding of the fossils, mainly from examination of the Cambridge Greensand material, with informed speculation about aerodynamics.

1.4.3 The pteroid debate

However, in 2006 he and others reported work (Wilkinson *et al.* 2006) which used wind tunnel tests to examine the role of the propatagium on the aerodynamic performance of the pterosaur wing section. Wilkinson *et al.* (2006) used the results of these tests to support an anterior orientation for the pteroid (Wilkinson *et al.* 2006, Wilkinson 2007; 2008) (Figure 1-15). The pteroid is a bone unique to pterosaurs, which is attached in the region of the wrist and positioned on the anterior side. Historically it had been assumed that the pteroid articulated with the fovea in the preaxial carpal and was orientated so as to point medially, a view that retains support (Bennett 2007, Prondvai & Hone 2008). Bennett, a vociferous advocate of the medial orientation, maintains that the pteroid is located at the side of the pre-axial carpal and that there was a sesamoid located in the fovea. As early as 1914 however, Hankin (1914) proposed that the pteroid might have been directed anteriorly but this was not supported by others until 1981 (Frey & Riess 1981), in a paper that argued for an anterior orientation and a very extensive propatagium. Frey no longer holds this view and now advocates (Frey *et al.* 2006) the medial orientation and an articulation directly onto the proximal carpal.

The views of Wilkinson and co-authors (2006, 2008) are at odds with this. They proposed that the pteroid was not only articulated with the preaxial carpal but was also directed anteriorly, thus providing a very much larger propatagium area than in other reconstructions, with the pteroid deployed to depress the propatagium in a morphology analogous the the Krueger flap used on aircraft (Fullmer 1948),

enabling the wing to generate high lift. They undertook wind tunnel testing (Wilkinson *et al.* 2006) to investigate these effects, results that were at the time the only tests that specifically represented possible pterosaur wing sections. Wilkinson *et al.* (2006) used a circular cross section spar and investigated a wing bone/patagium and also two propatagium/wing bone/patagium configurations. At face value the results of the wind tunnel tests look impressive, but on closer examination they proved to be less convincing and contain little that could not have been found by consulting the aerodynamic and sailing yacht literature.

When testing wing sections, two key parameters of interest are the lift and the drag. Conventionally, (Anderson 2007:24) these values are non-dimensionalised by the dynamic air pressure in order to allow comparison with other results, giving two coefficients, the lift coefficient (C_l) and drag coefficient (C_d) (with lower case suffixes: see Glossary for derivations). C_l is used for the results from 2D tests and C_L for those from complete aircraft.

The values of C_l and C_d vary with the characteristics of the airfoil section and the angle of attack relative to the on-coming flow. As angle of attack increases, so too do C_l and C_d, to a point where C_l reaches a maximum (C_{lmax}) at the stall, where the airflow breaks down across the section.

A common way of presenting these data for both evaluation and comparison with other results is in the from of a polar plot, where C_l is plotted against C_d (Figure 1.16).

To a lesser extent, the values of C_l and C_d are dependent upon the Reynolds number (Re) of the airflow, a dimensionless index that characterises fluid flows (Vogel 1985:84, Anderson 2007:38; Hoerner 1965:1-9). (See Glossary for derivation).

The value of Re ranges over many orders of magnitude for living organisms - from 0.00001 for a bacterium to 300,000,000 for a large whale (Vogel 1985:86). Most flying vertebrates fall in the range from around 50,000 to 500,000, which happens to be the so-called transition region - where flows change from being largely laminar to largely turbulent and consequently the flow characteristics around a body are very sensitive to the shape and conditions of the surface. Typically, the Reynolds number for large pterosaurs is in the range from 200,000 to 500,000 (assuming flight speeds in the 15m/s to 20m/s range and wing chord of around 0.3m to 0.5m, based on reconstructions in Bramwell & Whitfield (1974) and Bennett (2000)). For a more detailed discussion, see Section 2.3.3.

The Reynolds number of the tests reported by Wilkinson *et al.* (2006) were not given, which complicates their interpretation and the results are in places inconsistent with other well established data. For example, the spar diameter to wing section chord ratio was 9.2% for the patagium configuration, but the minimum profile drag coefficient was only 0.02 - an implausibly low value for such a section since a value of 0.02 is associated with a flat plate or low camber thin airfoil (Marchaj 1988:312-325). Therefore the results for the patagium only configurations should be treated with considerable caution. The sections with fore-wings (propatagia) had higher minimum drag coefficient values - in the range from 0.05 to 0.10, which are more in line with other result (Marchaj 1996:103, Chaplin *et al.* 2004). However, Wilkinson *et al.*

(2006) reported a maximum lift coefficient (C_l) of only 1.5 at a camber ratio of 15%, a low value compared to other published results and it appears that the value was still increasing when the tests were curtailed. In the case of the section with the broad propatagium, higher values of lift coefficient were recorded - up to 2.5 for the highest camber section. Measurements from the figures in Wilkinson *et al.* (2006) indicate that the overall camber ratio for this section was in the order of 20%, so the C_l value of 2.5 is not unexpected or in any way exceptional (Milgram 1971, Hoerner 1985:Chapter 4). The same camber applied to the patagium-only section may well have produced similar results had the experiments been extended to full stall, so it does not appear necessary to invoke a broad propatagium as the only possible high lift mechanism for a pterosaur wing.

It is well established in the aeronautical literature that high camber results in high lift coefficient and also that thin airfoils can be efficient at low Reynolds number (see for example Marchaj (1979:302-326) and Hoerner (1985:4-11). Hoerner (1985) also presents data which shows the effect of camber on C_{lmax} for thin sections, peaking at $C_{lmax} = 1.8$ for a camber ratio of 15% (the highest for which data was available). Milgram (1971) investigated highly cambered sections at Reynolds numbers below 10^6 and measured C_{lmax} of up to 2.6 at a camber ratio of 18%. He found a slight variation with the shape of the mean line (the distribution of the camber across the chord) but this was a much less significant than the camber ratio. NACA tests of the Krueger flap (Fullmer 1948) were carried out at a higher Reynolds number than is appropriate for pterosaurs, but nonetheless demonstrated that the device can produce a substantial increase in C_{lmax} (from 1.1 to 1.8). All these results are therefore generally supportive of the results reported by Wilkinson *et al.* (2006), but they do not provide any reason to suggest that the pterosaur wing sections achieved a unexpectedly high lift performance. Increased camber results in an increased maximum lift coefficient and the results in Wilkinson *et al.* (2006) serve only to confirm what is already well known in the aerodynamic literature.

The fact remains that there is potential for the proximal wing to generate high lift with a depressed, anteriorly oriented pteroid since this increases the local camber of the wing sections. However, with such a pteroid orientation, the inner portion of the wing is in effect twisted nose down by around 10 degrees relative to the distal regions, resulting in the these sections being at or beyond stall, which would greatly reduce the overall effectiveness of the wing. In additions to this aerodynamic reservation, there are a number of other reasons to be sceptical of an anterior orientation for the pteroid:

- the bending strength of the pteroid;
- the lack of evidence for restraining tissue;
- the requirements for excessive propatagium strain;
- some evidence for longitudinal curvature in pteroids giving an upturned tip, and finally
- the poor aerodynamic performance of a stepped leading-edge,

These views are developed in more detail in a paper published in 2009 (Palmer & Dyke 2009), which strongly argued for a medial orientation.

1.4.4 Coming up to date

Returning to the more general history of biomechanical studies of pterosaurs, Strang *et al.* (2009) theoretically modelled the flapping flight of pterosaurs using panel codes (see Chapters 3 and 7 for more detail of these approaches to aerodynamic modelling) as part of a programme to develop flapping micro air vehicles. Their results suggest that even large pterosaurs could be efficient flapping fliers and that a high flapping propulsive efficiency (>70%) could be achieved without the varying wing span (reduced span during the upstroke) seen in birds, a behaviour that is less likely to have been practical for pterosaurs since it would result in reduced membrane tension and an associated drag penalty (see Chapter 6).

Most recently, a comprehensive paper (Witton & Habib 2010) represents the published "final word" on the general biomechanics of pterosaur flight, with particular emphasis on the limits to size. They review the literature and fossil evidence for large pterosaurs and conclude that there is little support for sizes above 10-11m wing span and an associated mass of around 250kg. They note that large pterosaurs, the azhdarchids in particular, have very robust forelimbs when compared to birds, and relatively gracile hind limbs, a morphological trend that they attribute to the proposed quadrupedal launch behaviour (See Chapter 8). They modelled the flight of these large animals using Pennycuick's FLIGHT program (Pennycuick 2008), which was developed for relatively smaller birds with very different wing aerodynamics and morphology, so it may not be entirely reliable for pterosaurs. Witton & Habib (2010) showed that large pterosaurs could have had sufficient flight muscle mass to undertake flap-gliding, but most likely not continuous flight. Using aerobic muscle power they could climb to sufficient altitude to have a good chance of finding thermal or ridge lift.

Crucially to these calculations, the authors note that pterosaurs most likely had a higher flight muscle mass fraction than birds as a result of their "front heavy" anatomy. For this reason, and others based on a range of morphological characters, they make the important point that pterosaurs are not birds, and that extrapolating from bird behaviour and capabilities is of limited usefulness in understanding pterosaurs. They are not new in noting this. Bramwell & Whitfield (1974:533) said *"Pteranodon is not a bird, nor a bat, but a pterosaur with its own peculiar structure."* but Witton & Habib (2010) bring together more lines of evidence to support this view. Lastly, Witton & Habib (2010) note that pterosaurs varied substantially in morphology and that the two giants, *Pterandon* and *Quetzalcoatlus* were far from similar. Thus not only is it unreliable to use birds as analogues, but even general statements about giant pterosaurs are difficult due to large differences in morphology.

1.5 Flight simulation

Several of the existing studies of pterosaur flight have been largely based on biological approaches to understanding flight mechanics (Padian 1985, Padian & Rayner 1991; 1993, Hazlehurst & Rayner 1992a; 1992b). They demonstrate that the fossil record provides a reasonably comprehensive data source for overall skeletal dimensions and to a lesser extent for wing geometry and this allows allometric approaches to the effects of size to be studied. When combined with estimates of wing area and total mass, these allometric approaches have provided some insight into the possible flight style of pterosaurs and how this compares to extant birds.

However, from an engineering point of view, the available data is very limited since in order to analyse gliding flight capabilities it is necessary to have information about the basic performance of the aerofoil sections (so called 2D data) and to then assemble the aerofoils into a three dimensional wing, which will have a specific outline shape and distribution of aerofoil orientation (twist) along its span (3D aerodynamic data). These data, combined with estimates of total mass and wing area can then be used to reconstruct flight performance, often presented in the form of flight "polars" - curves that relate horizontal speed to sinking speed. This basic data can then be used to make first approximations to the power required for level or climbing flight. This approach to modelling flight has been central to the development of aircraft and more detail of the aerodynamic background is given in Chapter 3. An overview of the variable that need to be considered is shown in Figure 1.17

Historically scant information has been available on the likely airfoil sections (2D data) applicable to pterosaurs. Comparison of the available cambered plate data from early aeronautical sources (as used by Bramwell & Whitfield 1974) with more recent results from masts and sail tests demonstrate significant efficiency degradation due to the presence of a leading edge spar (see Figure 1.18 and Chapter 2), but these results are insufficient to create 2D data for likely pterosaur wing sections, and certainly totally inadequate to understand their sensitivity to different assumptions about the wing morphology.

1.6 Modelling the complete animal

In order to model the complete animal, the results of the aerodynamic modelling must be combined with the structural characteristics of the wing spar and wing membrane. While wing bone morphology was apparently well described in the literature, on close inspection the available information was completely inadequate for calculating the structural strength of the wing since details of wing bone cross sectional morphology was almost completely absent save for frequent reference to pterosaur wing bones being thin walled and a few representative sections in sources such as Bramwell & Whitfield (1974). However, a model of the structural characteristics of the wing spar is crucial to understanding the role of structural flexibility, the structural limits of the flight envelope and possible limits to size since the wing

spar was likely to have deflected significantly under load, changing the shape of the wing and affecting its dynamic response to aerodynamic forces.

1.7 New approaches

This study therefore sets out to redress some of these deficiencies and produce new, more complete models of pterosaur flight. Specifically, the research asks the following questions and sets out to test a related hypothesis:

Overarching question

How did wing flexibility shape the aerodynamic performance of pterosaurs and did it influence the limits to their size?

Supplementary questions

i. What was it about their morphology that enabled pterosaurs to achieve such large sizes?

ii. Were the Late Cretaceous giants pushing against these physical limits, or given the right environmental circumstances, could they have become larger still?

Related hypothesis

Wing flexibility was a significant factor in determining the aerodynamic performance.

Approach

The approach adopted was a mix of physical and computer modelling:

- Experimental and theoretical investigations to quantify the two dimensional performance of likely pterosaur airfoils.
- Construction of three-dimensional gliding flight computer models to predict overall flight envelopes.
- Computer modelling of wing morphology to define likely planform and flight stability.
- Examination of museum specimens (including the use of CT scanning) to build a structural definition of the wing bones.
- Development of a computer model to analyse the wing spar structure.
- Estimation of wing spar deflection, stresses and structural factors of safety for different loading cases.
- Investigation of the interaction between the wing spar structure and the membrane in order to infer membrane properties.
- Extrapolation of the results to investigate the upper limits to size.

The first steps in the research were to fill two key gaps:

- to quantify the performance of candidate 2D wing sections and
- to obtain details of the internal wing bone morphology in order to build a structural model.

This is the work which constitutes the bulk of this study and in itself has resulted in two papers (Palmer 2010, Palmer & Dyke 2011) and a number of presentations to conferences such as Flugsaurier (2010, 2015), IPC (2010), SVPCA (2011, 2014, 2015) and SVP (2014).

Chapter 2 describes the design of the wing sections and the wind tunnel testing and Chapter 3 the application of these results to the prediction of the flight performance, as quantified by glide polars. These results was published in the literature in Palmer (2010). Chapter 4 describes the construction of the wing spar structural model and Chapters 5 and 6 the effect of dorsoventral and anteroposterior loading respectively, with the implications for the wing membrane properties. Chapter 7 draws on the foregoing results to establish constraints on the morphology of pterosaur wings (published in Palmer & Dyke 2011). Lastly, Chapter 8 uses the data obtained as a baseline from which to project the possible limits to size of giant pterosaurs, presented at SVP in 2014 and Flugsaurier 2015.

Chapter Two

Wing Airfoil sections

2.1 The pterosaur wing

The pterosaur wing is unique in many ways and there are no direct analogues in mechanical aerodynamics, the closest being the mainsails of sailboats. However, because the vast majority of sailboats are required to operate with the wind incident on either side of the sail, the sections comprise a flexible sail attached to the centre of a symmetrical mast. In contrast, the wing section of a gliding pterosaur can be asymmetrical since the main lift force only acts in one direction (Figure 2.1).

Determining the relative positions of the bones and wing membrane from the fossil record is difficult due to the limited number of specimens with soft tissue preservation and the problems of interpretation in three dimensions. Padian & Rayner (1993:132) noted that *"This topic is one of the most important aspects of the mechanical problem of reconstructing the pterosaur wing, yet so far as we can tell no previous author has described or attempted to reconstruct the attachment of the patagium onto the bones of the skeleton."* In fact, Frey & Reiss (1981) included a sketch that suggested that the propatagium and the patagium attached midway between the dorsal and ventral sides of the wing bones (which is analogous to the yacht mast geometry). Padian & Rayner (1993) concluded, without explanation that *".... it is apparent that the patagium originated from the dorsal side of the [wing] spar."* (Padian & Rayner 1993:158), thus resulting in an asymmetric airfoil section (Figure 2.2). This section geometry was adopted by Wilkinson *et al.* (2006), but again without explanation or justification.

Lastly, to the extent that contemporary bats might inform the reconstruction of pterosaur wings, Norberg (1972) indicated that the bones in bat wings are positioned as in the Frey & Reiss (1981) reconstruction, but the bat wing bones are much smaller in diameter in relation to the width of the wing than in pterosaurs (Figure 2.3).

2.2 Analogues from other disciplines

While results from theoretical analysis and experimental tests on airplane airfoils and sail boat sails are not directly applicable to the aerodynamics of a pterosaur wing, they can provide some general insights. Compared to most airplanes, the Reynolds number of pterosaur flight (around 2×10^5 - see below) is very low and much closer to that of sailing boats. It is known that as Reynolds number reduces, the relative performance of thick and thin airfoils changes. Marchaj (1979:302-326) presented results that compared a curved plate airfoil with more conventional thick airfoils (Figure 2.4) and showed that at

Reynolds number below 1 x 10^5 the thin, curved plate airfoil has lower profile drag and was capable of generating a significantly higher maximum lift coefficient than thicker sections. As Reynolds number increases above 1 x 10^5, thicker airfoils slowly become superior and when Reynolds numbers reach those applicable to aircraft (>10^6), thicker airfoils show overwhelming superiority, hence their almost universal use in aircraft. In the range of Reynolds numbers over which pterosaurs operate (200,000 to 500,000) the differences between thick and thin airfoils are small, so as Marchaj's (1979) results described above show, pterosaurs would not have been fundamentally disadvantaged by having a single skinned membrane.

The profile drag (the pressure and frictional drag of a two-dimensional section) of a thin airfoil is primarily a function of the curvature or camber of the section (Shyy *et al.* 2008:46). Conventionally, the camber is defined as the ratio of the depth of the curvature (f) to the local chord (c) of the wing, and often given as a percentage. For a flat plate (zero camber) section, the profile drag coefficient is around 0.02 (Marchaj 1979:320), becoming 0.05 at 15% camber and 0.10 at 18% (Milgram 1974). Low camber sections show a marked minimum in the curve of profile drag coefficient against lift coefficient, but as camber increases the profile drag becomes nearly constant with lift up until the point where stall starts, at which point it starts to increase rapidly. Consequently, as camber increases, so too does the lift coefficient associated with maximum lift:drag ratio (Milgram 1974).

As discussed above, the other effect of increasing camber is an increase in maximum lift coefficient (C_{lmax}). For a flat plate the maximum lift coefficient is less than 1.0, but this increases in an approximately linear relationship to 2.5 at 18% (Marchaj 1996:319 (Figure 2.5) and Milgram 1974). Beyond 18% camber there is evidence that the rate of increase declines and that such high absolute values may not apply to sail sections (Collie *et al.* 2004). Indeed, the precise value of C_{lmax} achieved *"can be very sensitive to the test conditions."* (Hoerner 1985: 4-11 *et seq.*) and will also depend upon the surface roughness of the wing section, the Reynolds number of the tests and, to a much more limited extent, the actual shape of the camber line (Hoerner 1985:4-12, Marchaj 1996:144, Shyy *et al.* 2008:48). However, a figure approaching 2.5 appears achievable with camber alone.

A pterosaur wing, like the mainsail of a yacht, is supported by a rigid structure - the wing bones in the pterosaur, the mast in a yacht. As noted above, most mast/sail combinations comprise a fixed mast to which a membrane sail is attached, generally such that the mast is symmetrically positioned across the leading edge of the membrane. This is the main reason why most data for mast/sail combinations has limited usefulness in helping us to understand the effects of variation in the relative positions of the rigid and flexible parts of the pterosaur wing. Marchaj (1996:103) presents the most useful data in this respect. It shows that attaching a mast (with diameter = 7.5% of the width of the sail) symmetrically to the leading edge of a cambered airfoil reduces the maximum lift coefficient by 15% and doubles the profile drag. A 12.5% mast has a much greater adverse effect upon maximum lift and a further increase in profile drag (Figure 1.17). However, if this larger diameter mast is offset towards the high pressure side of the

airfoil (the ventral side of a pterosaur wing), the profile drag is unaffected, but the maximum lift coefficient improves greatly, to become similar to that of the smaller diameter mast.

Chaplin *et al.* (2005) used Computational Fluid Dynamics (CFD) techniques to examine the effect of the presence of a circular mast (5% of sail width) on the anterior margin of a cambered sail. Like earlier workers, they found a substantial increase in drag (up to 100%) which had the effect of reducing the maximum L:D ratio (L/D_{max}) from 70 to 25! They also examined the effect of varying sail camber for the sail and mast combination and found an optimum camber (based on L/D_{max}) of 12%. This optimum results in a lift coefficient of 1.3 at L/D_{max}.

Maughmer (1979) reported the results of wind tunnel tests on a flexible wing concept, the Princeton Wing (Figure 2.6). The Reynolds number of the tests (around $1x10^6$) were somewhat higher than the range applicable to pterosaurs so results need to be interpreted with caution, but they serve to confirm the superiority of the asymmetric spar/membrane geometry. Typically Maughmer's (1979) results show a profile drag coefficient of 0.08 for an asymmetric geometry as compared to 0.06 for a symmetrical one, but a much higher Cl_{max} and consequently a 60% increase in maximum lift:drag ratio. These conclusions are further supported by results of comparative tests of different mast/sail geometries in Marchaj (1979:338) which show superior L/D for a configuration with the mast offset to the windward (ventral) side of the sail.

More recently Paton & Morvan (2007) used Reynolds Averaged Navier Stokes (RANS) based CFD to analyse different mast/sail geometries. Their results are restricted to only one angle of attack, but suggest that an asymmetric section can give a significant improvement (50% or more) in L/D ratio and that the details of the spar section can have significant (though lesser) influences. They propose that the main mechanism by which these gains are realised is the reduction in lee side (dorsal) flow separation.

The variation in drag for different configurations is primarily the result of different degrees of flow separation as separated flow is a major source of airfoil profile drag (Eppler 1979:132) and becomes an increasingly important consideration as Reynolds number is reduced and laminar flow starts to predominate (Russell 1979, Eppler 1979, Katz & Plotkin 2001:497, Shyy *et al.* 2008:31). At low angles of attack, thin, cambered sections experience laminar separation on the lower (ventral) surface and this switches to upper surface separation as the angle of attack increases. Depending on the pressure distribution, Reynolds number and surface roughness, the separated flow may or may not re-attach to form a separation 'bubble' (Mueller & Batill 1980, Lissaman 1983). The presence of a mast or wing bone on the anterior edge of a membrane airfoil greatly increases the drag due to the flow separation around the relatively 'bluff' mast/wing bone. Typical separation regions are shown in Fig 2.7 (from Chaplin *et al.* 2005) and for a detailed exploration of the phenomena, see Wilkinson (1984).

At higher Reynolds numbers (around $1x10^6$ and above), surface roughness on an airfoil has the effect of increasing drag and reducing C_{lmax} as roughness increases (Hoerner 1985:4-20). However, at lower Reynolds numbers, the effect is different in that surface roughness can have the effect of triggering

transition from laminar to turbulent flow and thus reducing the adverse effects of laminar separation and resulting in an overall improvement in aerodynamic efficiency (Lissaman 1983). Consequently, the inevitable presence of aerodynamically significant surface roughness on natural wing structures may not be a disadvantage in the Reynolds number regime where pterosaurs operate.

2.3 Experimental testing

Because data from contemporary analogues (yacht sails, "soft" aircraft wings) is not directly applicable to pterosaurs and Wilkinson *et al.'s* (2006) results contain anomalies as well as covering only a very restricted range of wing geometries, it is not possible to determine from earlier work the effect of varying the location of the wing bone relative to the lifting surface nor the effects of different wing bone sections or sizes relative to the local chord of the wing. In the absence of such 2D wing section data it is not possible to reliably predict the aerodynamics of the complete wing and thus the flight performance of the animal.

To address this deficit, two-dimensional models of a range of wing sections were made and tested in a low speed wind tunnel and the results used to produce comparative flight performance curves for large, generic ornithocheiridomorph (*Pteranodontidae, Istiodactylidae, Anhangueridae* etc) pterosaurs. The models were made intentionally generic so that the results would be widely applicable and not species specific. Rigid models were used to investigate the effects of different wing bone cross sections and surrounding soft tissue morphology and flexible membrane models were made to investigate the differences between rigid and flexible wing membranes appropriate to the range of pterosaur taxa listed above.

Wing sections were also modelled using the XFOIL computer program (http://web.mit.edu/drela/Public/web/xfoil/), a code developed specifically for the viscous flow analysis of low Reynolds number, 2D isolated airfoils.

2.3.1 Wind tunnel testing

The use of a wind tunnel for testing the properties of airfoils was first recorded by Horatio Phillips in the UK in 1884 and used extensively by the Wright brothers in their development of the first powered airplane (Anderson 2007:300). Since these early days, an extremely extensive body of work has been created, covering all wing types from the smallest insects to hypersonic spacecraft. There must be many, many thousands of references resulting from these studies (See Anderson 2007 and Hoerner 1965 & 1985 for examples). The fundamental properties of an airfoil are quantified by means of two dimensional tests - in which a prismatic wing section is placed across the full width of the wind tunnel. In this way, end effects are avoided and the characteristics in two dimensional flow are measured.

The conventional procedure is to measure the forces generated by the models and to present them in non-dimensional forms for ease of comparison. The most important forces are lift and drag, non-

dimensionalised to lift and drag coefficients, but the moments of these forces are also often measured as they have important implications for flight stability.

2.3.2 The wing sections

Pterosaur wings comprised two distinct regions – the proximal region where a propatagium was present and the distal region where it was absent (Wellnhofer 1991a, Padian & Rayner 1993, Bennett 2000). The distal region of the main wing membrane, the cheiropatagium, was supported by wing bones situated along the anterior margin whereas in the proximal region the wing bones lay within the margins of the membrane, with the propatagium extending anteriorly and the cheiropatagium extending posteriorly. (Figure 1.6, 1.7 and 1.12)

Test sections were designed to be representative of the wing of a large pterosaur – nominally 2.88m in length (5.8m wingspan in total) and with a geometry based upon Bennett (2001), Wilkinson (2008) and Prondavai & Hone (2008) - see Figure 2.8. The wing bone cross section morphology was based upon measurements taken from SMNK 1133 PAL, the Cambridge Greensand specimens at NHMUK, Cambridge and York and illustrations contained in Wellnhofer (1985) (see Chapter 4 for more details of the specimens consulted). While the cross sections of the bones can be reliably measured from these sources, the extent of the wing membranes is more speculative, in particular its width. Accordingly, models were made that represented two different ratios of wing bone diameter to membrane width. This also reflected the variation of bone cross section between diaphysis and epiphysis.

The wing membrane in the rigid models was modelled by thin curved plates made from epoxy resin/carbon fibre moulded composite (Figure 2.9 and Annex 1). Since the actual camber of the pterosaur wing membranes cannot be known with any precision, models were made with three different values (nominally 10%, 12% and 15%) to provide a range of results. The model of the proximal part of the wing was given greater camber since depression of the legs would have been capable of inducing deep camber in that part of the membrane (assuming the current view that the wing membrane is attached to the legs from hip to ankle (Elgin *et al.* 2009)). More distally this effect would weaken and the membrane tensions are likely to have reduced the camber, so less camber was incorporated in the models of the distal sections.

The models represented wing sections in the proximal, mid-span and distal parts of the wing at four locations, A, B, C and D shown in Figure 2.10. The two proximal sections (A and B) modelled the propatagium, humerus or radius/ulna and cheiropatagium, the mid-length section (C) the cheiropatagium and first wing phalanx and the distal section (D) the cheiropatagium and second wing phalanx. The wing bone sections used are shown in Figure 2.11.

A model incorporating a flexible membrane was also made (Figure 2.12). The membrane was 190 mm wide when stretched flat and attached to a circular section carbon fibre tube of 13 mm diameter, the mean depth of the two wing bone sections used on the rigid models. The membrane was made from latex

rubber, reinforced in the mediolateral direction with thin cotton fibres to represent the aktinofibrils. The membrane properties were scaled to be equivalent to 2mm thick skin with properties the same as those reported for the skin of bat wings (Swartz *et al.* 1996).

The posterior edge of the membrane was held in place by a 3mm diameter carbon fibre rod that could be moved in the anteroposterior direction so as to change the slackness in the membrane and thus its camber. Three locations were tested to give a wide range of different membrane curvatures, from which intermediate values could be interpolated. The upper limit was set beyond values generally found in yacht sails and is likely to be a form that experiences substantial regions of separated flow and consequently with drag and low aerodynamic efficiency. The complete range of bone sections and wing sections evaluated are shown in Figure 2.13. In the text that follows they are referred to by the relevant letters and numbers associated with them on that Figure, so the 160mm chord curved section with no attached wing bones is A1 for example.

The models were tested in a small wind tunnel situated in the Department of Engineering at University College Dublin. The Plint TE 44 Subsonic is an open jet wind tunnel with a working cross section of 457 mm x 457 mm. The mean turbulence level is less than 0.7% r.m.s. and velocity variation less than +/- 1.0% outside the boundary layer. Forces were measured with a Plint three component balance. Lift and drag forces were measured and converted to non-dimensional forms for ease of comparison with results from other sources.

2.3.3 Flight Speed and Reynolds Number

The full scale width of the wing at locations A to D along the wing was assumed to be 0.7, 0.5, 0.4 and 0.3 m respectively. In order to achieve fluid dynamic similarity, it is necessary to conduct tests at a Reynolds numbers similar to that of the full sized wings, which in turn depend upon the flight speed assumed. The flight speed of any flying body depends upon three main parameters:

the total weight,

the lifting surface (wing) area

the airfoil lift coefficient.

(It also depends on the air density, which varies slightly with temperature and pressure, but this is a second order effect.)

To a close approximation, the lift is the same as the weight.

The weight of pterosaurs is a much debated topic as noted earlier and as reviewed in Palmer & Dyke (2009). The published estimates in the literature were used to establish likely upper and lower limits, which give a weight range of 13.9kg to 32kg (Palmer & Dyke 2009) for a 5.8m wingspan ornithocheirid. The wing area is another parameter that cannot be determined with precision. An estimate based on the reconstruction shown in Figure 2.10 gives a wing area of 2.50 square metres, a little higher than the value

of 2.29m^2 used by Palmer & Dyke (2009). Witton (2008) gives a wing area of 1.99m^2 for a 5.96m wingspan *Pteranodon*, which if scaled isometrically results in a wing area of 1.88m^2 for a 5.8m wingspan individual. These estimates suggest a range of 1.9 to 2.5m^2. Lastly, an estimate of the overall lift coefficient of the wing is required. Bramwell &Whitfield (1974) proposed a value of 1.2, Brower (1983) predicted values in the range of 1.2 to 1.4 for optimum soaring performance. The results reported in later sections of this paper indicate that the optimum lift coefficient depends upon the wing section configuration, but that in most cases it falls in the range between 1.2 and 1.6, which encompasses the estimates made by others. These values are considerably higher than values estimated for birds (Pennycuick 2008 for example) and those applicable to man-made gliders. The difference is a reflection of the characteristics of high camber wing sections, wherein the best lift:drag ratio occurs at a relatively high value of lift coefficient. The range of cruising flight speed that results from these estimated ranges of weight, wing area and lift coefficient is 7.5 to 15m/s.

Using standard values of air density and viscosity at 20°C, the Reynolds number thus ranges from 1.5 x 10^5 for the narrowest section at the slowest speed, to 6.9 x 10^5 for the widest section at the highest speed. While the whole speed range is of potential interest, it was not practical due to limitations on the experimental time to measure the performance of each wing section over this entire Reynolds number range. It was therefore decided to bias the experimental range towards the low speed end of the range, since performance at low Reynolds numbers is inherently more variable due to laminar separation effects and because the low speed flight characteristics of the animals are of particular interest if estimates of minimum sink speeds and landing speeds, two important parameters for large, soaring animals, are required.

2.3.4 Validation of Test Procedures and Models

The rigid models were first tested without wing bone sections over a range of Reynolds numbers to ascertain the sensitivity of the results to this parameter. At Re=1.2 x 10^5 the maximum lift coefficients were reduced by approximately 6% when compared to results between Re = 1.6 x 10^5 and 2.0 x 10^5, but there was little difference in the results at lower lift coefficients. Within the higher range of Re values, any differences between the results were almost indistinguishable over the complete experimental range. All the remaining tests were therefore conducted at Reynolds numbers of 2.0 x 10^5 as this gave larger absolute forces and thus minimised the signal to noise errors in the instrumentation. Due to excessive distortions in the flexible membranes, it was only possible to achieve a Reynolds number of 1.2 x 10^5 for those tests.

The results of the cambered plate models were compared with those published by other workers to validate the model making quality and the performance of the wind tunnel. A comparison of the 14.6% camber ratio test with the most comprehensive comparative data available (Milgram 1971) is shown in Figure 2.14. While the correspondence is not perfect, the overall shape of the results is very similar and

follows the pattern of Milgram's (1971) results, giving confidence that the results being reported here are reliable. The detailed differences are most likely due to differences in the section shapes and the characteristics of the air flow in the wind tunnel but are unlikely to affect the validity of comparisons between results obtained the same test facility (Hoerner 1985:4-7). To quote the American home of aeronautical testing: (NACA 1921:259) *"It is a well known fact that the results obtained in different laboratories, because of their individual methods of testing, are not strictly comparable even if proper scale corrections for size of model and speed of test are applied. It is, therefore, unwise to compare too closely the coefficients of two wing sections tested in different laboratories. Tests of different wind sections from the same source, however, may be relied on to give true relative values."*

2.4 Results

2.4.1 Proximal sections

The 14.6% camber wing section (A1) was tested with a notional proximal wing bone situated at 20% and 40% of the wing chord from the anterior margin (A2, A3 and A4, A5 respectively). It was tested in a faired (A2 and A4) and unfaired geometry (A3 and A5). The fairing was applied with plasticine and was shaped by eye. No doubt other shapes are possible, but these must be the subject of further studies.

Figure 2.15 shows the polar curves (C_l vs C_d) for these sections. The section without any attached bone demonstrates a very similar shape to that reported by Milgram (1971), with a minimum profile drag coefficient of 0.1, a best L/D of 18 at a C_l of 1.8 and a maximum lift coefficient in excess of 2.0.

The addition of the wing bone (faired or unfaired) reduced the maximum C_l that was achieved but did not increase the minimum drag (although this was achieved at much lower value of lift coefficient.) The overall effect was a reduction in the best L/D ratio and a small reduction in the C_{lmax}.

The more anterior location of the wing bone gave the greatest reduction in performance and in both cases the effect of the fairing was small. The location of the bone was the more powerful effect. At the 20% location, the best L/D ratio was 9, increasing to 12 for the 40% location. Both locations gave a C_{lmax} of at least 1.8 (the tests had to be curtailed due to excessive vibration from the model, due to extensive separated flow.)

In summary, the proximal wing bone positioned at 40% of wing chord (faired or unfaired) reduced maximum lift but did not increase minimum drag, resulting in only small reduction in aerodynamic efficiency. A more anterior (20% chord) location for this wing bone resulted in a greater reduction in performance. In both cases the effect of the fairing was small.

2.4.2 Wing Phalanx Sections

The first wing phalanx (WP1) was modelled as an oval section (C3, C4, D3, D4, E2), with (C4 and D4) and without the soft tissue 'fairing' on its posterior face that has been proposed by other workers as

necessary to reduce aerodynamic drag (Padian & Rayner 1993). The second wing phalanx (WP2) was subtriangular in section, with slight concavity on the posterior face (C5, C6, D2 and E3). Both these wing sections were attached to two wing sections, one with 11.6% camber, the other 8.7%. (E1 and D1)

Figure 2.16 shows the results obtained with the 11.6% camber section. With no bone attached, it had a minimum drag coefficient of 0.05 at C_l=1.5, and a maximum L/D of 33. Attaching the wing bones increased the minimum drag substantially in all cases and moved the minimum to a lower value of C_l - around 0.8, and increased the C_{lmax} (with one exception - see below).

The small WP1 section was tested on the ventral side of the wing section, faired and unfaired. The shape of the fairing was based on an illustration in Padian & Rayner (1993). The two results were almost indistinguishable, both giving C_{lmax} = 1.9 and L/D = 15. While both the limited morphological evidence from the palaeontological literature (Padian & Rayner 1993) and the results from the aerodynamic literature discussed above suggest that a section with the wing bone offset in the ventral direction is more likely, one test was conducted with the WP1 section fitted on the dorsal surface of the wing section. It gave a slightly higher minimum drag and lower L/D than on the ventral side, as well as a substantially reduced maximum lift coefficient.

The smaller WP2 section had a slightly higher minimum drag than the WP1 section, the same maximum L/D ratio (15) and gave a small increase in C_{lmax} (2.0 as compared to 1.9). The larger WP2 section increased the drag substantially, but also resulted in an increase in C_{lmax} (to 2.25). The best L/D for this geometry was 10.

The 9.7% camber section alone (Figure 2.17) had a slightly lower minimum drag than the 11.6% section, but because this occurred at a lower value of C_l, the best L/D for this section was actually slightly lower (28.4). Attaching the large WP1 section increased the minimum drag as before (to 0.07) and again it moved to a lower C_l (0.5) than for the section alone. In this case, adding the fairing increased the minimum drag to 0.09 but gave very similar performance at high C_l. Consequently the maximum C_l of the two sections were the same (1.85) and the best L/D very similar (13.5 with fairing, 14.5 without). The large WP2 section increased the C_{lmax} to 2.15, had similar minimum drag but more drag at intermediary values of lift coefficient, resulting a reduced L/D max of 12.0.

As discussed above and illustrated in Figure 1.16, the parameters that are arguably most important in assessing the merit order of different wing sections are the maximum C_l that can be achieved (which determines the minimum flight speed), the maximum C_l/C_d ratio (which determines the aerodynamic efficiency) and the lift coefficient at which this occurs, which is an indication of cruise speed. These parameters are summarised in Figure 2.18.

2.4.3 Flexible sections

At low lift coefficients the taut and low camber section (F1 and F2) and gave similar drag to a comparable rigid section (C_d = 0.1), but closer to stall the drag became higher, thus reducing the

maximum L/D (12.5 for 0% camber, 9 with 10% camber) (Figure 2.19). However, a more notable result was that the maximum lift coefficient was greatly increased. In the cases of the high slack configurations the maximum lift coefficient reached 2.7, almost 25% greater than the highest result for any of the rigid sections (compare results in Figures 2.15 and 2.18). For these flexible sections, the maximum lift:drag ratio of 6 was achieved at a lift coefficient of more than 2.0. The exceptionally high maximum lift coefficient of these flexible sections was coupled with a gentle stall characteristic, as for the rigid sections. The key parameters are summarised in Figure 2.20.

2.4.4 XFOIL simulations and wing bone fairing

Attempts were made to apply the XFOIL low Reynolds number airfoil analysis code to the sections but panel codes of this nature have a limited capability to accurately model the effects of (as distinct from the occurrence of) large areas of separated flow and consequently underestimate the drag (Paton & Morvan 2007). The analysis was consequently of no use for producing reliable, absolute values for lift and drag of pterosaur type wing sections. XFOIL does however predict the shape of the boundary layer (Figure 2.21) and the location and extent of separation, which is useful in understanding the potential effect of different amounts of fairing around the wing bones. Figure 2.22 shows a summary of a typical set of XFOIL results for a WP1 wing bone section. With very little fairing, the program shows a region of separated flow posterior to the wing bone. As the extent of the fairing is increased the extent of the separated flow region reduces. The final section shows very little separation and represents the extent of fairing likely to be required to reduce drag to a minimum.

This approach was used to design a fairing for the medium camber section and resulted in a large (35%) reduction in minimum drag from 0.083 to 0.055 (Figure 2.23), but a more modest improvement in the aerodynamic efficiency, from a L/D ratio of 16 up to 22 since the maximum lift coefficient achieved was unchanged.

Results from wind tunnel tests of optimised low Re wing sections (S1223 and UF) (Shyy *et al.* 2008) (Figure 2.24) shed additional light on the section shapes required for minimum drag. The main difference between the two sections is their thickness and the thinner section had a higher peak L/D, but this was only sustained over a restricted range of angle of attack. The thicker (S1223) section had a lower maximum L/D but sustained good performance over a wider range of conditions. Both sections have enhanced trailing edge camber, something that is difficult to envisage on a pterosaur wing membrane. For comparative purposes, data for a thin plate section (Gottingen 417a from Schmitz 1952) is also included and demonstrates a lower peak L/D and a narrow performance range. The Gottingen 417a section was the one used by Bramwell & Whitfield (1974) and Brower (1983).

2.5 Discussion

In summary, tests with the WP1 and WP2 phalanges showed that:

- With the sections on the ventral side, drag increased substantially (as compared to a cambered section alone), with little difference between the two shapes. There was almost no effect on the maximum lift (in fact a small increase with the WP2 phalanx).
- A phalanx located on the dorsal side of the wing reduced the section performance substantially, increasing drag and decreasing the maximum lift coefficient. Positioning the bone on the dorsal side greatly reduced the section performance and similar results are apparent from sail/mast tests. These results strongly support the ventral positioning proposed by Padian & Rayner (1993).
- The larger the bone section relative to the width of the wing section, the greater the drag.
- Fairing the phalanx sections to the extent previously suggested (Padian & Rayner 1993) did not reduce the drag or influence the maximum lift.
- A more extensive fairing, designed to minimise separation, reduced the drag by 35% with no change in maximum lift.
- The flexible section had similar minimum drag but greatly increased maximum lift (>25%) (at the cost of high drag).
- The maximum lift coefficients produced by the rigid sections approached 2.0 and were higher still for the flexible section (approaching 2.7), values considerably in excess of those reported for birds (Pennycuick 1968, 1983, Tucker and Heine 1990).

More generally, the results show that the airfoil section efficiency is sensitive to the wing bone diameter (strictly, the ratio of local diameter to local wing membrane width) and is maximised when this ratio is minimised. The humerus and radius/ulna are the largest diameter bones in the wing and are surrounded by soft tissue, further increasing their size. Thus the proximal regions of the wing are likely to suffer the greatest loss of performance due to the presence of the wing bones. However, this is the region where the propatagium is present, resulting in a section that does not have a bluff anterior edge to trigger separation and high drag. Indeed, the test results showed that a wide propatagium resulted in a section with less aerodynamic drag than a section with a narrow propatagium, pointing to an advantage from positioning the wing bones on the ventral side of the wing membrane and posterior to the leading edge. Thus, the propatagium acted more as a drag reduction device than as a means of lift enhancement, *contra* Wilkinson *et al.* 2006.

When soft tissue around the wing bone of this configuration was modelled, the section characteristics changed little, indicating that in the proximal regions of the wing the aerodynamic performance is insensitive to assumptions about the extent and shape of the soft tissue surrounding the wing bones. This is most probably due to the bone being in the separation 'shadow' of the leading edge at low angles of attack, thus having no effect on the minimum drag, but then causing new regions of separation as it is exposed to the incident flow at higher angles of attack. This would reduce the positive

pressure on the ventral side of the section and thus reduce the maximum circulation and C_{lmax} that could be achieved.

Wing bone sections situated on the ventral side of the membrane gave maximum lift coefficients that were comparable to or greater than the sections without a wing bone, indicating that the presence of the bones on the anterior edge had no detrimental effect on the lifting capability of the wing, although they did result in a substantial increase in drag.

There was little difference between the two different wing bone cross sections tested: the only parameter that proved significant was the wing bone depth. As this increased relative to the section width, the drag increased, L/D decreased and C_{lmax} increased, so moving the most efficient operating condition to a higher value of C_l.

XFOIL modelling and reference to optimised low Re airfoils indicates that substantial drag reductions could result from extensive fairing behind the wing bones. However, this would imply very extensive soft tissue which, unless it was heavily pneumatised, would have large weight penalties.

Taken together, it appears from these results that in order to approach the low values of minimum drag that are possible with optimised airfoils, a considerable extent of fairing behind the wing bones will be required and that L/D is maximised by having a thin section, which implies the smallest possible bone diameter.

For the flexible wing sections, the performance at low camber was similar to that of the rigid sections, but as the camber (and flexibility due to slackness) increased the C_{lmax} became very high and the best lift:drag ratio was achieved at a lift coefficient of more than 2.0.

2.6 Summary

In summary, these tests have allowed the two-dimensional characteristics of possible pterosaur wing sections to be quantified for the first time. They reveal sections that were well adapted to low speed flight and controlled deceleration for low speed landing. Since the bones of pterosaurs are very thin walled and consequently very susceptible to impact damage, such a flight capability could have made an important contribution to avoiding injury.

Chapter Three

Flight capabilities

3.1 Modelling a flying animal

As outlined earlier, the standard aeronautical engineering approach to determining the flight performance of an aeroplane is to start with the 2D wing section data and to assemble this into the complete, three-dimensional aeroplane (or flying animal). The fundamental theory underlying this approach has long been known (Lanchester 1907, Prandtl 1921b) and relies on a body of analysis known as lifting line and lifting surface theories. (See Katz & Plotkin 2001, Anderson 2005 and more accessibly Marchaj 1979.) These approaches enable the calculation of the aerodynamic performance of finite wings, taking account of the induced flow patterns, energy losses due to the formation of tip vortices and variations in wing section and section orientation (twist) along the span. This analysis can also be used to understand the pitching moment characteristics of the wing and thus inform and understand the flight stability about the transverse axis. (Figure 3.1)

At the simplest level, the effect of moving from a 2D (effectively infinite) analysis to a finite one in three dimensions is the introduction of the tip effects, wherein energy is lost due to the formation of wing tip vortices, an effect captured by the concept of induce drag.

The well established formula for induced drag (Anderson 2005:395) is

$$C_{di} = \frac{C_l^2}{e\Pi AR}$$

(See Glossary for more details). From this it is apparent that induced drag depends on the square of lift coefficient (and the inverse square of flight speed), so it increases rapidly as speed decreases. Induced drag also depends on the inverse of Aspect Ratio (AR), (a measure of the slenderness of a wing). Long thin wings have higher aspect ratio and consequently less induced drag than short, wider wings, which explains why gliders are the shape that they are. A price paid is a loss of manoeuvrability. The final factor is 'e', a semi-empirical correction that varies with the lift distribution along the wing. Pandtl (1922) showed that the optimum lift distribution (the one giving the lowest induced drag) for a planar wing is elliptical, the shape of the iconic Spitfire fighter wing of WWII. Any deviations from that shape generally result in an increase in induced drag (Figure 3.2), represented by e in the equation above. Typically the value of 'e' lies within the range between 0.8 and 1.0.

The factor e can be estimated using lifting line and lifting surface theory, and over the years numerous computer codes have been developed to undertake this analysis (the so called "vortex lattice" and the more complex "panel codes" collectively referred to as panel codes in the what follows) which are the inviscid (meaning that the solutions take no account of viscous and thus boundary layer effects) forerunners of the more recent viscous flow computational fluid dynamics (CFD) codes, (which are based on solutions to the fundamental Navier Stokes equations of fluid flows and incorporate the effects of friction). While these new codes offer the promise of greater accuracy, versatility and the representation of viscous flow phenomena, they are computationally intensive and panel codes are to this day the workhorses of aircraft design (Woodward 1968, Erickson 1990). Panel codes are by their nature limited to an inviscid analysis, so are unreliable in cases where separated flow is present (such as stall) but for cruising flight they can give very reliable results. The vortex lattice method of 3-dimensional lifting surface aerodynamic analysis (technically a discrete co-location finite-difference method for obtaining numerical solutions to the loading integral equation relating normal velocity to wing loading (DeYoung 1976)) has been in use since the 1940s (Falkner 1946). Typical modern implementations are Tornado (http://www.redhammer.se/tornado/index.html), XFLR5 (http://www.xflr5.com/xflr5.htm) and AVL (http://web.mit.edu/drela/Public/web/avl/). I selected XFLR5 for this study for a number of reasons:

- It readily runs on a Mac computer using an accessible graphical interface, so the learning curve is shallow.
- It is free and open source.
- XFLR5 has been shown to provide similar results to other comparable codes and wind tunnel results (Deperrois 2011).
- It incorporates XFOIL, Mark Drela's open source 2-dimensional airfoil design code, a very powerful low Reynolds number 2D panel code that can take account of boundary layer (but not full separation) effects (http://web.mit.edu/drela/Public/web/xfoil/). This allowed a variety of airfoil sections to be modelled. XFOIL has been used in a very large number of airfoil studies and is known to provide reliable results over normal flight ranges (e.g. Bertagnolio *et al.* 2001, Windte *et al.* 2006, Kay 2010).
- It was designed for model aircraft, so is tailored to the Reynolds number range of relevance to pterosaur flight (10^5 to 10^6).
- Validation work for the analyses that follow was conducted on well-known configurations including uniformly tapered wings and elliptical wings and yielded correct results.

3.2 Weight and Wing area

In addition to the aerodynamic characteristics of the wing sections, the calculation of flight performance requires knowledge of the total weight and the area and shape of the lifting surface(s). As

discussed in the introduction section, the question of pterosaur body mass is not resolved, but it does appear that most workers now more or less support the results obtained from Witton's (2008) analysis. Consequently, this formulation was used to provide central values, although in some cases the effect of variation was also investigated. The same source was used for the wing area.

3.3 Calculation of polar curves

In order to compare and quantify the effects of the different wing section characteristics, the lift:drag relationships were used to calculate the flight performance of a notional three dimensional pterosaur with a wing area of 2.2m^2, wingspan of 5.8m and mass ranging between 13.9kg and 32kg . The drag was calculated as the sum of the section profile drag measured in the 2D tests, the parasitic drag of the body and the induced drag (drag due to lift). The resulting lift and drag values were then used to calculate a glide polar curve (the variation of sink speed with forward speed). A generalised polar curve is shown in Figure 3.3, highlighting the areas of particular interest with regards understanding animal flight performance.

The parasitic drag of the body was calculated using the methodology of Bramwell & Whitfield (1974) in order that comparisons could be made with their work. The induced drag was calculated using the standard aerodynamic formulation described above, and for the purpose of this initial study a constant value of e=0.9 was used, applicable to a highly tapered wing (Marchaj 1979). The aspect ratio was calculated from $AR=B^2/S$ (where B = the total wing span and S the wing area). The polar curve was calculated using the identity $C_T=W/(0.5\rho SV_a^2)$, where C_T is the resultant of C_L and C_D (the wing lift and drag coefficients), W the weight of the animal, ρ the mass density of air and Va the airspeed. This is solved to give the airspeed vector, from which the horizontal and vertical speed components can be derived.

The resultant curve is an inverted U shape, and the maximum of the curve is the point of minimum sink (Figure 3.3). The point where it is tangential to a line through the origin is the maximum aerodynamic efficiency (L/D_{max}) and also the maximum range in still air. It is important to be aware of this distinction. At minimum sink, time in the air is maximised whereas at L/D_{max} the range is maximised. The former matters more for behaviour that relies on soaring in rising air (Vogel 1994). Minimum sink can be improved in two ways: by increasing the L/D_{max} and/or by reducing the flight speed by reducing the wing loading, since moving towards the top left of the graph improves the sink rate without an increase in aerodynamic efficiency.

One other region of the polar curve deserves attention - the bottom left of the graph. This is where speed becomes very low and flight can only be sustained by achieving high values of lift coefficient. A precipitous drop in the polar curve reflects a sudden stall and most likely, loss of control. A more rounded shape reflects a more gradual and controlled transition from flight to stall.

Figure 3.4 shows the polar curves using the WP1 wing section at two different values of mass, compared with polars calculated by Bramwell &Whitfield (1974) and Brower (1983). It is immediately apparent that the WP1 data results in a halving of the L/D ratio when compared to the earlier estimates, although at the lighter weight the flight speed is similar. At the higher weight the flight speed is increased as is the minimum sink rate, but the flight efficiency (L/D ratio) remains constant. These results suggest that the flight efficiency (as quantified by the L/D ratio) of large pterosaurs was significantly inferior to previous estimates, and somewhat lower than the best extant soaring birds. (Pennycuick 1983, Tucker & Parrott 1970). However, due to the potentially low flight speed, the minimum sink rate was comparable to extant birds.

Figure 3.5 compares the results of the wind tunnel tests at a constant mass of 23kg (mid way between the two extreme estimates.) For comparative purposes, results were also calculated using data from the 471a Göttingen section (a simple cambered plate that was used by Bramwell & Whitfield 1974) and the Selig S1223 section, an airfoil optimised for low Reynolds number flight. The two airfoil sections give similar peak efficiencies of 20:1 (similar to the values predicted by Bramwell & Whitfield 1974), but the S1223 section maintains good performance at higher values of lift coefficient, so shifts the polar curve to the left, resulting in lower flight speeds and improved minimum sink (0.5m/sec). This result is in effect the upper bound for an 'ideal' pterosaur with an optimised airfoil section that requires assumptions of a thick wing section. For comparative purposes, the results of the camber only section are also shown. It has a lower flight speed than the 417a section due to its higher lift capability, but is inferior to the S1223 section.

The results in Figure 3.6 show the effect of camber with the WP1 wing bone. As camber increases the polar curve moves vertically downwards, resulting in a increased sink rate and reduced aerodynamic efficiency (L/D ratio.) The flight speed at minimum sink for the low camber section is 10m/s increasing to 12m/s at maximum range (L/D max). Figure 3.7 shows that the wing bone to chord ratio is a very important parameter. An increase from 7.0% to 9.4% increases the minimum sink rate from 1.0 to 1.5m/s, whereas the differences between the WP1 and WP2 profiles of the same depth are relatively small.

The flexible sections (Figure 3.8) cover a wider range of performance, with the lowest camber section giving similar performance to the rigid sections at speeds above the minimum sink condition, but a less precipitous increase in sink rate at low speeds (due to the 'soft' stall.) This effect becomes more marked as the camber is increased, thought it is achieved at the price of poorer efficiency and higher sink rates. An envelope around these curves suggest that if pterosaurs could control wing camber (which is certainly plausible in the proximal regions of the wing where the camber is under the control of the ankle attachment), then they are capable of maintaining control at very low flight speeds.

3.4 Summary

The glide polars show the flight efficiency is significantly inferior to previous estimates (Bramwell & Whitfield 1974, Brower 1983), and somewhat lower than some extant soaring birds (Pennycuick 1971a, Tennekes 1997, Alexander 2003, Pennycuick 2008). However, due to the low flight speed, the minimum sink rate (approx 1.0m/s) was comparable to extant birds (Azuma 2006, Pennycuick 1971a, Tennekes 1997, Alexander 2003, Pennycuick 2008) and bats (Pennycuick 1971b). As wing bone size increases (relative to the wing chord) the sink rate increases with little effect upon flight speed.

The flight performance was improved by extensive fairing of the wing bones, and while the presence of such a fairing is entirely speculative, it may have been provided by pneumatised tissue (Claessens *et al.* 2009). The fairing increased the aerodynamic efficiency and flight speed but had only a limited effect upon the minimum sink speed, the parameter that determines the loitering and thermal/slope soaring capability.

With a flexible membrane, the flight envelope was extended to lower speeds due to the enhanced high lift capability and progressive stall of these sections. Since the animals presumably had some control over the wing camber (Kellner *et al.* 2010, Bennett 2000), the envelope curve around the results with the flexible membrane best shows the full range of performance. When compared to the rigid wing section results, the low speed flight capability is extended and combined with a softer stall, which would have enhanced control during landing manoeuvres when low speed, high drag and high lift are required.

Chapter Four

Wing spar structural model

4.1 The pterosaur wing spar

The gross morphology of the complete wing bones of large pterosaurs has been well described by Bennett (2001) and Wilkinson (2008) in particular, although other authors have provided descriptions of specific features or made inferences about the attachment of soft tissue and thus the ways in which the wings may have been deployed (Elgin & Hone 2010). In addition to describing the morphology and relative sizes of the different bones, Bennett (2001) and Wilkinson (2008) also discussed the degree of mobility likely to have been possible in the joints. What follows relies heavily on these sources and for the sake of clarity they are not repeatedly referenced.

This literature describes what the bones looked like, how they articulated with each other and how they were constrained and moved by the soft tissue (muscles and tendons) attached to them. However, all the authors have been more or less silent on what the bone morphology may say about them as structures. The one point that has been repeatedly made is to the effect that the bones were thin walled "for lightness and strength", but that is all and of itself a rather meaningless phrase. The same claim has been repeatedly made with respect to birds (see Dumont 2010 for a review), but as Dumont (2010) points out, the skeletal mass of birds contributes the same proportion of total mass as does the skeleton of mammals, because bird bones are more dense than mammals. Dumont (2010) interprets this as a response to the stiffness and strength requirements of flight. It is likely that the same evolutionary forces shaped the bones of pterosaurs.

4.2 What the morphology may reveal about load bearing function

What follows contains a degree of subjectivity and speculation, but is an attempt to infer the structural behaviour and possible loading cases by examination of the bone morphology. I start at the glenoid and work towards the distal end of the wing. While the precise shapes and sizes of the bones vary from species to species (and indeed from individual to individual) the well described bones of *Pteranodon* and *Anhanguera* are sufficiently typical for the purposes of illustrating the discussion that follows (Figure 4.1).

4.2.1 Humerus

The humerus is the most robust wing bone in that it is not only large in diameter at mid shaft but has greatly expanded epiphyses and a large deltopectoral crest. In contrast to its relatively massive overall dimensions, the cortical bone thickness is low compared to the diameter and the bone has a dense network of "foam-like" trabeculae in the epiphyseal regions (Steel 2005) and a network of slender transverse trabecular struts in the mid shaft (personal obs. Figure 4.2). The cross section of the mid shaft is typically close to circular and overall the bone is very stout when compared to more distal bones such as the ulna and wing phalanxes.

From a structural point of view this morphology suggest a bone that is heavily loaded in compression - its stoutness ensuring that it does not suffer from an Euler bucking failure. The flared epiphyses are presumably also a response to high compression loading since, while bone may be strong in compression, the joints are filled with much softer cartilage so the local stresses must be reduced. As Rogers & LaBarbera (1992) and Reich & Gefen (2006) show, the presence of trabeculae increases the energy absorption capability (strain energy) of bones, again pointing to a bone heavily loaded in compression, perhaps experiencing shock loading due to landing impact.

The large deltopectoral crest that extends laterally from the proximal end of the humerus is the wings' main attachment to the flight muscles and the offset nature of the attachment means that the humerus will be subject to torsional loads as well as the mediolateral pull of the muscles (the lateral component of which imparts compressive loading onto the bone). A circular cross section is the most efficient structural form to resists torsional loads (in the absence of other loading - but see section describing the wing phalanges for more on this) and the combination of large diameter and thin walls is the most weight efficient way to distribute the cortical material. The slender trabecular struts, which appear to be oriented at an acute angle to the long axis of the bone may also contribute to the torsional stiffness of the bone. They are most likely too slender to be effective when loaded in compression, but would be able to resist deformation when loaded in tension. Some would be effective in this way on the downstroke, others on the upstroke.

In summary, the humerus has the hallmarks of a structure optimised to resist compressive and torsional loading and to be capable of absorbing impacts.

4.2.2 Radius and Ulna

From a structural point of view (resistance to bending or compressive loading) the radius is of little consequence since its cross section dimensions are substantially less than those of the ulna it accompanies, so the discussion will now focus on just the ulna. The ulna is more slender than the humerus, but also exhibits large differences between the epiphyseal and diaphyseal diameters (most marked at the proximal end) and extensive trabeculae in the epiphyseal regions, again a likely response to high compressive

loading on the joints. The joint facets themselves do not have any obvious locking mechanisms, so this invites the question of how the joints resist the bending loads applied the lift forces in the wing. Why does the wing not simply fold up? The restraining mechanism must be a tendon acting across the joints.

Theses tendons/muscles are clearly illustrated by Bennett (2007 and 2008) (Figure 4.3) and imply that at least as far distally as the joint between the metacarpal and the first wing phalanx, the wing bones are constrained against dorsoventral bending by tendons/muscles acting as tension members in what in engineering terms is a guyed structure. It seems likely therefore that the humerus, ulna and to some extent the metacarpal are adapted primarily to resist compressive forces rather than bending - they are buried in a mass of soft tissue which is loaded in tension and it is this that locks them in position and applies the compressive loads.

4.2.3 Wrist

The wrist bones are very short and in structural terms are no more than an extension of the ulna, and as in the case of the ulna they are retained in place by compression.

4.2.4 Metacarpal

The metacarpal (strictly speaking McIV as McI-III are typically much reduced or absent) exhibits lesser differences in diameter along its length, but as in the ulna, the proximal diaphysis is the larger of the two. The most striking character of this bone is the "pulley" shaped joint at the distal end, which joins with the first wing phalanx. This shape provides a degree of locking of the joint in the dorsoventral direction, but again, to be effective, the two bones have to be held against each other by the action of a tendon stretched across the joint. These tendons appear to be on the anterior and posterior faces of the metacarpal, so unlike the more proximal bones of the forelimb, it is exposed to the bending loads produced by the wing lift forces.

The cross section of the shaft of the McIV shows relatively thick walls (as compared to the ulna and humerus) and reduced dimensions, but a marked difference between the width (anteroposterior dimension) and the depth (approaching a ratio of 1.0:1.5). Consequently the second moment of area (a measure of the resistance to bending loads) is at least twice as high dorsoventrally as anteroposteriorly.

4.2.5 First wing phalanx

The wing phalanges are relatively slender bones with extensive mid-shafts of more or less constant, parallel cross section. The first wing phalanx is distinctive in that the proximal end is more flared than the others, where it locates with the "pulley" joint to the metacarpal. As before, this swelling is presumably a response to the high compressive forces across the joint, applied in particular by the large tendon attached proximally to the anterior face of the phalanx.

The first wing phalanx has a distinctive cross sectional shape in the shaft - somewhat sub-triangular and with regions of thicker cortex in the corners of the triangle (Figure 4.4). A shape such as this is optimum for resisting a combination of bending and torsional loads (Karihaloo & Hemp 1987). The orientation of the shape is such that the anteroposterior dimension is larger than the dorsoventral, resulting in the dorsoventral second moment of area being around half that in the anteroposterior direction (the opposite of the case for the metacarpal).

The mid-shaft region is typically 30mm wide and 20mm deep, with a wall thickness of 1.0 to 2.0mm. As a general statement, a thin walled structure such as this is an efficient disposition of material to resist bending and torsion, since for a given mass, a large diameter, thin walled section has a higher second moment of area (a measure of bending and torsional stiffness) than one of lesser diameter and increased wall thickness. However, as the section becomes increasingly thin walled, there comes a point where, instead of failing in bending due to rupture of the structural material, local bucking occurs and places an upper limit on the load bearing capability of the structure. However, as will be discussed later in this Chapter, it appears that thin-walled as they were, pterosaur bones were unlikely to be subject to local bucking failure.

4.2.6 Second and third wing phalanges

Most of the above discussion of WP1 applies equally to WP2 and WP3. The main difference is that the proximal epiphyses of these bones are not as expanded as in WP1 and they do not show any obvious signs of joint flexibility, suggesting that they were more or less locked together (Wellnhofer 1991a:46), in effect making the four wing phalanges into a continuous structural unit.

4.2.7 Fourth wing phalanx

The fourth wing phalanx is different from its more proximal neighbours. The cross section is more nearly circular and the wall thickness is much increased (as compared to the overall diameter). This is a structure that is not optimised for bending stiffness, but for toughness. The thick walls mean that it is relatively resistant to impact damage and the small diameter means that it can bend with less chance of failure - specifically, for any given bending deflection (radius of curvature) the surface strain will be less than for a larger diameter, thinner walled alternative.

4.2.8 Overall dimensions

The external diameter of the wing bones that comprise the wing spar decreases progressively from the glenoid to the distal end. This is characteristic of a structure that is fixed at one end and primarily loaded in bending, practical analogues being fishing rods, flag poles or unstayed yacht masts.

4.2.9 Discussion

From a purely structural point of view, the pterosaur wing bone morphology implies overall bending loading, but locally high levels of compressive loading.

The morphology of the first proximal bones implies structures subject to compressive loading. All the bones are weight efficient (in that they are thin walled) and the wing phalanges are shaped to resist a combination of bending and torsional loading. The bending stiffness of these more distal bones is greatest in the anteroposterior direction, suggesting that membrane tension is more of a structural driver than the loading from lift in flight.

The most distal wing phalanx is more thick walled and (possibly) flexible, suggesting that it maybe imparts some aeroelastic flexibility to the wing membrane whilst also resistant to impact loads, perhaps the result of the wing tips touching the ground on take-off or landing.

Against this general background the remainder of this chapter, and the two which follow, will discuss the development of a structural model of the wing spar, the likely loading and the response of the structure to this loading.

4.3 Limits to load bearing: the bending and buckling of thin walled structures

4.3.1 Scaling effects

Simple beam theory (Den Hartog 1949:79) shows that the deflection (δ) of a uniform cantilevered beam is:

$\delta = PL^3/(3EI)$ or $\delta = wL^4/(8EI)$

Where:

P is a point load at the end of the beam

w is load per unit length

E=Young's modulus of the beam material

I=second moment of area of the beam cross section.

The wing spar of a pterosaur is more complicated than this in that the second moment of area varies along the length as does the loading, however the underlying dimensional characteristics do not change, so it is instructive to briefly examine the scaling of these relationships.

In order to do this, another key formula of beam theory must also be considered. The formulae above are for the complete beam, but at any location along its length there will be a transverse stress distribution that is characterised by the following formula (Den Hartog 1949:39)

$\sigma = My/I$

Where σ is the local stress at distance y from the neutral axis

M is the local bending moment

y is a distance from the neutral axis

I as above.

Under the assumptions of simple beam theory, the stress distribution will be linear across the section (see Fig 4.5) but if the neutral axis of the section is not equidistant from the opposite sides the maximum surface stress will be larger on one face than the other.

Returning to the deflection, as pterosaurs vary in size it is likely that the ratio of deflection to span will need to remain constant. The upward curvature of a wing subject to bending will have two effects - it creates dihedral, which increases the roll stability and also reduces the projected area, which reduces the aerodynamic efficiency (Hoerner 1965:7-9, Kuenn 2013) (although this is to some extent offset by an increase in span efficiency Cone 1962, Kroo 2005). Whatever the precise effects, they are effects that will vary little with scale and consequently it is reasonable to assume there are no strong reasons why the shape of the wing deflection curvature should not remain more or less constant with scale.

If this is valid, then δ/L is constant, and so:

δ/L is proportional to PL^2/I for a constant material (i.e. E=constant). For isometry, the force will vary as L^3 so

$\delta/L \propto L^5/I$.

So for constant δ/L, the second moment of area I must be proportional to L^5. Since I$\propto$to section depth^4, the bone depth will increase faster than the bone length (with an exponent of 5/4), i.e. the bone must become relatively more robust as size increases. However, Witton (2008) calculated that pterosaur mass is allometric with span, having an exponent of around 2.5, meaning that I is proportional to $L^{4.5}$, reducing the relative rate of the increase in section depth (to an exponent of 1.125). Either way, larger pterosaurs are likely to require relatively larger diameter wing bones, resulting in a reduction in the aerodynamic performance (as well as in increase in skeletal mass - see Chapter 8 for more discussion of this point).

Returning now to the second key formula:

$\sigma = My/I$,

It can be shown that $\sigma \propto L$ since $M \propto L^4$ and $I \propto L^{4.}$ However, for any given material, i.e. bone, the value for allowable stress does not change with animal size - bone is bone regardless of the animal it is in and its strength does not increase with animal size (Currey 2006:130).

Consequently for isometry:

I/y must be proportional to M and since $M \propto L^4$, $I/y \propto$ to L^4. Now, for a cylinder, $I \propto D^4$, so $I/y \propto D^3$ and thus $D \propto L^{4/3}$, which reduces to $L^{1.17}$ (for Witton mass scaling). So here again the wing bone diameter must increase proportionately more quickly than bone length, but by a different (higher) exponent to the rate driven by bending deflection. Consequently it appears that surface stress rather than deflection may well be the limiting factor.

4.3.2 Non-linear effects

The foregoing discussion is based upon simple beam theory equations, which assume small deflections and no distortion in the structural cross section. In practice thin walled tubes (such as the long bones of pterosaurs) may be subject to more complex phenomena, in particular the possibility of local bucking. Anyone familiar with a drinking straw will know that if it is bent it initially takes up a smooth curved shape but as the bending is increased there comes a point where it suddenly kinks, but does not fail in the sense that the material ruptures. What has happened is that the cross section of the straw deformed due to second order effects and it became oval, with the long axis in the plane of bending, thus reducing the second moment of area of the cross section, reducing the bending stiffness at the same time as the bending moment was increasing, resulting in catastrophic failure. This phenomenon is known as Brazier buckling (Brazier 1927). It is also possible for local wrinkling to occur on the compression side of the structure, so called "bifurcation instability" (Karamanos 2002). These effects are very complex and the subject of extensive research (for example Wadee *et al.* 2006 and Corona *et al.* 2006).

In practice, there is a minimum level of wall thickness at which this effect occurs, and for thicker walled structures the failure occurs as rupture of the material. This limiting value of wall thickness depends upon the Young's modulus and Poisson's ratio of the material (Brazier 1927, Young & Budynas 2002:735).

Brazier's formula for the critical bending moment of a tube was given as:

$$\overline{M} = \frac{2\sqrt{2}}{9} \frac{E\pi r t^2}{\sqrt{1-\sigma^2}}.$$

Where, r=radius of curvature of the tube and confusingly, based on the earlier terminology in this document, σ=Poisson's ratio.

The Young's modulus (E) of bone varies a great deal (Currey 2006:130). Typically, the value for mammal long bones ranges from 15GPa to 25GPa and it can be as high as 28.2GPa for the tibiotarsus of a flamingo. Since pterosaurs are clearly highly adapted for flight, and as Dumont (2014) has shown for birds, bone stiffness is important, it is reasonable to assume that the forelimb long bones of pterosaurs will have E values towards the upper end of the range that is available from the material - in other words somewhere between 20GPa and 30GPa.

There is some debate about the appropriate value of Poisson's ratio for bones. Currey (2006:56) gives a range of values that have a mean of around 0.4. Rupin *et al.* (2008) note that the common value given in the literature is 0.3, but they measure a value of 0.42. However, Shahar *et al.* (2007) give values in the range from 0.10 to 0.20. From the formula above it is clear that the larger the value of Poisson's ratio the larger will be the critical bending moment. Accordingly, to be on the conservative side, a value of 0.2 will be used in the analysis that follows (though a brief sensitivity analysis showed that the difference in the results between using 0.2 and 0.4 is very small.)

Referring again to the classic beam theory equation for the stress distribution of a section subject to bending:

$\sigma=My/I$ (with σ having its original meaning of stress).

Brazier's formula above can be inserted into this equation to give the critical stress at which buckling occurs based on different value of Young's modulus (E) and the wall thickness ratio (r/t). Currey (2004) presents data that links E and tensile strength of cortical bone (Figure 4.6). There is scatter in the data but for E of 20GPa and 30GPa, typical yield stress values of 150MPa and 200MPa respectively. The result of using these values in the relationship described above is shown in Figure 4.7. The critical stress increases with E and decreases with r/t ratio. Using the appropriate values for the stress for each value of E gives critical wall thickness ratios of 46 and 51.

An alternative and more generalised approach to determining the critical wall thickness ratio is given by Reddy (1979) in the form of experimental data that relates yield strain to critical wall thickness ratio (Figure 4.8). This figure combines Reddy's (1979) result with data from Currey (2004) that relates yield strain to E. Projecting the Currey (2004) results onto the Reddy (1979) graph predicts critical wall thickness ratios ranging from 30 to almost 60, bracketing the values calculated above.

Overall then, it appears that for high modulus cortical bone, tubular bones with a wall thickness ratio (r/t) of at least 30, maybe as much as 60, are unlikely to suffer buckling failure when loaded in bending.

This r/t value implies a wall thickness of 0.2mm to 0.4mm for a 25mm diameter tube. As such the WP1 wing bone mid shaft sections, which are around 20mm to 25mm wide and have minimum wall thicknesses of around 1.0mm (Figure 4.4), are unlikely to be vulnerable to local buckling failure. It is apparent from the relationship above that the buckling resistance is inversely proportional to the radius of curvature. Consequently a circular approximation for the WP1 section is actually unrealistic since the radius of curvature in the dorsal side (which is subject to compression due to flight loads and thus vulnerable to bucking) is less than for a circle of comparable dimensions.

A better approximation is a 1.5:1 ellipse, for which the greatest radius of curvature is $a^{2/b}$ (Chan *et al.* 2010) where a and b are the major and minor radii respectively. Chan *et al.* (2010:394) note that a number of investigations have shown that the buckling of an elliptical section (about the long axis) *"could*

be accurately predicted by the buckling stress of a circular hollow section with a radius equal to the maximum radius of curvature of the elliptical hollow section."

Very roughly then, comparing an 1.5:1 ellipse with a circle of comparable area (with a radius equal to the mean of the radii of the ellipse) the maximum radius of curvature is 80% larger (almost twice) that of the circle (Figure 4.9). Consequently the critical r/t value will be around half that of the circular section, somewhere between 0.36mm and 0.72mm, which becomes close to the minimum thickness in this region. The foregoing suggests that the WP1 mid-shaft section is likely to be close to failing in bucking but providing the wing bone material has an E value towards the upper end of the possible range for bone, this might be avoided.

There are clear weight advantages in making the wing bones as thin walled as possible. A simple parametric study of an elliptical cross section beam sized for constant bending stiffness showed that weight decreased in almost direct proportion to the wall thickness (Figure 4.10). As is clear from the cross sections in Figure 4.4, the ratio of wall thickness to radius is higher for the more distal phalanges, so they too will not fail by local bucking.

4.4 Wing spar loads

As noted earlier, in mechanical terms the wing spar of a pterosaur is primarily a cantilevered beam loaded in bending and torsion. The proximal end is embedded in and restrained by the musculature around the humerus but more distally the bones are unsupported. The flight loads on the spar come from the aerodynamic forces generated by the wing membrane - primarily the weight support forces (lift) required to maintain flight and the membrane tension required to resist flutter. Since the spar is at the leading edge of the membrane the centre of action of the lift force will be everywhere posterior to the local wing bone resulting in torsional loading in addition to bending.

While it is relatively easy to estimate the lift forces and moment since lift is almost exactly equal to weight and can be assigned a span-wise variation, the torsional loads are much less tractable. The aerodynamic centre of lift is approximately 25% of the local chord from the leading (anterior) edge of the section (Katz & Plotkin:113) so the applied torsion will depend upon not only the span-wise lift distribution but also the planform shape. As discussed in Chapter 7, it is likely that the pterosaur wing planform was one with substantial forward sweep (see Figure 7.3), which would not only have the effect of balancing the centres of mass and lift, but also reducing the torsional loads, particularly on the proximal wing bones, for the following reason. The predominant membrane tension is in the span-wise direction, so the vertical component of that tension at the attachment to the distal wing bones will result in a torsion moment about the more proximal bones. However, from inspection of Fig 7.3 it is apparent that while the forces on WP3 and WP4 may be exerting a torsion moment in a head down rotation about the glenoid, the forces on WP1 and WP2 are having the opposite effect, as are any tension forces acting on the radius/ulna. In the absence of a full, detailed model of the wing bone/membrane interaction it is impossible to

quantify these effects but in view of the apparent cancellation of forces noted above, it was deemed reasonable to ignore the torsional loads in the following analyses. This is clearly a deficiency that could be remedied by the construction of either a fully detailed structural computer model or an instrumented physical model. Both are beyond the scope of this present work.

While the lift forces will load the wing spar in dorsoventral bending, the tension in the membrane will result not only in the torsional moments discussed above, but also substantial anteroposterior bending moments. The possible magnitude of these moments is discussed in Chapter 6, but suffice to say at this point that they appear to be considerably greater than the lift moments.

Whatever the loading, in order to understand its effect on the wing spar structure, the structural properties of the spar must be determined. As noted above, the deflection and local stress magnitudes in the structure depend primarily on two factors, the second moment of area of the cross section and the overall dimensions of the section. (Strictly speaking, the local stresses may also be influenced by stress concentrations - abrupt changes in cross section, but given the smooth, curved shapes of the wing bones this possible effect was considered to be negligible (Young & Budynas 2002:771-797).)

Therefore it was necessary to know the bone cross section geometry along the spar, data that had to be obtained almost exclusively from measurements of museum specimens since, with the notable exception of Steel's PhD thesis (Steel 2005) which contained a limited range of illustrations obtained from thin sections, the published literature was almost silent on the subject despite frequent comments on the exceptionally thin walled nature of pterosaur bones.

4.5 Wing bone morphology and measurements

In order to obtain the necessary wing bone morphology information, collections in a number of museums were visited:

Natural History Museum, London

Sedgwick Museum, Cambridge

Museum of York, York

State Museum of Natural History, Karlsruhe

American Museum of Natural History, New York

University of Portsmouth

Initially the approach was to use photography to obtain the required information. The external morphology was obtained by taking scaled images from which the external dimensions could be measured (with a focus on the dorsoventral and anteroposterior planes). The bone cross section was less readily obtained since it could only be seen in broken specimens, or a few thin sections (Steel 2005). All this changed with the advent of financially accessible CT scanning and in 2010 three fragments of ornithocheirid wing bone (NHM 33228, probably WP1 or WP2) were scanned at the NHM. Further

scans were commissioned from the NHM, specimen numbers R3877 (fragment, right ulna *Istiodactylus latidens*), NHM PV R3880 (fragment, ulna, *Istiodactylus latidens*), R39411 (an almost complete ornithocheirid WP1) and R41637 (Figure 4.11), almost complete ornithocheirid WP1. More details of the NHM specimens are contained in Steel (2012).

Ultimately the most relevant data was obtained from University of Portsmouth specimens, a complete WP1 and an articulated WP2 and WP3 from a similar sized individual (see Figure 4.12), which were scanned at μ-Vis (University of Southampton). Due to the size of the specimen, the scan was made as a series of slices 10mm apart, but for the calculation of structural properties this is more than adequate definition. These specimens, plus the almost complete NHM OR41637 WP1 provided most of the information required to create the structural model. Thin section results (Steel 2005) and measurements from fractured specimens were used for WP4, ulna and humerus.

4.5.1 Wing bone sections

The CT scan data of the wings bone sections (Figure 4.13) were analysed using ImageJ with MomentMacro. Slices were selected along the wing bones and "repaired" and partitioned by eye in ImageJ, (http://imagej.nih.gov/ij/index.html) then analysed using MomentMacro (http://www.hopkinsmedicine.org/fae/mmacro.html). The technique was validated against known shapes. This combination allowed the second moments of area about the two primary axes (Ixx and Iyy) to be obtained (required to estimate the bending stiffness and deflection), as well as the orientation of the neutral axis and the extreme values of surface distance from the neutral axis (required for estimating the surface stress).

4.6 Structural modelling of the wing spar

4.6.1 Beam theory or FEA?

With the exception of the humerus, the wing spar bones are all relatively slender so conventional beam theory can potentially be used to analyse the deflection under load (Roark 2002:125). However, strictly speaking beam theory should only be used when the deflection is small (Den Hartog 1949:79) since intrinsic in the formulation is an assumption that the projected beam length is equal to the actual beam length. However, if the deflection is large, in the case of a cantilever for example, the free end not only moves vertically but also horizontally, which has the effect of reducing the bending moment if the direction of the applied force does not rotate with the beam.

In the case of a pterosaur wing spar, the deflection is likely to be larger than generally considered acceptable for the use of beam theory - maybe as much as 15% of the wing length (Browning 2007). In addition to the large deflection, the other characteristic that makes the pterosaur wing spar very different from most man-made structural beams is that the cross section varies along the length. Beam theory can

still be applied to beams with varying second moment of area, with the variation in I included in the integration that is required to obtain the deflection, but taken together these two factors suggest that a finite element approach may be more appropriate, and there is no doubt that if modelled in the requisite detail this approach would give a highly accurate result.

However, in order to create the necessary mesh models for the FEA analysis, either detailed scans with the slices at voxel spacing would be required, or 3D models prepared from widely spaces scans, thin sections and photographic information. Since the information for the former approach was not available (with the exception of the NHM WP1 scan) the latter approach would be required. In practice, "reverse engineering" complex shapes in 3D modelling packages such as Rhino is extremely difficult and time consuming (see http://wiki.mcneel.com/rhino/reverseengineering) and most of the available techniques are based on the use of point cloud datasets obtained from 3D scanners or photogrammetry, neither of which were practical for the available specimens since almost all were part encased in matrix. The only way that the modelling could have been undertaken was by lofting the cross sections (using a 3D CAD program to create faired surfaces through the cross sections), a very fiddly and time consuming process which might be viable for a model of the exterior surface, or a shell with an assumed constant wall thickness, but a forbidding task when the processes requires two slightly different shells to be accurately nested one inside the other.

4.6.2 A beam theory model

In view of these difficulties, a simpler beam theory based approach was developed and calibrated against known analytical solutions and simple FEA modelling. The key simplification was to model the bones as a series of parallel sided sections rather than a continuous curve. Clearly a trade-off between accuracy and the number of sections was to be expected, so this was investigated. For a beam with a constant cross section (for which an analytical solution was calculated) convergence to within 1% of the analytical solution for the end deflection was achieved with 10 sections, but more were needed for a beam with variable cross section. The WP1 bone was selected since the variation of the second moment of area with length is similar for the Ulna, WP2 and WP3. In this case 20 sections gave a result within 5% of the likely asymptotic value computed for 500 sections (an analytical solution not being readily calculated), and 50 sections were within 2% (Figure 4.14). Accordingly, it was decided to use a figure of 50 sections per bone for the calculations to keep the process manageable and computationally efficient.

In order to produce data for 50 cross sections of each bone, the variation of second moment of area along the length of each bone as measured from CT scans and other sources was plotted and curves fitted to the data so that precise values could be interpolated at each of the 50 locations along the length. Figure 4.15 shows a typical example of the shape of the variation (for WP1) and the nature of the fitted curve. The overall bone width and depth were also included in the model so that the surface stress could be estimated. In order to do this the simple approximation was made that the distance from the neutral

axis to the outer surface was half the relevant section dimension. This is likely to be very reliable in the proximal bones as the mid shaft bone cross sections are close to symmetrical for the humerus, ulna and metacarpal. It is also reliable for the distal bones (the wing phalanxes) in the anteroposterior direction since they are more or less symmetrical in this orientation, however in the dorsoventral direction the asymmetry of the wing phalanxes means that this assumption is slightly in error. Comparison of the calculated distance from the neutral axis to the outer surface and the half the section depth showed that in the mid shaft region (where surface stresses are highest) the error in making this assumption was less than 10%, in the direction that results in an underestimation of the tensile stress on the ventral extreme of the bone. The maximum error occurred in the first wing phalanx, and reduced to only a few percent in WP2 and WP3.

4.7 Stiffness distribution

The distribution of Ixx and Iyy along a typical individual bone is shown in Figure 4.16 and for the complete spar in Figure 4.17, from which a number of characteristics are apparent. As might be expected, the average value of I decreases along the length of the spar, as does the bending moment. However, within any particular bone, the values of I are more or less constant in the diaphysis but increase substantially in the epiphyseal regions (even when the effects of the trabeculae are ignored), despite the cortical thickness being much reduced towards the ends of the bones. Perhaps most significantly, the relative values of Ixx and Iyy change along the spar. In the proximal region, distally as far as the metacarpal, the value of Ixx (which relates to bending in the dorsoventral direction) is greater than Iyy, but at the first wing phalanx the relative values are reversed and the anteroposterior stiffness is twice that in the dorsoventral direction (at last as far as WP4, where the values are similar.)

This change had not been previously identified and yet appears to be present in all pterosaur wing fossils that I have examined. The functional interpretation is that the wing spar structure is balancing the requirements of controlling the dorsoventral wing tip deflection with providing sufficient anteroposterior stiffness to ensure adequate membrane tension. Since the tip deflection is particularly sensitive to the stiffness of the proximal bones, this region is biased towards dorsoventral stiffness, but since the membrane tension is more or less span-wise, the more distal regions are subject to bending due to the membrane tension, so must be adequately stiff.

4.8 Summary

The gross morphology of the pterosaur wing spar suggests a structure that has evolved to resist compressive loading in the proximal bones (proximal to the wrist) and bending loads more distally. In flight, the applied loading is primarily dorsoventral due to the aerodynamic lift on the wing and anteroposterior due to the tension in the wing membrane. While some torsional loads are also likely to be

present, their quantification is problematic and they are considered likely to be small compared to the other loads.

Since the distal wing bones, which are subject to bending loads, are relatively slender, beam theory is considered to be sufficiently accurate as a modelling approach. It provides sufficient accuracy to allow reliable estimation of deflections and local stress loading and is computationally far less demanding than an approach based on finite element analysis.

Initial assessment of the distribution of cortical material in the wing bones shows that the proximal bones (as far as the metacarpal) have greater stiffness in the dorsoventral plane than anteroposteriorly, whereas more distally the opposite is the case, by a factor of around 2:1. This is interpreted as a structure that minimises the overall wing deflection whilst also providing adequate stiffness in order to tension the wing membrane.

Chapter Five

Dorsoventral Wing spar loading

5.1 Distribution of Lift loading

The aerodynamic forces on the wing comprise the lift force required to balance the weight of the animal and keep it in the air and the drag forces generated by the wing, which are a combination of profile and induced drag. In practice the drag forces are much less than the lift forces, typically no more than 10%.

In steady flight, the total vertical aerodynamic force must equal the weight of the animal. This aerodynamic force is the resultant of lift and drag, but since the drag component is less than 10% of lift, it is a good approximation to assume lift is equal to weight (for a lift:drag ratio of 10:1 for example, the error involved in making this simplification is approximately 0.5%).

Since the lift force acts in a more or less vertical direction it imposes dorsoventral bending on the wing spar. The magnitude of the bending moments will depend not only on the total lift force but also the distribution of lift along the wing. The lift distribution is aerodynamically significant because it affects the magnitude of the induced drag, a significant component of the total drag particularly in soaring flight. It has long been known from lifting line theory that for a simple planar wing the induced drag is minimum when the lift distribution is elliptical. However as will be discussed in Chapter 7, there is in practice an unavoidable interaction between the requirements for pitch stability and the lift distribution along the wing. For example, in conventional flying wing aircraft with posterior sweep, pitch stability is achieved by twisting the wing such that the angle of attack in the distal regions of the wing is reduced; so-called washout. In such a wing, lift distribution deviates greatly from the elliptical optimum and there is a significant induced drag penalty, which is the aerodynamic price of pitch stability. Alternatively in flying wing configurations with anterior sweep the wing must be twisted such that the angle of attack is increased towards the wingtips, again resulting in a sub-optimum lift distribution (and a structurally challenging geometry.) These considerations apply to man-made aircraft which are more or less aerodynamically stiff structures, at least within the safe flight envelopes. However the membrane wing of the pterosaur is inherently flexible and subject to rather different aerodynamic considerations. Most importantly, the membrane and the wing spar are sufficiently flexible that they will deflect significantly under the influence of aerodynamic loading and as is shown in Chapter 7 this flexibility may be beneficial to the extent that it enhances pitch stability whilst allowing an efficient lift distribution.

In addition to quantifying the induced drag efficiency and the pitch stability of the different wing configurations considered, the XFLR5 program also provides output in the form of the variation of lift coefficient along the wing. A typical example is shown in Figure 5.1. By combining this variation of the local lift coefficient with the local chord along the wing the variation of lift force could be calculated. The result is shown in Figure 5.2. This lift distribution was then used as input to the wing spar model described in Chapter 4, with the input values being generated from a seventh order polynomial curve that was fitted to the load distribution using the CurveExpert Pro program (http://www.curveexpert.net/products/curveexpert-professional/).

5.2 Lift magnitude

Two mass estimates were used, at the lower end of the range that by Bramwell & Whitfield (1974) and at the upper end the estimate using Witton's methodology (Witton 2008). Whilst the lift forces subject the wing spar to a dorsally directed bending moment this is offset to some extent by the mass of the wing which is directed in the opposite sense. Thus in order to obtain the actual bending moment the applied load is a lift minus the wing weight.

In the literature there are three papers that discuss the distribution of mass between the different body parts, Henderson (2010), Bramwell & Whitfield (1974), and Strang *et al.* (2009). Henderson gives a range of values which appear to centre around 20% for the wing mass, whereas Branwell & Whitfield (1974) give a figure of around 35%. Strang *et al.* (2009) calculate a value of 43%. Witton & Habib (2010) criticised Henderson's (2010) work for underestimating the muscle mass on the forelimbs so it seems probable that his mass allocation underestimates the wing proportion. Accordingly, a somewhat arbitrary figure of 40% was used, perhaps towards the high end of the likely range which means that the bending moments are if anything underestimates, which should be borne in mind in the interpretation that follows.

5.3 Wing spar dorsoventral deflection

With these reservations in mind Figure 5.3 presents the calculated wing deflection assuming that the wing spar behaves as if all the joints were rigid and that the proximal end is firmly fixed into the glenoid. This is of course not a very anatomically realistic assumption but is used here as a starting point for this analysis. On this basis it is immediately apparent that with the Witton (2008) mass estimate the deflection of the wingtip is just over 1m, in other words about one third of the span, which seems high, certainly when compared to birds. Since if all other things are equal the deflection is directly proportional to the mass then obviously the deflection for the Bramwell & Whitfield (1974) mass estimate is much less than for Witton (2008). On this basis then it would appear that the Witton (2008) mass estimate is too high.

5.4 Effect of proximal fixity

However as noted above, the assumption that the wing spar is a simple built-in beam attached to the glenoid is far from realistic. In reality the proximal bones at least as far distally as the wrist are surrounded by heavy musculature and constrained by tendons. Thus in structural terms this region of the wing is more akin to a stayed structure than a built-in beam and as such it is a very complex structure to analyse. As an extreme simplification that would bracket the plausible range of different geometries, modifications were made to the model such that the wing was made extremely stiff between the glenoid and the wrist and the glenoid and the end of the metacarpal. These assumptions are the equivalent of the animal being able to actively control the location of the wing bones distally as far as either the wrist or the distal end of the metacarpal, by applying tension to the appropriate controlling muscles and tendons. This would have the effect of changing the loading on the bones from bending to primarily compression, which might explain in part why the proximal bones are closer to circular in cross-section than those situated more distantly. In this case the tip deflection is substantially reduced to between 0.6 and 0.7 m depending on the extent of the assumed high stiffness region of the wing. Since it appears that the unloaded shape of the wing phalanxes is such that they have a degree of ventral curvature, the combination of the deflection and this curvature would mean that the actual elevation of the wing tip was quite small (Figure 5.4).

5.5 Material stresses and safety factors

When the structure is subjected to bending the deflection is obviously one important consideration but it is also important to understand the local stresses to which the structure is subjected. In order to do this the surface strain along the ventral side of the wing bones was calculated and compared to published values of the bending strength of bone. Using data from Currey (2004) a value for bending strength of 300MPa was selected as an appropriate upper limit for bone with a high Young's modulus of around 25 to 30GPa (see Figure 5.5). Using this value, the factor of safety (the ratio of the calculated stress to the maximum bending strength, or the likely ratio between the typical loading in life and the failure load of the material) was calculated. The results are shown in Figure 5.6, for a calculation which assumes the beam fixed at the glenoid. It is immediately apparent that the lowest factor of safety occurs in the ulna but for the reasons given above this simple model is inadequate and in fact the ulna will most likely not be subjected to significant bending load.

However regardless of the assumptions about the fixity of the proximal regions of the wing spar, from the end of the metacarpal the structure will be subjected to pure bending so these calculated safety factors are probably reasonable for that region. They show that in the mid shaft region of the first wing phalanx the safety factor drops to 2.5, which is very low for a natural structure subjected to dynamic loading (Palmer & Dyke 2010), particularly when bearing in mind that the bone structural parameters

used in the analysis are right at the upper end of the plausible range. A more likely factor of safety is somewhere between four and six, though given the somewhat extreme nature of the pterosaur structures it is likely that they operated towards the lower end of this range. Here again the value calculated using the Bramwell & Whitfield (1974) body mass methodology is very different and gives a factor of safety of just over five.

From the foregoing it would appear that on the basis of both wingtip deflection and more importantly the stresses in the wing bones, the combination of the Witton (2008) mass estimate and the optimal lift distribution calculated using the XFLR5 program is unlikely to have been a practical condition for the pterosaur. To understand the sensitivity of the results to assumptions about the lift distribution, the lift distribution was modelled as a simple linear variation from a maximum at the proximal end of the wing to zero at the wingtip: a triangular lift distribution and one which would not be unreasonable for a wing that generated a roughly constant lift coefficient along its length. This lift distribution would incur an induced drag penalty but result in reduced bending loads in the wing structure. The induced drag penalty would typically be around 10% to 15% of induced drag, which would in turn represent just 2% to 3% of total drag - not a very large increase. Adopting this assumption the deflection of the wingtip for simple "fixed at the glenoid" model reduced from just over a metre to 0.7m (23% of the wing length), which would reduce further in the more realistic case of high stiffness in the proximal wing bones. More tellingly this modification has the effect of reducing the surface stress and thus increasing the factor of safety to around 4.5, a low value but not an impossible one.

The foregoing analysis has used a mixture of relatively robust information, the overall bone dimensions obtained from CT scans and the properties of bone in combination with more speculative variables, the total body mass, the acceptable structural factors of safety and the patterns of load distribution. As such it cannot give a precise answer but it does strongly suggest that the Witton (2008) mass estimate is towards the upper end of what is possible for a bone structure.

5.6 Structural efficiency

It is also instructive to examine the distribution of the structural strength as compared to the pattern of loading since, for an optimal structure, these two are expected to be in correspondence. At the simple level of visual observation this is clearly the case for the pterosaur wing spar in that the humerus is much more robust than the more distal wing bones. However as Figure 5.7 shows this correspondence is actually close over the full extent of the wing. The graph shows the modulus of the wing bone sections (a proxy for the maximum surface stress) overlaid with the bending moment, scaled so that it fits on the same axes. Clearly the wing bones have local regions of very high modulus (and hence low stress) at their ends, but in the central region of the bone shafts the modulus closely follows the distribution of bending moment. Given that large pterosaurs were clearly highly adapted to the structural demands of flight it is

reassuring that the calculated bending moments appear to correspond so closely to the structural properties of the fossil bones, increasing confidence in the quality of this result

5.7 Summary

The wings of pterosaurs deflected substantially, maybe as much as 25% of the length of the wing, under both aerodynamic lift and membrane tension loads and the deflection was limited by the bending strain in the bones before it became sufficient to be aerodynamically detrimental.

The distribution of bending stiffness along the wing spar varies along its length. In the dorsoventral plane it closely follows the applied lift loading, pointing to a refined structure optimised for flight loads. Distally (from the first wing phalanx) the bending stiffness in the anteroposterior plane is as much as twice that dorsoventrally, a likely response to the need to resist high membrane tensile loads required to suppress aeroelastic flutter.

Chapter 6

Wing spar anteroposterior loading

The foregoing sections showed that the pterosaur wing spar has a biased stiffness distribution with greater dorsoventral stiffness in the proximal regions, presumably to limit the deflection of the wingtip, but this switches over to greater stiffness in the anterior posterior direction at the first wing phalanx, presumably to maintain adequate the tension in the membrane.

Can this result be used to infer information about the membrane?

6.1 Maximum membrane tension loading

One approach is to apply the membrane tension as a load in the wing spar model, bending the spar in the anterior posterior direction. The maximum load that the spar can withstand will be an indication of the maximum membrane tension assuming the parsimonious view that the wings bones will only be as strong as they need to be to withstand the flight loads. The simplest way to model this is to assume that the tension is uniform across the membrane and oriented in a mediolateral direction, as sketched in Figure 6.1. In this case, since the local wing chord is approximately 0.5m, the moment experienced by the bones that run more or less parallel with the loading direction (WP1 and Mc4) will be T x 0.5 x 0.25Nm (where T= tension per metre width of membrane.) Thus, for tensions of 500 and 100N/m respectively, the bending moment will be 62.5Nm and 125Nm. The minimum values of second moment of area in the anteroposterior direction are 7000mm^4 and 3000mm^4 for the WP1 and Mc4 respectively, and the half width of the sections are 14.7mm and 8.5mm. Consequently the maximum local stresses on the two bones will be 130MPa and 180MPa for a tension of 500N/m respectively, which gives safety factors of 2.3 and 1.7 (assuming a bending strength of 300MPa). These values are implausibly low, so if this assumed loading pattern is correct, the maximum membrane tension can only be 280N/m or less (to give safety factors of at least 3).

Closer inspection of the probable orientation of the aktinofibrils and the pressure distribution due to lift (concentrated towards the leading edge) suggests that a uniform tension distribution is actually unlikely. An alternative loading assumption is shown in Figure 6.2. It assumes that the load bearing aktinofibrils are attached to the three most distal wing phalanxes and are directed medially towards the elbow region, thus containing most of the tension within the "bow" of the wing anterior to a line between the elbow and the wing tip.

The calculations for this are more a little more complex than for the uniform load due to the direction of the loading. In theory it is possible that as the wing bones deflect under load, the applied

bending moments increase due to a change in the geometry of the aktinofibrils relative to the wing bones. If this is the case, the loading becomes extremely difficult to analyse since the result can only be determined by iteration or a full FEA type analysis. Fortunately, by inspection it became apparent that this effect was unlikely to be large. Comparison of the undeflected and possible deflected shapes of the wing spar showed that the geometry of the loading does not change if it is assumed that the aktinofibrils must remain more or less at constant distances from the wing bones (in other words that the membrane does not stretch significantly in the anteroposterior direction).

Using the estimates of bending moment described above, it is possible to make estimates of the maximum surface stress in the wing bones by examining the bending moment at the points of minimum second moment of area. These occur at roughly the mid length of the WP1, 75% of the length of WP2 and 67% of the length of WP3. The bending moments were calculated using the geometry in Figure 6.2 and taking the possibly conservative assumption that the tension is evenly distributed along the three distal-most bones, WP2, WP3 and WP4. (In fact in the case of WP4 this is almost certainly conservative since these bones taper to a very fine point at their extreme distal ends, so would probably bend excessively if the tension were applied evenly.) However, in the absence of a viable way to make a more refined estimate, the assumption of uniform distribution will tend to give a high value of the bending moment. The results of this analysis are presented in terms of bending stress safety factor in Table 6.1 below.

Table 6.1 Predicted membrane tension

Wing bone	Tension 500N/m	Tension 1000N/m
Mc4	8.8	4.4
WP1	11.9	5.9
WP2	5.8	2.9
WP3	9.3	4.6

It is apparent that at a tension of 500N/m the safety factors are in excess of 5 on all the bones, but drop to 2.9 and 4.6 in WP2 and WP3 respectively at 1,000N/m. Given the close correspondence between the dorsoventral loading and the structural strength of the wing spar demonstrated above, the low value in WP2 is possibly anomalous. But even if this is "averaged out" between WP1 and WP3, the result is still less than 5 in WP3, suggesting that the wing spar becomes maximally loaded as the membrane tension approaches 1,000N/m.

In summary then, the crude uniform tension distribution, an undoubtedly extreme load case suggests that the membrane tension could have been at least 300N/m and the more likely concentrated load distribution raises this to at least 500N/m, maybe as much as 1,000N/m.

Is this level of tension adequate to control the possible flutter in the membrane, which is important since a fluttering membrane increases drag dramatically (Morris-Thomas & Steen 2009).

6.2 Flutter limits to membrane tension

The fluttering of membranes is a very complex phenomena and none of the sources on the fluttering of flags (such as Morris-Thomas & Steen 2009) provided results from which the necessary tension could be calculated. However, tests conducted by the newspaper industry (Watanabe 2002) proved to be a suitable source. It appears that the industry has considerable problems with large rolls of paper running fast through machines: if the paper starts to flutter it tangles up and a whole production line comes to a halt, with severe commercial consequences. They have therefore looked at how thin membranes behave under these conditions. Figure 6.3 shows a typical test rig in one of a series of experiments.

The results of a large number of tests with many different membrane materials were condensed down to one graph (Figure 6.4), which has a clearly defined boundary between conditions where there is flutter and where there is no flutter. The equation defining that line is:

$U_w=4(m/\rho d)^{-1/3}(Td^2/EI)^{1/3}(EI/\rho d^3)^{1/2}$

Where:

U_w=flutter airspeed

M=membrane mass per unit area

ρ=air density

D=unsupported span of membrane (in direction normal to air flow)

T=membrane Tension per unit length

EI=bending stiffness per unit width

E=Young's modulus of membrane material

I=second moment of area per unit width

This equation can be transposed to give the following relationship for the required tension:

$T=0.0156U_w^3\rho^{1/2}d^{3/2}m(EI)^{-1/2}$

What does this say about the conditions that influence flutter?

For practical purposes, the air density ρ is constant and I is proportional to the membrane thickness, t^3. Thus the formula can be further reduced to:

$T \propto U^3d^{3/2}m/(E^{1/2}t^{3/2})$

This relationship shows that speed is very important - it is a cubic relationship, the span of the membrane is somewhat less important and the tension is directly proportional to the mass per unit area,

so a light membrane is better. Conversely, the stiffer the membrane material (the higher the value of E) the lower the tension required, and more importantly, the greater the thickness the lower the tension. At constant material density, the requirement for minimising mass per unit area and maximising thickness are therefore apparently in direct conflict.

If the membrane material density is assumed to be more or less constant, the mass per unit area, m will be proportional only to the membrane thickness, so the relationship can be further simplified to become:

$$T \propto U^3 d^{3/2} / (Et)^{1/2}$$

This implies that for any given membrane span, the tension is minimised by high modulus and thickness, since the proportionality of t in the denominator in the first equation above is greater than in the numerator, so the effect of thickness on stiffness is more important than its effect on mass per unit area.

Using the above equations the wing membrane was modelled in a variety of different possible materials. First a membrane with the same properties as extant bat wing membrane (taking the maximum values in Swartz *et al.* 1996), gives a Young's modulus of 0.05GPa. The result is shown in Figure 6.5. In order to give results that were roughly in line with the requirements for flight speed and membrane tension, it was necessary to assume a membrane thickness of 4mm in this case. (It should be noted that this thickness would result in a membrane weight of 13kg, around a third of the likely total weight of the animal and therefore somewhat unlikely.) Next a membrane which is notionally heavily reinforced with ligament type material, giving it a significantly higher Young's modulus - assumed to be 0.2GPa was modelled. (The modulus of ligament is in the range 0.2 to 0.8GPa (Ashby *et al.* 1995) so this is notionally a membrane comprising at least 25% ligament in a matrix of much lower modulus soft tissue). Finally, a high tensile membrane material assumed to comprise a matrix of skin-like soft tissue and embedded fibres (aktinofibrils) made from nature's highest modulus material, keratin, was modelled. The maximum modulus of keratin is 5GPa (Ashby *et al.* 1995) and if it is assumed that the fibres comprise from 20% to 40% of the membrane (the latter being a much higher figure than implied by the membrane descriptions in the literature) the combined Young's modulus will be 1.0GPa to 2.0GPa.

Comparing the likely membrane tension that is implied by the previous analysis, in the range of 750 to 1,000N per metre, it is apparent that when the membrane is made of 4mm thick bat wing tissue, flutter starts at a flight speed of just 12m/s. Given that for this animal the likely stall speed is around 9m/s, this is a very narrow flight envelope indeed and seems very unlikely. Even with a ligament reinforced membrane of the same thickness, the speed range is only increased to a maximum speed of 14 to 15m/s and it is only with keratin reinforcement properties that a wide range of flight speeds becomes possible.

As noted earlier, a 4mm thick membrane would weigh around 13kg, a very high fraction of the total weight, and thus unlikely. Figure 6.6 shows the effect of membrane thickness variation at flight

speeds of 10m/s and 14m/s (for only the ligament and keratin reinforcement assumptions.) In the case of the ligament reinforcing at a thickness of around 2.5mm is required to achieve a maximum flight speed of 14m/s. However, in the case of the keratin reinforced membrane, the thickness can be reduced to 0.5mm to achieve the same flight envelope.

Overall, this analysis, which admittedly relies on many assumptions and approximations, suggests that for flutter stability the wing membrane must be reinforced with high modulus fibres, and that without such reinforcement the membrane would have to be excessively thick, with associated weight penalties. This provides support of the view that the aktinofibrils were made from keratin (Bennett 2000).

6.3 Membrane strain and deformation

So far this analysis has only considered the applied tension loading, but in an elastic material load results in extension or strain and in the case of a membrane wing, high strain results in a membrane that rapidly balloons out of shape. So not only must the membrane not exceed its tensile strength limits but the strains must be relatively low in order to control the shape of the membrane.

Here the interpretation becomes more subjective, but the basic calculations required to estimate the effects are straightforward. The effect of extension on the membrane curvature can readily be determined by comparing the length of a circular arc to that of a straight line joining the ends of the arc. The results (Figure 6.7) shows a strain of just 10% produces considerable curvature or camber (camber is the ratio of the displacement to the span of the membrane) of 5 to 1. The strains need to be less than 2% or less to keep the camber below 10 and approaching 20. Subjectively, based on observations of sails and flexible wing aircraft (Pers. obs, Polhamus & Naeseth 1963, Kroo 1981, Marchaj 1996) the camber will have been needed to be between 10:1 and 20:1 (which requires strains of less than 2%).

Using the membrane properties derived for the flutter analysis it is possible to calculate the membrane strains that result from the tensile loading. The results in Table 6.2 show that for the bat membrane the strains are 50% to 100% at 4mm and 2mm thickness respectively, which would clearly result in totally excessive deformation of the membrane. With the ligament reinforcing the strains are still high at 25% for the 2 mm thick membrane. Only with the keratin reinforced membrane were the strains limited to the 1% - 2% range which is needed to control the spanwise camber.

Table 6.2 Variation of membrane strain with composition and thickness

Membrane tissue	Strain at 4mm thickness	Strain at 2mm thickness
0.02GPa bat	50%	100%
0.2GPa ligament	12%	25%
2.0GPA keratin	1%	2%

As an alternative approach to determining the effect of membrane properties and loading, the tensile loads induced in a membrane due to the aerodynamic pressure load were estimated. Under such loading, the tension is directly related to the camber - for the membrane to have low curvature it has to have high tension. The tension is related to the lift forces, and thus the mass of the animal and the tension was calculated using a result for thin walled pressure vessels (Young & Budynas 2002).

Figure 6.8 summaries the results. The diagonal shaded band is the variation of membrane tension with camber ratio for the likely range of weight estimates for the animal. To achieve a camber ratio of 20:1 it is necessary to have a tension of 500 to 750N/m, and 750 to 1000N/m for 30:1.

6.4 Summary

The membrane tension is large compared to lift loads. It acts more or less parallel to the wing spar, with the majority of the tension balanced within the length of the wing spar between the elbow and wing tip, a structural geometry that minimises the bending moments and allows the wing to have high tension regions in the distal part and lower tensions more medially. Membrane tension values obtained from flutter analysis and membrane curvature considerations all appear to converge on a tension of around 500 to 1000N/m, which corresponds with the wing bone strength. Values of this magnitude point to a membrane with very different properties from that of extant bats. It needed to be extensively reinforced, to bring the tensile modulus up to values only achievable with high modulus, keratinous tissue, which sheds new light on the likely nature of the aktinofibrils.

Chapter 7

Morphological constraints

7.1 Mechanical and aerodynamic constraints

There are a number of physical conditions that can be used to infer the constraints on the wing morphology of pterosaurs. These conditions do not so much say what the morphology was, but more what or how it could not have been. As such, when they are applied together they can be used to constrain the shape within quite tight boundaries. The conditions used will be:

Static balance in steady flight

Wing bone limiting strain under loading from membrane tension

Free margin behaviour

Aerodynamic efficiency

Static stability

7.1.1 Static balance: the requirement for coincidence of Centre of Mass (CM) and Centre of Pressure (CP)

For steady flight in any system, the CM of the body and the CP of the aerodynamic forces must be coincident so there are no applied moments and the total aerodynamic force (the resultant of lift and drag) and total weight are equal and opposite in order to satisfy Newton's third law of motion. (Figure 7.1).

7.1.2 Surface strain on wing bones

Structures deflect under load and their failure is the result of interactions between the material properties and geometry. The distal wing bones of pterosaurs were slender, thin-walled beams and thus might fail by either section buckling or rupture as local strain exceeds the yield strain of the material. However, as was discussed in Chapter 4, it appears unlikely that pterosaur long bones failed in buckling, despite their thin walls.

Thus, for the purposes of a structural threshold of a pterosaur wing bone, what matters is the point at which surface strain exceeds a limiting tensile strain (since in bone the tensile strength is less than the compressive strength). Because strain is a geometric quantity, it can be used to define the limiting

deflection of the wing bones and can be used to make predictions about the likely deflected shape of bones under load.

7.1.3 Shape of the free margin

The margin of the pterosaur wing membrane was unconstrained posteriorly and attached distally to the ankle and body (Elgin *et al.* 2010, Kellner *et al.* 2010). Under flight loads the membrane will deflect and experience tension. It must not flutter as this creates high levels of drag, so it must have a shape that is everywhere in tension. This has a direct bearing on the shape of the free edge.

7.1.4 Aerodynamic efficiency and induced drag

For sustained, unpowered flight, one measure of aerodynamic efficiency is the ratio of lift to drag. Since lift is fixed and equal (to a first order) to an animal's body weight, drag must be minimised to achieve the highest lift:drag ratio and thus maximum aerodynamic efficiency (Azuma 2006:50). Strictly speaking, although maximising lift:drag ratio will maximise flight range, for some birds (and perhaps some pterosaurs) flight endurance appears to be a more important parameter. This is maximised by flying at the lowest descent (sink) speed, which does not coincide exactly with the maximum lift:drag ratio. However, in practice it is generally the case that increases in lift:drag ratio tend also to reduce sink rates, so low drag matters.

7.1.5 Static stability

While the most basic requirement for steady flight is that the aerodynamic resultant and weight are equal and opposite, any configuration must also be such that if its flight path is disturbed the animal (or airplane) can return to a stable condition. The most demanding stability requirement is in pitch (i.e. rotation in the sagittal plane) because an animal's mass moment of inertia is much less for this axis than for yaw and roll (the other axes in which stability is important) and so response rates have to be much faster. Pitch stability is determined by the interaction of aerodynamic and weight forces and depends on how they move relative to one another under the influence of changes in the airflow over the wing. For example, if a wing encounters a gust that increases the angle of attack on its wings, the transient aerodynamic resultant increases in magnitude and may move anteroposteriorly, the magnitude and direction of the movement being related to the local wing section.

For a simple cambered wing section, this movement is anterior (Katz & Plotkin 2001:113), inducing a nose-up pitch rotation which increases the angle of attack still further and is thus destabilising (Figure 1.11). Returning to an original flight path under these conditions can only be achieved by active control, which requires very rapid reaction times and precise manipulation of control surfaces. Such 'active stability' can be provided by computer control in specialised, agile aircraft but it remains unclear whether, or not, it can be achieved by flying animals. The alternative, passive pitch stability, has been shown to be

likely in large birds (Krus 1997, Thomas & Taylor 2001) and may confer energetic advantages as it reduces muscular and neurological activity in flight.

If we assume that large pterosaurs were also statically stable in pitch (a likely assumption), their wing characteristics must be such that not only must CP coincide with CM in a static sense, but when the incident flow direction changes, CP must also move in a direction to stabilise flight. In aircraft this is achieved in two ways, either by fitting stabilisers on the end of a long tail behind the main wing (or ahead of the wing in the case of a canard configuration) or by adopting specific wing geometries in the case of flying wings. There are some wing sections, so called reflex sections, that do not generate nose up pitching moments, which can be used on flying wings. Alternatively, or in addition, the combination of wing sweep and wing twist (in which the posterior edge in the distal regions of the wings are twisted dorsally) or anterior sweep and the opposite twist will provide static stability, at the unavoidable cost of reduced aerodynamic efficiency. Hoerner (1985:Chapter XI) provides a comprehensive introduction to the physics of static stability. Since pterosaurs most probably had cambered rather than reflex wing sections, they must have secured static stability from some combination of wing section properties, wing sweep and twist.

7.2 Centre of mass calculations for static balance

Bramwell & Whitfield (1974) made estimates of the mass and centre of mass (CM) locations for a 6.95 m wingspan specimen of *Pteranodon*. They used a slicing method for the body and neck and made individual mass estimates for the head, arms and legs. The total mass estimated was 16.6kg, which is considered low by present workers (Witton 2009, Henderson 2010). Bramwell & Whitfield (1974) also concluded that the CM was 6.3 cm posterior to the glenoid cavity, which in non-dimensional terms is 0.9% of the wingspan. Unfortunately, they did not provide sufficient details of how they made their calculations for it to be possible to reproduce their result.

In order to establish independent values for the CM, new estimates were made as follows.

Strang *et al.* (2009) provide mass estimates for the individual regions of the wing (bone-by-bone) and these data were used to estimate the longitudinal and transverse locations of the wing CM in the position used by Henderson (2010). This wing geometry was used as the starting point for the analysis of relative CM and CP locations.

Henderson (2010) also provided estimates of the total mass and CM as well as the mass and CM of body parts for the large pterodactyloid pterosaurs *Anhanguera santanae* and *Pteranodon ingens*. Strang *et al.* (2009) provide a mass estimate (but no CM) for *Anhanguera piscator.* These results are summarized along with those of Bramwell & Whitfield (1974) in Table 7.1.

The CM of *Anhanguera* was estimated in two different ways. First, the body part CM locations given by Henderson (2010) were applied to the weight fractions given by Strang *et al.* (2009). Secondly, CM

locations were estimated from the original reconstruction, using the following assumptions. The head was treated as a cone, so the CM was located at 33% of its length. The neck was assumed to be of constant cross section and the body to be comprised of two opposing cones, attached to a conical hip region. It was assumed that the majority of the mass (bone + soft tissue) of the legs was concentrated around the upper regions.

Table 7.1 Mass of body parts: % total

	B&W	Henderson	Strang
Head	5.2	12.0	6.1
Neck	4.9	4.0	6.1
Body	52.4	55.0	36.3
Legs	5.0	5.0	7.9
Wings	32.5	24.0	43.6

The CM of *Pteranodon* was estimated using the body part CM locations given by Henderson (2010), (having noted that his reconstruction was in exact register with that of Bennett (2001)). These body part CM locations were applied to the different mass allocations provided by Bramwell & Whitfield (1974) and Henderson (2010).

These approaches gave CM locations ranging from 1.03% of wingspan anterior to the glenoid to 0.44% posterior to the glenoid (Table 7.2).

Table 7.2 Estimates for locations of the CM

Species	Mass allocation	Reconstruction	CM % span
Pteranodon	B&W low	Henderson/Bennett	-0.17
	B&W medium	Henderson/Bennett	-0.33
	B&W high	Henderson/Bennett	-0.44
	Henderson	Henderson/Bennett	0.35
Anhanguera	Strang	Kellner & Tomida	-0.11
	Strang	Henderson	-0.22
	Henderson	Henderson	1.03

As noted above, these CM locations are calculated with the wing in the position shown by Henderson (2010). The aerodynamic centre of pressure (CP) for this wing geometry was calculated using XFLR5 program. The location was 2.3% of wingspan posterior to the glenoid, indicating a state of aerodynamic imbalance. To achieve balance the wing needed to move anteriorly – to have anterior sweep.

Accordingly, the wing was then morphed to give 200, 400, 600 and 700 mm anterior sweep. The CP locations were -1.4%, -0.05%, 1.5% and 2.21% respectively.

Since the wings are a significant proportion of the total mass, anterior sweep will also result in an anterior movement of the CM. This effect was calculated for the reconstructions listed in Table 7.2.

The variation of CM and CP locations with wing sweep were then compared (Figure 7.2). The Strang *et al.* (2009) based estimates indicated a more posterior CM location in the baseline case, but more rapid anterior movement of the CM with anterior sweep due to the higher wing mass fraction. In contrast, the Henderson (2010) based estimates started with a more anterior CM location, but the rate of movement with sweep was less due to the lower wing mass fraction. The overall result was that for all the different estimates, the CM and CP locations became coincident with the anterior sweep in the 600 and 800 mm range. The resulting wing shape has more than 10° of anterior sweep (Figure 7.3).

From this result it is apparent that the CM and CP locations are not coincident in many of the wing shape reconstructions currently in the literature, in other words pterosaur wings had more anterior sweep than is shown in almost all modern reconstructions. Interestingly, the relatively early reconstruction produced in Bramwell & Whitfield (1974) is very close to being balanced according to this analysis. In particular, this approach clearly demonstrates the implausibility of shapes with high posterior sweep (e.g. Witton 2009) because they would be aerodynamically unbalanced.

7.3 Shape of free margin

The wing membrane did have some internal structures: one (Bennett 2000, Padian & Rayner 1993) or possibly more (Kellner *et al.* 2010) layers of 'aktinofibrils' - fibres with a higher modulus of elasticity than the surrounding tissue. The recent fossil evidence indicates that these fibres were of a diameter comparable to human hair (circa 0.1mm) and were probably comprised of a collagenous or keratinous tissue (Bennett 2000, Kellner *et al.* 2010). These fibres would have increased the in-plane tensile strength of the membrane but in view of the thinness of the membrane (<1mm) (Kellner *et al.* 2010), they would have contributed very little to its bending or compressive strength even if they had been arranged in two layers on opposite faces (a configuration for which there is no fossil evidence but which would be mechanically the one to give the greatest out of plane bending stiffness).

A thin membrane with no significant out-of-plane bending stiffness can only be constrained from instability by in-plane tension, which is unavoidably absent in a region with a convex margin (Jackson & Christiet 1986) unless it is supported by stiffening structures capable of resisting bending and compressive loads, like the batten stiffened regions of yacht sails and hang-glider wings (Figure 7.4). This universal requirement for a concave margin to maintain membrane tension is apparent from examination of man-made structures like tents and sails that lack battens, as well as the membranes of bats that use extended fingers to stabilise and support their wing membranes, yet have a very marked concave membrane margin

between the fingers (Norbert 2002, Norbert *et al.* 2003) and Figure 7.4. Following this line of reasoning, reconstructing a convex wing margin for pterosaurs must be incorrect: without in-plane battens, the membrane would have flapped uncontrollably, greatly increasing the drag (Morris-Thomas & Steen 2009) and destroying the shape required for flight.

A possible solution to the problem of membrane instability is the suggestion that pterosaurs may have possessed a tendon that ran along the posterior margin of the wing (Pennycuick 1988). When tensioned, this tendon could have stabilised the free margin, allowing an almost straight (but still necessarily concave) edge. However, fossil evidence for such a tendon is equivocal, and non-existent in larger species where preserved membranes are unknown, and mechanically it was unlikely to have been present. In order to be effective at stabilising the membrane edge, a tendon would have had to have been under considerable tension to balance the chord-wise (anteroposterior) tension of the wing membrane. Such loading geometry would subject the wing bones to substantially greater bending loads than if the membrane tension was primarily subparallel to the wing bones (i.e. spanwise). Sneyd *et al.* (1982) estimated that chordwise membrane tension, reacted by a supporting tendon, would have increased bending moments in the wing bones by a factor approximately equal to the aspect ratio of the wing: a factor of more than 10 in a typical ornithocheirid pterosaur. Bramwell & Whitfield (1974), calculated a slightly lower difference factor of 6 for *Pteranodon*, which they estimated to be structurally unsustainable. Simple mechanics (as well as anatomical parsimony) thus imply that spanwise tension, with no requirement for a tendon, was more likely the case in pterosaur wings. Lastly, the argument is also supported by the position of the aktinofibrils which, when preserved, are orientated to produce anisotropic membrane properties that would have resisted spanwise tension (Bennett 2000, Padian & Rayner 1993). As Bramwell & Whitfield (1974) show, if the membrane were supported by a trailing edge tendon the primary direction of the membrane tension would have been chordwise, completely contrary to the orientation of the aktinofibrils and therefore very unlikely.

7.4 Wing planform and pitch stability

7.4.1 The effect of wing shape on flight efficiency

As noted earlier, aerodynamic theory and experimental data have shown that induced drag is primarily determined by aspect ratio (slenderness) and planform shape (especially the degree of wing taper), although wing tip shape and distribution of twist along the wing can also be important (Anderson 2007:435). Theoretical studies (Anderson 2007:411) have shown that to minimise induced drag, the lift distribution along a wing must be elliptical, but in practice, a simple prismatic wing with 50% taper is very nearly as efficient as this ideal wing (Figure 3.2). However, as taper increases further it rapidly becomes more and more detrimental to performance (Marchaj 1988:420). A highly tapered wing not only has high induced drag but is also prone to tip stall (early stalling of the wing tips relative to the more proximal

regions of the wing) (Marchaj 1988: 430), which is detrimental to control during low speed flight. These simple parameters have been used before to explain the relatively conserved range of wing shapes found amongst flying animals (Rayner 1988) and because some wing shapes work better than others under certain conditions, predictive methods can be used to inform choices between competing wing reconstructions, especially in extinct vertebrates.

To examine the effect of shape variation in more detail, an appropriate computational method is required. The XFLR5 implementation of the Vortex Lattice Method (see Chapter 3 for the justification for using this program) was used for the investigation. A typical input screen for the program is shown in Figure 7.5, illustrating the range of parameters that can be investigated and Figures 7.6 to 7.8 illustrate the range of graphical output available.

The range of shapes evaluated is shown in Figure 7.9. The shapes to the left (columns A and B) in Figure 7.9 were taken from published sources (Bramwell & Whitfield 1974, Bennett 2001, Unwin 2005, Witton 2008 and Wilkinson 2008), with the exception of the "Lunate" shape, which is discussed below. The shapes to the right in Figure 7.9 are a set of variations on the shape in Bennett (2007): all of very similar aspect ratio, but differing in taper, sweep, wing bone curvature and body length.

The relative performance of the different shapes is compared in two ways. First the induced drag was compared with the induced drag of an ideal elliptical wing of the same aspect ratio, to yield a ratio (the "e-ratio") related to the well known span efficiency "e". This ratio is a measure of the aerodynamic efficiency of the shape of the wing, corrected for aspect ratio. These results are shown in the left hand column for each set of morphologies. The shapes were also compared on the basis of a direct comparison of the increase in induced drag coefficient (% increase) shown in the right hand column.

As is to be expected, the aspect ratio of the shapes has a strong influence. The Witton 3 (azhdarchid) shape produced almost twice the induced drag (93.6% increase) of the best shape (Bennett 2007). In part this increase is due to the difference in aspect ratio (8.2 compared to 14.5) but it is also to a less efficient shape (e ratio = 11.6% as compared to 2.3% for the best shape, again Bennett 2007). The ranking on the basis of e ratio shows that the highly tapered Witton 2 and Wilkinson (2007) and (2008) shapes are amongst the least efficient, while the forward swept Bramwell & Whitfield (1974) shapes and the lunate shape are amongst the best. The presence of the Rhamph 1 form near the bottom of the scale may at first appear inconsistent since it is superficially similar to the Bennett (2007) shape. However, the XFLR5 analysis allows interrogation of the supporting calculations of the induced drag (Figure 7.10). These graphs compare the underlying characteristics of the Bennett ornithocheirid and Witton rhamphorhynchoid shapes with an ideal elliptical shape. The most striking difference is in the proximal region, where the induced drag coefficients of both pterosaur forms are much higher than for the elliptical shape, due to the posterior extension of the membrane to the ankle. This is more marked for the rhamphorhynchoid shape and accounts for most of the increase in the induced drag of this shape. The aerodynamic penalty of this posterior extension of the proximal region of the wing membrane also has a

negative effect on the performance of the azhdarchid and rhamphorhynchoid shapes proposed by Witton (2008) and Unwin (2005) respectively.

Since these forms do not represent a systematic range of variations, but reconstructions taken from a number of disparate sources, it is difficult to draw detailed conclusions from these results. In order to better understand the effect of changing morphology, the Bennett (2007) shape was taken as a basis from which a range of related, varied shapes were derived (Figure 7.9 - columns (C) and (D)). The form with the most efficient shape is the basic shape modified to have a concave posterior margin and modest posterior sweep. It is just 1.5% less efficient than the elliptical ideal. With less sweep the efficiency reduces very slightly. Anterior sweep of the wing results in a 5.3% reduction in efficiency, almost the same as the basic shape with an anteriorly projecting propatagium, the shape that corresponds to an anterior pteroid orientation (Wilkinson 2008). The least efficient shapes in this series were forms with a 50% increase in proximal width (a relatively longer body) and a highly tapered form with large sweep and a straight taper.

7.4.2 Lunate planform

The pterosaur wing has an obligatory highly tapered planform due to the basic structure of the wing bones and membrane. While there is some evidence (Bennett 2000) of preserved wings having a small, finite width at the tip, the extent is such that the overall wing is still highly tapered (pointed) in an aerodynamic sense. The shape is well into the range where it will exhibit a high induced drag due to the degree of taper (Anderson 2007:420). There is however a feasible geometry that may have mitigated this disadvantage - a lunate or doubly-elliptical crescent shaped planform found widely in fast swimming marine creatures (Figure 7.11) and in many bats (Norbert 2002, Norbert *et al.* 2003) and some birds (Videler 2005). It was first noted in the context of possible pterosaur wing morphology by Hazlehurst & Rayner (1992). As Hazlehurst & Rayner (1992) observed, this geometry both reduces the tendency to tip stall and lowers the induced drag, observations that have been reinforced by more recent research, which has also shown that 'lunate' curvature can be concentrated towards the tip of the wing and still be effective (van Dam 1987, Burkett 1989, Marchaj 1996:95 and 208).

The same XFLR aerodynamic modelling approach as described earlier was used to calculate variations in lift along the span of the wing, in order to analyse the likelihood of tip stall. Comparison between a triangular, tapered wing and the same basic shape but with the distal regions curved anteriorly to give a lunate shape were made. In the proximal regions, lift distribution was more or less identical for the two geometries, but in the distal tip regions lift distributions deviated significantly from each other with the triangular shape showing an increasing lift coefficient right to the tip. In contrast, the lunate shape exhibited a maximum lift coefficient followed by significant reduction towards the tip (Figure 7.12), confirming that it would be less prone to excessive lift coefficients and thus local stall propagating from the tip. This analysis was then extended to more pterosaur-like wing morphologies and further confirmed the benefits of the lunate tip in reducing the propensity for tip stall (Figure 7.13).

7.4.3 Anterior sweep effects

Next the effect of anterior sweep on induced drag was investigated using the XFLR5 program. With a plain untwisted wing the span efficiency reduced with increasing anterior sweep, suggesting that while an anteriorly swept planform may be required for aerodynamic balance, it is disadvantageous in terms of the induced drag ((a) to (c) in Figure 7.14). Another variation (Figure 7.14 (d)) was investigated which represented an anteriorly swept wing where the relatively more elastic proximal regions of the membrane (the cruropatagium between the legs and the membrane that might have been controlled by leg movement Kellner *et al.* 2009) was held at a different angle to the rest of the wing. Consequently the wing sections in this region had reflex - a local reversal in the section camber towards the posterior margin. With this reflex applied to the most proximal one third of the wing, the span efficiency approached a value of one, the highest that is theoretically possible for a planar wing (Figure 7.14).

7.4.4 Leading edge shape

Calculations of surface strain were used to estimate the bending deflection of pterosaur wing bones (Figure 7.15). While actual wing bone loading cannot be estimated, the possible maximum bone curvature can be calculated on the basis of acceptable maximum strain (Figure 7.15). Using a yield strain of 0.0075 (the upper limit for bone with a Young's modulus of 25GPa, Currey (2004)) and a safety factor of 3 (Kirkpatrick 1994, Palmer & Dyke 2010), the calculated average deflections are 8° for the first and second wing phalanges (WP1 and WP2), 10° for WP3, and 12° for WP4. It is also apparent from many fossil specimens (Lu & Ji 2005, Lu *et al.* 2006b, Andres & Ji 2008, Stecher 2008, Kellner *et al.* 2009, Lu *et al.* 2010, Lu 2010, Wang *et al.* 2010, Dalla Vecchio 2013) that WP4 frequently had natural curvature, typically around 15°. These bone deflections (assuming no flexibility in the interphalangal joints) were applied to Bennett's 2007 reconstruction of *Anhanguera santanae* (which was in turn modified from Bennett (2001)) and also to Wilkinson's (2008) reconstruction. The result produced wings with increased posterior sweep, the opposite direction to that required for aerodynamic balance. However, anatomical reconstruction of bone and joint geometry inevitably contains some imprecision (C. Bennett pers. comm. 2010) and it is known (Bennett 2001, Kellner *et al.* 2014) that the pterosaur elbow joint could flex through a large angle.

A 5° change in the angle of the humeroulnar joint and at the wrist results in moderate anterior sweep: if this is combined with a 10° flexure of the elbow then the forward sweep of the wing can be sufficient to provide aerodynamic balance. An anteriorly swept wing configuration is thus perfectly possible within the bounds of known pterosaur anatomy (Figure 7.16).

7.4.5 Static stability

The movement of CP with increasing angle of attack depends on the wing section and the wing geometry but, as noted earlier, this typically moves in an anterior direction with increasing angle of attack

for cambered wing section shapes, which is destabilising in pitch. As angle of attack increases so does the lift coefficient and XFLR5 allows the variation of CP location with lift coefficient to be determined as lift coefficient varies (Figure 7.17). This was first calculated for a rigid wing with posterior sweep and the analysis conducted for a range of values of distal wing twist (washout). As washout increased the curves moved bodily in an anterior direction, but also showed a change in the gradient such that by 15 degrees of washout the wing became statically stable in pitch - the centre of pressure moved posteriorly as lift increased. The effect of the washout is to change the lift distribution along the wing, which causes an increase in the induced drag. At 15 degrees twist the span efficiency drops by 15% (Figure 7.18), resulting in an increase in induced drag of 15%, which under soaring conditions could represent as much as 10% increase in total drag.

However, in response to an increase in lift (resulting, for example, from encountering a gust) the natural flexibility of the wing would in practice cause it to deflect due to changing loading, with the wing bones deflecting dorsally and also twisting along their length. This is because the applied lift force is posterior to the structural neutral axis of the wing bones. In consequence, the wing sections would experience twist along the length of the wing such that the posterior margin would rise relative to the leading edge, resulting in washout. To model this, the aerodynamic analysis was made for two wash-out configurations: 2.5° and 5° washout at the wing tip with on wings with anterior and posterior wing sweep. Variation of CP location with lift coefficient ran almost parallel to that for the rigid wing but was displaced in a posterior direction for the anterior sweep and the anterior direction for the posterior sweep (Figure 7.19).

This observation is relevant because of the situation where a flexible, anteriorly swept, wing experiences a gust the overall lift coefficient will increase but the twisting of the wing will off-load the distal regions so the total increase is likely to be less than for a rigid wing. Also, since for any given lift coefficient the location of the CP is shifted posteriorly with increasing washout, instead of CP moving anteriorly with increasing lift coefficient (along a line of constant wing twist), if the response is correctly tuned, it may move posteriorly, conferring passive pitch stability (Figure 7.19). The precise nature of the effect will of course depend on the flexural response of the wing and the determination of this is beyond the scope of this work. However, the fact remains that the above is a possible mechanism by which passive static pitch stability might be achieved as a result of the natural flexibility of the wing. This possibility, that wing flexibility actually can provide pitch stability, was first proposed by Sneyd *et al.* (1982).

This current application of vortex lattice code shows that it is possible to investigate the likely effect and to confirm a possible mechanism. It is also well worth noting that the opposite effect is true for a posteriorly swept wing – wing flexibility reduces pitch stability, casting doubt on the applicability of stability analysis based on aeronautical flying wing experience (which are for practical purposes rigid wings) and reported in Wilkinson (2008).

7.5 Summary

By their very nature, pterosaur wings were tapered mediolaterally and consideration of the requirement for the membrane to be everywhere in tension means that the posterior, free margin was concave. Membrane tension is required in order to suppress aeroelastic flutter and consideration of the structural strength of the wing bones indicates that the tension was directed mediolaterally, following the orientation of the aktinofibrils and confirming their role as structural reinforcing fibres.

While basic aerodynamic analyses show that highly tapered, straight wings (with a triangular planform) generate high levels of induced drag and are prone to tip stall, more sophisticated analysis using a vortex lattice approach shows that lunate shapes, which combine taper to a sharp, pointed tip with a concave posterior margin and moderate posterior curvature can actually be as efficient as shapes that are close to the so-called ideal elliptical shape. Lunate shapes also induce lower lift coefficients towards the tip, so are less vulnerable to tip stall. Analysis of the possible surface strain on the wing bones loaded by the membrane tension show that the distal bones are subject to substantial deflection and as a result allow the wing to take up a lunate shape, suggesting that in practice pterosaur wings could be aerodynamically efficient despite the obligate taper to the membrane shape.

The vortex lattice modelling also shows that reduction in body length:arm length ratio is doubly beneficial. It increases aspect ratio and reduces the adverse effects of the wide proximal regions of the membrane. Consequently the ornithocheirid bauplan was superior to the rhamphorinchoid (and azhdarchid) in terms of induced drag and thus aerodynamic efficiency, supporting the view that the former were open ocean foragers, very reliant on sustained soaring flight. For similar aerodynamic reasons, a wing with an anteriorly projecting pteroid and a very wide propatagium has a reduced aerodynamic efficiency, although this effect can be reduced if the proximal wing sections are reflexed, a shape that might have been achieved by appropriate flexing of the legs.

The basic mechanical need for the CM and CP to be coincident in steady flight imposes limits to the relative positions of wings and body and points to a requirement for anterior wing sweep. This requires an anterior centre of mass - which might explain long necks.

For passive pitch stability in the absence of a tail, posteriorly swept wings require wash-out, which greatly reduces the aerodynamic efficiency, typically resulting in a 18% induced drag penalty. In contrast, anterior sweep and wing tip twist results in a small efficiency loss (about 5%), but confers pitch stability provided that the wings are flexible and responsive to gust input.

This examination of the various constraints on wing reconstruction provides predictions for actual wing shape reflecting the mechanical and physiological demands of flight, which place a great premium on aerodynamic and structural (weight) efficiency. If these were the significant evolutionary drivers then the foregoing provides many new insights into pterosaur wing performance and morphology.

Chapter Eight

Limits to size

8.1 Effects of scaling

The maximum possible size of animals has long been a source of fascination for scientists and the wider pubic alike. Giants abound in folk-lore and gigantism is a much debated topic of biology and palaeontology. A typical example of the latter is Alexander (1998), entitled *"All time giants: the largest animals and their problems"*. The subtitle is revealing in suggesting that giant animals face problems, which, by inference, ultimately limit their potential size. As Alexander (1985, 1998) and others have shown, these problems are a direct result of scaling effects, which influence the effects of size in all animals and indeed man-made structures (see Liu 2006 for a comprehensive overview).

It is also important to bear in mind that animal size is clearly a response to adaptive, complex and multifaceted evolutionary pressures (Biewener 2005, Sander *et al.* 2011, Habib 2013) and so even if a particular body plan has the potential for large size, for evolutionary reasons there is no absolute requirement that real animals will actually grow to that size. However, estimating the maximum potential sizes so as to place limits on what was possible and determine whether giants were constrained by mechanical or other limits can provide useful evolutionary and functional insights

The questions to be addressed herein are, what are the physical constraints on size and consequently what could be the maximum size of pterosaurs, assuming gigantism confers an adaptive advantage. The approach will start with a review of published work on flying vertebrates, carried out mainly on birds and then by analogy and example apply the conclusions to gigantism in pterosaurs.

As long ago as 1638, Galileo noticed that the bones of large animals were more robust than those of smaller animals, in other words that as animals increased in size their proportions changed. It is not possible to scale up a mouse to the size of an elephant and retain the same proportions: due to the way that strength scales, mouse legs on an animal the size of elephant would be impossibly weak.

This scaling is not simply a feature of biological systems, it is equally well established in engineering where it is more commonly known as the "square cube law", a name reflecting the fact that as a body increases in size the volume increases as length cubed whereas the area only increases as the length squared. Since, in very general terms, loads are related to mass, and therefore volume, and strength to area, it follows that geometrically scaled shapes become weaker as they become larger if they are simply scaled geometrically. Geometric scaling is also referred to as isometry, which is a special case of the more generalised allometric relationships that reflect changes in morphology with size (Alexander 1985).

Isometry, as it applies to natural systems was very eloquently described by Haldane (1926) in his essay *"On being the right size"*, where amongst other things he pointed out that as the size of a flying animal or indeed aeroplane increases, the power required to fly increases more rapidly than the weight. Since the power available is proportional to the weight, these trends converge and where they come together sets the upper limit to practical size.

8.2 Power as a limit to size

This concept of the convergence of the two trends has been invoked on other occasions (Pennycuick 1996, Sato *et al.* 2009, Norberg & Norberg 2012), but there is still considerable debate about the maximum practical size of flying vertebrates. For example, Pennycuick (1996) concluded on the basis of power required and power available that the maximum size of a bird which can undertake sustained flight is around 15kg and was sceptical of claims of the flight capabilities in much larger birds. However, Chatterjee *et al.* (2007) suggested that while the 70kg *Argentavis* may not have been capable of sustained flight, it could have flown using anaerobic power for long enough to secure lift from rising air. Similarly, a recent analysis of *Pelagornis*, a 35kg, 7m wingspan seabird from the Oligocene (Ksepka 2014) used Pennycuick's FLIGHT program (Pennycuick 2008) to calculate that this bird was likely capable of sustained flight.

The situation is no clearer when it comes to estimates of the maximum size of pterosaurs. While no one appears to doubt that the 6 m to 7 m wingspan *Pteranodon* was a capable flyer (Bramwell & Whitfield 1974, Bennett 2001, Strang *et al.* 2009, Witton 2013), there is less consensus on the flight capabilities of the largest azhdarchids, which might have reached 10m wingspan or more, with body masses in excess of 250kg (Chatterjee & Templeton 2004, Sato *et al.* 2009, Witton & Habib 2010, Habib 2013).

If the determination of maximum size is a matter of finding the crossover point between two convergent lines, why is there such a range of opinion as to where this crossover occurs? Conceptually there are two different factors at play, one is the gradients of the lines and the other their position relative to one another, as illustrated in Figure 8.1 for isometric scaling. Consider first the gradients of the lines. Schmidt Nielsen (1984) noted that in practice the scaling of birds deviates from strict isometry and is more generally allometric. The result of this deviation, according to Schmidt Nielsen (1984), is that the power required for flight is directly proportional to body mass, although he noted that the power available scales at a lower power meaning that the two relationships do still converge, but differently from the isometric scaling. Alexander (1998) also suggested, on the basis of constant sink rate, that the power required for steady flight was directly proportional to the mass of the animal. However in a much more recent study prepared from an aeronautical perspective, Liu (2006) examined the scaling of small fliers (birds and bats) and concluded that the power required varied as body mass to the power of 1.17 and power available as body mass to the power of 0.97 assuming a constant muscle mass specific power output of 141W/kg (Weis-Fogh 1977). Using this relationship he predicted that the upper size for a

practical bird would be between 165 ±102N, the wide range resulting from the inclusion of many different bird species, a key point that will be discussed below. However this result was calculated using the required power at maximum range speed, which is higher than the speed at minimum power. Reworking the calculation using the minimum power required for flight increases the weight range to between 313±102N.

Greenewalt (1975) undertook a comprehensive analysis of the morphometric parameters of birds, which he grouped by behaviour and lifestyle and presented as bivariate plots, for example a relationship between total weight and wing area. Using units of grams and centimetres he retrieved a power law relationship with a gradient of 1.28 for these parameters. This gradient applied not only to the average of all the birds in the sample but also to the linear regression lines through the various subsets, resulting in a series of parallel lines separated vertically, and the separation was substantial. At the extremes, the intercept for his shorebirds grouping line was 0.044 and for ducks 0.08, a difference of almost a factor of two.

Using the various relationships which he established, Greenewalt (1975) derived an aerodynamic analysis to calculate the minimum power required for flight. The exponent of the variation of power required with mass was very slightly less than one (typically around -0.003 as compared to 1.17 for isometric scaling), but as in the case of the relationship between weight and wing area, there was substantial difference in the intercepts of the different morphological groupings. The effect of this was that the predicted specific power requirement for the wandering albatross was half that of the similarly sized great bustard. Greenewalt (1975) did not use his analysis to try to make a prediction of the maximum size of birds and concerned himself more with the power required to fly than with the power available. However he did provide information on the flight muscle mass (the "engine" of the bird) and his data showed that as a fraction of total mass it reduced slowly with increasing mass (exponent -0.033), but with a constant that varied between 0.15 and 0.28, equivalent to flight muscle mass fractions between 12% and 22% for 1.0kg bird, representing almost a factor of two difference in available power. Consequently, at the extremes of his data sets, the power required varies by a factor of two as does the power available, implying possibly a four to one range in the ratio of power available to the power required.

In the time since Greenewalt (1975) undertook his study a great deal has been learnt about muscle power output and there is reasonable consensus (but see later for more detail and relevant references) that a sustained power output in excess of 100W per kilogram is achievable. The variation of this output with muscle mass and bird size is poorly understood and a matter of discussion (again see later), but clearly if it is a constant value and Greenewalt (1975) and others (e.g. Alexander 1998, Schmidt Nielsen 1984, Ellington 1991) are correct in the view that due to allometric effects the power required for flight in birds is directly proportional to the body mass, or maybe even slightly negatively correlated, then there is in

practice no crossover between power required and power available, rendering this approach to determining the maximum size of birds, and by extension other flying vertebrates, doomed to failure.

In contrast, the analysis presented in Pennycuick (1996) uses this approach and appears to result in a relatively tightly defined upper estimate of size. Pennycuick (1996) used results from his bird database and FLIGHT program (Pennycuick 2008) to calculate the power required by birds. He retrieved the relationship that power required varies with mass to the power of 1.167, in common with the isometric approach. Where his analysis differs is in the estimation of available power. Pennycuick (1996) argued that muscle strain is a constant (25%) and that there is an upper limit to the stress in muscle fibres. Therefore it follows that there is an upper limit to the work that muscles fibres can do (the product of force and strain) and Pennycuick (1996) calculated this to be 57J per kilogram. As power is the rate of doing work, muscle power is the product of work and flapping frequency. Pennycuick (1996) used the results of his own regression analysis (Pennycuick 1990) for the calculation of the flapping frequency as a function of mass, wingspan and wing area and calculated the ratio between power required and power available for the birds in his database and plotted the results against body mass. The definition of the ratio is such that the level at which the ratio exceeded unity sets the upper limit to the size of bird that can undertake sustained flight. Pennycuick (1996) The crossover of the standard major axis regression line through the data occurred at a mass of around 15kg, (close to the observed upper limit of mass of extant birds). This figure is reproduced in Figure 8.2.

8.3 Not an average bird

This conclusion is based on the projection of the regression line through the data and as such represents the maximum size of a notional "average bird". As Greenewalt (1975) and Alerstam *et al.* (2007) have shown, the range in values of a dataset such as that which Pennycuick (1996) used is not so much scatter in the sense of inaccuracies in the data points, for which the use of a regression line would be appropriate, as variation between but many different, consistent morphological datasets overlaid on each other. Consequently, the variations in the data points captures real differences between birds of different morphologies (which may reflect functional as well as phylogenetic differences), so it is instructive to fit a series of lines to the data, reflecting these differences and thus investigating the effect of morphology on the potential maximum size. As Greenewalt's (1975) data showed, it is very likely that these lines will be parallel to one another (though further work is required to confirm this view) . However, if this suggestion is correct and in the case of Pennycuick's (1996) data upper and lower boundary lines are drawn parallel to the his regression line, the cross over points for the limiting power ratio occur at body masses of 2kg and 100kg respectively.

Thus the maximum size that can be achieved by a bird is dependent not only on the allometry of scaling but also the underlying "prototype" or morphology. Some birds are simply better starting points or prototypes for scaling up that others - in other words they have fundamental morphological characters

that have the potential to allow them to reach large size if that is a beneficial evolutionary trajectory. From Pennycuick's (1996) data it would appear that Charadriiformes are amongst the best prototypes for large size. Greenewalt's (1975) results also place the Laridae in this category, as well as the specific species *Fregata aquila* and *Diodmedia exulans*, which share many morphological similarities with *Pelagornis sandersi* (an extinct giant bird of the Oligocene, which is thought to have reached at least 6.4m in wingspan and weighed as much as 400N (Ksepka 2014)).

Overall morphology is not the only potential cause of variation in the predicted maximum size from Pennycuick's (1996) approach. He does not state the assumed flight muscle mass fraction explicitly in the paper, but clearly a "prototype" with a high flight muscle mass fraction can reach potentially larger size. Similarly there are other formulations for flapping frequency (Rayner 1988, Taylor *et al.* 2003) and reason to believe that in large birds the frequency may tend towards mass to the power of 0.167 (Rayner 1988), which would reduce the gradient of Pennycuick's (1996) data points and thus result in even higher prediction of maximum size. The limitations of drawing conclusions from single linear regression lines through data derived from many different species are discussed in great detail and sophistication by Taylor & Thomas (2014).

Marden (1994) adopted a different approach based on the results of studies that determined the maximum weight that birds and bats can carry and still manage to take off. He demonstrated that the lift force per unit mass was constant with size, but that the power required to generate this lift increases with size, creating another analysis with convergent trends that can potentially be used to estimate maximum size. Marden (1994) argued that the specific power available from flight muscle is a constant 100W per kilogram because the work loop is not constant but expands with reducing frequency, thus resulting in a constant power output. Using this data he projected that at a muscle mass specific power of 100W per kilogram the largest body size can be no more than an improbably low value of 0.1kg. However he also noted that under anaerobic burst conditions the muscle mass specific power available was much greater (around 225W per kilogram). When this value was used, his analysis resulted in an asymptotic relationship rather than a crossover between two trends and implied that even a 250kg *Quetzalcoatlus* would be capable of flight.

This is therefore another approach which is not helpful in establishing upper limits to size since depending upon the starting assumptions, the maximum size projected ranges from 0.1kg to no limit. The result for sustainable flight predicts an upper limit of only 0.1kg, a value which is clearly confounded by even casual observation of bird flight. In the case of burst flight the asymptotic nature of the relationship does not define an upper limit though it does give some support to the view that the largest azhdarchid's were capable of leaving the ground.

8.3.1 Quantifying power required

It appears that the reason Marden's (1994) analysis gives such a low value for the mass of sustained flight is that his data is based on takeoff power, which he argued was also the minimum power. He recognised that in theory birds should have a U-shaped power curve but maintained that there was little experimental evidence to support this view. If this were the case, it would be very difficult to reconcile with the experience of aircraft since it is well known that helicopters require a great deal more power to take-off vertically than a fixed wing aircraft of the same weight does to take off from a runway.

In the intervening years new experimental techniques have been developed (Hedrick *et al.* 2003, Tobalske 2007, Jackson *et al.* 2011, Robertson & Biewener 2012) that have demonstrated quite clearly that real power curves are indeed U-shaped, although close correlation between experimental results and theoretical predictions remain elusive (Tobalske 2007, Morris & Askew 2010). In fact, these results typically show that the takeoff power can be as much is twice the minimum power required for steady flight, a difference which will clearly have a profound effect on Marden's (1994) conclusions regarding sustained flight.

8.3.2 Power available

A critical factor in all the foregoing analyses is the value of the muscle mass specific power. At one extreme are Pennycuick's (1996) arguments that muscle mass specific work is constant and therefore the power must vary as flapping frequency, consequently with a negative exponent of mass. Ellington (1991) presented experimental data which challenged this view and suggested that the results lay between 100 and 200W/kg, with a tendency to increase slowly with the total body mass. He argued that if the exponent for available power was approximately unity, the comparison of available power and required power could not be used to set the upper limits to the mass of flying vertebrates. He suggested that the reasons for the limits were perhaps to be found in limits to takeoff capability, which arose from reductions in aerodynamic performance (specifically maximum lift coefficient) with increasing size, but left this simply as a speculation. Later work by Askew *et al.* (2001) concluded that in the size range up to at least 5kg, muscle mass specific power during short bursts was constant with body mass. Thus taking a conservative lower bound, one possible value is a constant 100W/kg.

Since the early 90s (Biewener *et al.* 1991, Dial & Biewener 1993 for example) it has become possible to make reliable measurements of the *in vivo* power output of muscles and data is available over a limited range bird sizes. The largest birds for which reliable steady power output levels have been measured are 1kg mallards (Williamson *et al.* 2001), for which a value of between 100 and 200W/kg was recorded. On the basis of experiments with corvids ranging in size from 0.07kg to 0.9kg, muscle mass specific work scales with positive allometry, with an exponent of between 0.11 and 0.18 (Jackson & Dial 2011) and consequently muscle mass specific power scaled with only a small negative exponent. (-0.18 or less). These authors note that: *"These empirical results lend minimal support to the power-limiting hypothesis, but also suggest that*

muscle function changes with size to partially compensate for detrimental effects of size on power output, even within closely related species. Nevertheless, additional data for other taxa are needed to substantiate these scaling patterns". (Jackson & Dial, 2010, p452)

Extreme extrapolation of these relationships is however problematic because they imply that either the stress in muscle fibres increases continuously and/or that the strain does so as well. Clearly there will come a point at which these become impossibilities and the scaling will tend more towards the exponents proposed by Pennycuick (1996).

The foregoing review shows that the power required versus power available approach to determining the limits to size of birds, and by extension, other flying vertebrates, is extremely problematic. Even with scaling assumptions that result in the largest differences between the exponents of the two relationships, the point at which crossover occurs is very sensitive to the underlying assumptions. At the other extreme, where scaling assumptions imply there is no convergence between the trends, cross over simply does not occur. It is also clear that the starting point for the scaling matters. As noted above, "Average birds" are not the best prototypes: some body plans are better starting points for large size than others.

8.4 An alternative approach

Against this background, is there an alternative approach that can be used to estimate the maximum size of pterosaurs? For these animals we have, when compared to birds, comparatively poor behavioural and phylogenetic data sets, so trends extrapolated from scatter plots of morphological data are even less likely to be useful than for birds. Consequently, noting that the starting point is important, an alternative approach is proposed. Take a well documented "prototype" and produce scaled up, "*in silico*" versions using established allometric trends and mechanical constraints. The properties and performance of these specific scaled up individuals can then be calculated, making it possible to examine more aspects than simply the comparison between sustained power and available power. Since fossil evidence points to the azhdarchids being the natural "models" for pterosaur gigantism, the morphology of this group was adopted for the study.

As size increases, allometry dictates that structural loading will increase disproportionately and consequently either stronger materials or proportionately larger structural members will be required. Clearly in nature only the latter option is possible, so the increasing size of structural members like the wing spar may have a detrimental effect on overall mass and perhaps aerodynamic performance. The allometric scaling of kinetic energy also works against increasing size, making safe landings increasingly problematic. These are potential limits that can be examined for individual "designs" more readily than by adopting a generalised, parametric approach. And lastly, even if an animal is strong enough to fly and to land safely and has the power required for sustained flight, it has to be able to get into the air. Take off can be onerous. Airspeed is low and consequently the power requirements are increased, albeit

temporarily, and once in the air the animal requires sufficient excess power to gain height and fly for sufficiently far to escape predation and/or find lifting air to keep it aloft.

8.5 Modelling azhdarchids *in silico*

8.5.1 Overview

The following sections develop a range of scaled azhdarchid "designs", selecting the best available data from the fossil record to establish an initial prototype, which is then scaled and adapted to reflect the known morphology of azhdarchids. Calculations were made for scaling from 6m to 9m and 12m wingspan (Table 8.1). The 6m ornithocheirid wing model described in Chapters 3 and 4 was taken as the starting point and scaled to consistent structural strength to withstand the imposed aerodynamic loads (see Section 8.5.2 for more detail). In each case the resulting aerodynamics characteristics were calculated. This data was then used to predict the performance of these individuals in terms of cruise power, landing dynamics and take-off dynamics (as described in Sections 8.5.3 to 8.5.5. In the case of cruise power, the power required was compared to the power available for a range of assumptions regarding muscle mass specific power and flight muscle mass fraction, for landing the ability of the skeleton to absorb energy was compared to the kinetic energy at touch-down speed and for take-off the power available was used to calculate the leaping dynamics and thus the ability to leave the ground and take to the wing.

Table 8.1 Calculated azhdarchid dimensions

Span (m)	Weight (N)	Wing area (m^2)	Wing loading (N/m^2)	Flight speed (m/s)
12.00	4,653	18.06	258	17.5
9.00	2,098	10.04	209	15.8
6.00	683	4.39	156	13.6
3.00	100	1.07	94	10.6
2.00	33	0.47	70	9.1

8.5.2 Scaling of structural strength

The strength of the bones in the wing, the wing spar, was selected as the variable to be scaled from 6 m to the 9m to 12 m size range. The reason for this choice was that in the case of pterosaurs the forelimbs are the structures that bear the brunt of not only the aerodynamic loading but also the loading on takeoff and most probably landing. Two limiting criteria were set, first that the deflection of the tip of the wing should be a constant percentage of the wingspan and second that the surface stress on the most highly loaded bones should not require a factor of safety of less than three (Kirkpatrick 1994 and Palmer & Dyke 2010). The baseline data was obtained from the large ornithocheirid wing spar described in Chapter 4. While this is not a perfect representation of an equivalent azhdarchid wing spar, with presently available data it is not possible to create such a wing spar in the same manner as was achieved

for the ornithocheirid. However, as will be seen later in this section, the results that are particularly sensitive to the assumed wing bone morphology (mainly the aerodynamic performance was affected by the change in wing airfoil as the wing bone diameter to wing chord ratio varies and the wing skeletal mass), did not prove to be strong limiting factors.

Witton (2008) estimates that the mass of azhdarchid pterosaurs is, for a given wingspan, considerably greater than for the ornithocheirids. The body mass of azhdarchids scales as $8.52\ b^{2.52}$ whereas for ornithocheirids the relationship is $4.42\ b^{2.43}$ (Witton 2008). The structural properties of the wing spar (specifically second moments of area in the dorsoventral plane) were therefore scaled to be able to resist the increased loading that would result from the azhdarchid body plan. As noted above, two different constraints were applied, firstly that the tip deflection should remain a constant fraction of the wingspan and secondly that the surface stress on the most highly loaded sections of the wing bone should remain constant. In order to make these assessments it was assumed that the cortical thickness remained a constant fraction of the depth of the wing bone section. This is of course a somewhat arbitrary restriction, but it has practical support in that thin-walled tubes are susceptible to earlier failure due to local buckling if the wall thickness is below a critical level which is related to the ratio of the wall thickness to the diameter as discussed in more detail in Chapter 4. Consequently, keeping this value constant would ensure that the heavier and larger scaled up wing spars retained the same resistance to buckling failure.

The bending moment on the wing spar is directly proportional to lift generated by the wing which in turn is directly related to the total body mass. The resistance to bending of the structure depends on two parameters, the Young's modulus of the material and the second moment of area of the cross-section (see Chapter 4 for more detail). For structures made from bone it can be assumed that the Young's modulus remains constant and thus the bending resistance is determined only by the second moment of area. Since this varies with the fourth power the linear dimensions, a relatively small increase in size produces a very large increase in second moment and thus bending stiffness. However the surface stress that results from the application of the bending moment depends not only on the second moment of area but also the linear depth of the section. Applying these approaches to the critical region of the first wing phalanx where the surface stress was greatest (see Figure 5.5) showed that it was surface stress rather than tip deflection which was the limiting factor. So, perhaps slightly counterintuitively, as the models became heavier and larger the tip deflection actually reduced as a proportion of wingspan because of the constraint to maintain the same maximum surface stress. The results are summarised in Table 8.2.

Table 8.2 Wing spar scaling results using Witton (2008) mass estimates

Span m	Total Mass kg	Cortical thickness mm	Cortical area mm2	Section depth mm	Deflection m	Defln/length
6	79	2.00	142	24.7	0.34	0.113
9	214	3.20	368	39.8	0.44	0.098
12	476	4.60	755	56.9	0.59	0.099

There were two allometric trends revealed from the scaling of the different sized models that might be expected to have effects on their relative performance. Firstly the depth of the wing bone section increased more rapidly than the wing span and therefore wing chord. The scaling exponent was 1.16. However because the azhdarchids have lower aspect ratio wings than the ornithocheirid pterosaurs (Witton 2008), the ratio of the section depth to the wing chord was proportionally greater than for ornithocheirids. Since the wind tunnel tests (see Chapter 2) showed that the higher this ratio the better the aerodynamic efficiency of the wing sections, it will be better in azhdarchids than in ornithocheirids. Thus although with increasing size there is a weak tendency for this ratio to become larger, the starting point was favourable due to the large wing chord relative to the wing bone diameter, so it did not prove to be a large (and therefore potentially size limiting) effect as will be shown in the aerodynamic analysis.

The other effect of the scaling was a disproportionate increase in the cortical area and thus wing skeletal mass with size. The scaling exponent with mass was 1.3. This is to be compared with an exponent of 1.07 found for the scaling of the total skeletal mass in birds (Prange *et al.* 1979) (noting also that this skeletal mass scaling was the basis of the Witton (2008) body mass estimates). For birds and mammals Prange *et al.* (1979) showed that the skeletal mass was typically around 6 to 8% of total body mass, which is also implicit in the Witton (2008) mass estimate for pterosaurs. Consequently the scaling of the wing spar bones with a slightly greater exponent than the rest of the skeleton will only have a small effect on total body mass. The effects of these uncertainties will be discussed in more detail in relation to the analysis of the other proposed constraints on size.

The preceding analysis suggests that the structural performance of the wing spar is not a significant limitation to size. Even at 12m wingspan the required section depth is not excessive from the point of view of aerodynamic performance and the mass of the wing bone material not greatly out of proportion with the overall mass of the animal.

Using the information obtained from the foregoing analysis it is possible to make estimates of the aerodynamic performance of the three different models. This then provides a baseline from which the power required for level and climbing flight can be determined.

8.5.3 Parametric analysis of flight power requirements

Before undertaking such a detailed analysis, it is instructive to make a simpler parametric analysis to understand the likely boundaries of the results. When a flying animal is gliding, the angle of descent depends directly on the ratio of lift to drag (Vogel 1994:254), the gliding angle being the inverse tangent of this ratio. Thus to achieve level flight, a thrust is required that exactly balances the drag force and consequently the power required is the product of thrust (=drag) x flight speed.

In practice, the position is a little more complex in that the flapping action of the wing increases the speed of the airflow over the wing surface, resulting in an increase in profile drag. In addition, some power is required to overcome the inertial losses. However, in cruising flight the flapping frequency of a

large pterosaur will typically be around 1Hz and the flapping angle around 40 degrees (Strang *et al.* 2009) which equates to a tip amplitude of 0.17m and thus a flapping velocity of around 0.34m/s. This is clearly small compared to the likely forward speed of 15m/s, so the increased local flow speed is in fact very small, meaning that any increase in profile drag can be ignored.

The estimation of inertial power is more complex. Application of the methodology proposed by Salehipour & Willis (2012) predicts a value of approximately 15% of thrust power whereas van den Berg & Rayner's (1995) approach gives a value of around 10%. However, both approaches ignore any possible kinetic energy recovery, which would reduce the inertial power requirement. In the face of this uncertainty, inertial power will be ignored for the purposes of this analysis.

The aerodynamic thrust power is less than the applied muscle power since there will be losses due to the propulsive efficiency, which will always be less than unity. Typically for flapping flight in the efficient regime (Strouhal number around 0.2 to 0.4 Nudds *et al.* 2004) the efficiency can be as high as 75% (Liu 2007, Strang *et al.* 2009). Consequently the applied muscle power = thrust power/0.75.

The likely L/D ratio of giant azhdarchids will be calculated in detail later, but measurements on birds gives results of around 8 to 12 for comparable aspect ratios (Alexander 2002:40, Tennekes 1997:83, Pennycuick 2008:194).

The flight speed can be readily calculated from the assumed lift coefficient. The wind tunnel tests described in Chapter 2 showed that for pterosaur type membrane wing sections the best lift:drag ratio is obtained at a lift coefficient of around 1.4 (substantially higher than for birds.) Taking this value, the speed can be calculated and using the propulsive efficiency described above, the required muscle power can be calculated for animals of any size.

The available power depends on two parameters, the total mass of muscle that can be recruited to power flight, the flight muscle mass (FMM) and the muscle mass specific power (MMSP). In birds, the proportion of muscle mass devoted to powering flight, the flight muscle mass fraction (FMMF), ranges from 10% to 30% (Greenewalt 1975, Pennycuick 2008:364, Heers & Dial 2014). In birds the flight muscles and the leg muscles are separate modules (Gatesy & Dial 1996) with the result that, depending on behaviour, there has to be a trade-off between the two (Heers & Dial 2014). However for pterosaurs the picture is not so clear cut since they use the forelimbs not only for flight but to make a major contribution to take off (assuming they use a quadrupedal launch (Habib 2008)). For birds the muscle mass devoted to the legs can be as much as 15% or more (Heers & Dial 2014) and while it is impossible to be sure of how the trade-off splits for pterosaurs, it does not seem unreasonable to propose that the upper level of the flight muscle mass fraction could be as high as 40% since a lower proportion of leg muscle is required as compared to birds.

If it can be assumed that the ratio of burst to aerobic power is constant, then a constant upper bound for aerobic power of between 100 and 200W/kg can be expected to apply for body mass up to 5kg

(see Section 8.3 for sources). Further, if it assumed that for increasing mass the frequency dependent scaling applies, then the muscle power can be calculated for any body size. Values for power required for notional azhdarchid models ranging from 3m to 12m wingspan (see Table 8.2 for details) were calculated for L/D values of 8 and 12 (using the simple approach described above) and used to determine the flight muscle mass fraction for a constant muscle mass specific power of 100W/kg and for the specific power varying with flapping frequency as described earlier.

The results are shown in Figure 8.3 where the flight muscle mass fraction is plotted against wingspan. It is immediately apparent that the assumed limits result in a wide "map" of results. For example, at one extreme a FMMF of only 20% is required for a 12m span with L/D=12 and constant 100W/kg specific power, whereas for L/D=8 and specific power that reduces with size, and FMMF of more than 50% is required at 12m wingspan. Or examined another way, if it is assumed that the upper limit of FMMF is 40%, then the maximum size of azhdarchid capable of level flight is at least 8m wing span, but in excess of 12m for the most favourable combination of assumptions.

A more detailed calculation of flight performance (using wing section data that reflected the wing bone depth to wing chard ratios found above) gave a L/D ratio of 8.4 at 3m span increasingly a little to 8.5 at 12m span, placing azhdarchids at the lower end of the range of the analysis above (and on a par with many birds (Pennycuick 2008)). However, it is apparent from Figure 8.3 that even with this refined data the approach is unlikely to provide a highly bounded value for the upper limit to size since the muscle mass specific power and, to a lesser extent the flight muscle mass fraction are unavoidably subject to considerable uncertainty. In almost all cases the maximum size appears to be well in excess of 10m wing span.

8.5.4 Landing

A detailed mathematical description of the landing dynamics of pterosaurs is problematic, indeed such a description has not yet even been attempted for extant birds. However, observation of bird behaviour shows that large birds in particular tend to land by slowing their flight as much as possible (perhaps by extending their legs and tails as air brakes) then pitching up at the last moment, using a dynamic stall to come to a halt. If there is no wind they may also flap their wings briefly, but in many instances when landing into wind they simply hold their wings steady.

Using a time stepping calculation and estimated aerodynamic characteristics for the wings (Figure 8.4: based on data in Carruthers *et al.* 2009 and Palmer 2010) it is possible to model this as a dynamic process where the wings are not flapped. Typical output is shown in Figure 8.5. Modelling was undertaken for a range of different large birds (see Table 8.3) and the 6m, 9m and 12m pterosaur models described above in Table 8.1.

Table 8.3 Birds used to model landing dynamics

Bird	Common name	Mass (kg)	Wing area (m2)	Source
Answer albifrons	White fronted goose	2.58	0.184	Alerstram *et al.* 2007
Ciconia ciconia	Stork	3.43	0.533	Alerstram *et al.* 2007
Branta canadensis	Canadian goose	3.63	0.372	Alerstram *et al.* 2007
Pelecanus onocrotalus	White pelican	8.50	0.960	Alerstram *et al.* 2007
Gymnogyps californianus	Californian condor	9.50	1.32	Campbell & Tonni 1993
Cygnus olor	Mute swan	10.60	0.65	Alerstram *et al.* 2007

The results (Figure 8.6 and Figure 8.7) showed that the forward speed could be reduced for landing to 5m/s or less for large birds with low wing loading (pelican, condors etc) increasing to 6m/s for more highly loaded geese. The most heavily loaded, large birds such as swans gave much higher landing speeds (8m/s), which is presumably reflected in the swan's preference for water landing on a long runway and the albatross' preference for cliffs which provide a strong headwind.

Since a large pterosaur is most likely unable to land on water (Hone & Henderson 2013), this landing adaptation cannot be assumed. However, the simulated 6m, 9m and 12m azhdarchids had landing speeds of 4.8m/s, 5.7m/s and 6.2m/s respectively (scaling as span$^{0.373}$), well within the range for birds that do not rely on water or headwinds to facilitate landing.

Safe landing is not simply a matter of landing speed. It is also depends on the ability of the structures involved to absorb the impact (kinetic) energy. Kinetic energy varies as mV^2, so for isometric scaling it varies as $m^{4/3}$. Strain energy is a function of the maximum material stress, the Young's modulus and the volume of material. Thus if the material (bone) does not change (as it cannot for animals) then strain energy varies as structural volume, a proxy for which is bone volume, or mass assuming constant density. Consequently it is apparent that kinetic energy scales more rapidly than strain energy, so proportionately, larger animals either need more bone volume or to move more slowly than smaller ones in order to retain the same resistance to impact. This effect is graphically illustrated by J. B. S. Haldane's famous observation that *"You can drop a mouse down a thousand-yard mine shaft and, on arriving at the bottom, it gets a slight shock and walks away. A rat is killed, a man is broken, a horse splashes."* (Haldane 1926:1).

Since skeletal mass scales as $m^{1.07}$ (Witton 2008) the strain energy actually scales as $m^{1.07}$. For impact energy to scale at the same rate, speed must scale very weakly as $m^{0.07}$. Consequently since as Figure 8.6 shows, large slow flying birds such as White Pelicans and Californian Condors weighing up to 10kg can land safely at 5m/s, the safe landing speed of a 100kg individual would be 5.9m/s and 6.6m/s for a 500kg individual using this scaling.

If this scaling can be taken to apply to pterosaurs, then the calculated landing speeds for individuals of up to 12m wing span (474kg) fall under this limit, so based on this relatively simplistic analysis at least it appears that landing loads may not limit the size of giant pterosaurs of up to 12m wingspan. However, since the scaling of calculated landing speed is higher than the safe landing speed, there will be a cross-over that will determine the size at which the landing speed becomes unsafe. With the exponents found in this study it is around 15m wingspan.

8.5.5 Take-off

The foregoing leaves getting into the air as the last potential limit. Assuming a quadrupedal launch for pterosaurs (Habib 2008, Molnar 2009) means that a high proportion of the launching forces come from the forelimbs, primarily the same muscles that are used for flight. To estimate the power required for launch it is necessary to know the source of the forces that provide the vertical motion. Earls (2000) and Henry (2005) have shown that for birds 80% or more of the lift-off force comes from the hind limbs rather than the wings, so birds propel themselves ballistically into the air and then the wings take over. Presumably this was also the case for pterosaurs. On the basis of these assumptions (quadrupedal launch and ballistic launch propelled by the forelimbs) a leap into the air was modelled using a time stepping simulation created in Excel. It was assumed that the leap was to sufficient height that when the wingtips were at the end of the full downstroke of the first wing stroke they just cleared the ground and also that there was sufficient forward speed to avoid wing stall, so the wings could take over in a smooth transition without loss of height. Because the launch activity is very brief, it can draw on the anaerobic output of muscle, so a high specific muscle power of 400W per kilogram was adopted, a value that has been measured in extreme cases for birds (Askew *et al.* 2001). The analysis was run for a range of values of the wing flapping angle varying from 70 degrees to 120 degrees as well as for two different launch poses. Figure 8.8 shows an outline flow diagram for the calculation procedure.

A key aspect of the calculation is the determination of the skeletal geometry, which influences the range of movement in the launch. Illustrations from Witton & Naish 2008 and Witton (2013:252) - see Figure 8.9, were used to determine the morphology at the point of lift off and also the possible crouched positions from which the animal propelled itself into the air. These are important because the longer the launch "stroke", the greater the potential impulse and thus launch velocity. Scaling from these diagrams (Figure 8.9) gave stroke lengths of 1.0m from a typical walking pose and 1.48m from an extreme crouched pose.

The results of the simulations are shown in Figure 8.10 for both the "walking" and "crouched" launch strokes. It is immediately apparent that the required flight muscle mass fraction (FMMF) is very dependent upon the wing stroke angle - which is perhaps no surprise as this angle determines the required height of the launch trajectory. Consequently, an indication of the likely wing stroke angle is needed to interpret the results. While birds may not be the ideal analogues for pterosaurs (Witton & Habib 2010),

flapping flight has been shown to be subject to the same unifying fluid dynamic relationships regardless of the animal in question. In particular, recent work has shown the over-riding importance of Strouhal number equivalence in flapping propulsion (Rohr & Fish 2004, Nudds *et al.* 2004, Sato *et al.* 2007, Aditya & Malolan 2007) and for this reason it is considered reasonable to refer to birds for information on the likely range of wing stroke angles. However, as Nudds *et al.* (2004) noted, there are actually very few stroke angle measurements available in the literature, and what there are mostly apply to birds in cruising flight. For such flight, Nudds *et al.* (2004) retrieved a relationship between stroke angle and wingspan of the form:

$$\theta=67b^{-0.24}$$

Where θ=stroke angle and b= wingspan. On this basis, the cruise stroke angles of 6m to 12m pterosaurs range from 44 degrees to 37 degrees (which agrees approximately with results in the flapping flight simulation reported by Strang *et al.* 2009). However, even superficial observation shows that birds employ a much greater wing stroke angle when taking off. Parslew & Crowther (2010) and Parslew (2014) present results for pigeons which suggest that while the cruising flapping angle may approach 90 degrees (compare this to a predicted value of 73 degrees using the Nudds *et al.* (2004) relationship) the angle at take-off exceeds 150 degrees and is ideally 180 degrees. More subjectively, analysis of slow motion films and photographs available on YouTube and other sources suggests that large birds of prey flap their wings through at least 120 degrees, as do herons (long legged birds that use a leaping launch). See for example http://www.moorhen.me.uk/iodsubject/birds_-_herons,_egret_&_snipe_04.htm. This value would scale (assuming the Nudds *et al.* 2004 relationship) to 80 to 90 degrees for 12m and 6m sizes respectively.

Taken collectively, these rather varied results suggest that for large pterosaurs, the launch wing stroke angle probably need to be in excess of 80 degrees, but most likely does not need to exceed 120 degrees.

Referring again to Figure 8.10, it is apparent that if an 80 degree angle was adequate, then this could be achieved with less than 20% FMMF fraction for the 6m animals, increasing to 35% at 12m with the more conservative launch stroke length. However, to achieve 120 degrees, even the 6m animal with the extreme launch stroke length would require a FMMF of 40%, increasing to almost 80% for the 12m animal with a conservative launch stroke length. These results suggest that while the 6m wing span animal could achieve a good takeoff performance with FMMF less than 40% (the likely upper limit as discussed in Section 8.4), by 9m span the options are becoming constrained and at 12m the long stroke launch pose is required to avoid an extremely constrained envelope. Figure 8.11 presents these results in a different way, cross plotting at FMMF of 20% and 40%, the probable range for pterosaurs. It is now even clearer that at 20% FMMF the 12m wing span is unable to make a sufficiently deep initial wing stroke and requires the assumption of the highest FMMF and launch stroke length to achieve flapping angles that are likely to provide adequate margin to ensure safe launch.

As an independent check on this result, a relationship between maximum force exerted and animal size determined by Alexander (1985a) was applied to the launch results. Alexander (1985a) found that for a very wide range of animal species, the maximum force ratio (ratio of force to weight) they can exert on their environment scales as $20m^{-1/3}$. In Figure 8.12 the Alexander (1985a) values are plotted against the calculated maximum ground reaction force ratios for the short and long launch stroke simulations (since the forces are presented as ratios of body mass, they collapse onto each other for the three animals sizes). At 12m span, the maximum stroke angle that can be achieved is about 75 to 90 degrees, increasing to 85 to 115 degrees at 9m and more than 120 degrees at 6m. Here again the tight constraints on the 12m span are apparent, with the convex curvature of the relationship progressively easing the severity of the constraints as size decreases.

While none of these observations are definitive, it is apparent that the launch stroke length and required initial wing flap angle are very significant parameters. At 12m span the results push hard against the limits of both of these constraints, suggesting that for real animals, which must operate with some margin of safety for forced behaviour in non-optimal conditions, a wing span of 12m is very unlikely. That said, it may be that the actual limit can lie towards the upper part of the range because the assumptions used in this analysis do take any account of elastic stored energy. In small animals this can be a several times larger than the available muscle energy (Alexander & Bennet-Clark 1977), though as animals become larger this reduces. However the very long tendons in the pterosaur forelimb can potentially be a significant elastic energy store, providing added power margins for reliable launch.

[Authorship note: The concept of the quadrupedal launch of pterosaurs is original work by Mike Habib. He provided some preliminary calculations for the takeoff power requirements, but this was completely re-written and recast for the analysis herein by including the addition of the impulse area (Earls 2000), deriving the stroke length from skeletal illustrations and the using a time stepping method.]

8.5.6 The scaling of take-off dynamics

Before leaving the topic of take-off, the overall scaling will be investigated in order to provide another analysis of the severity of the constraints. For a ballistic limb powered launch, the applied impulse is equal to the change in momentum (Bedford & Fowler 2008: Dynamics:224) and since the initial velocity (and hence momentum) is zero:

Impulse (I) $=mV$ and hence $V=I/m$

Also for a projectile launched upwards against gravity with vertical velocity component V, the height it reaches (h) can be found from:

$h=V^2/2g$ (Bedford & Fowler 2008: Dynamics:51)

Now, assuming that the height reached is a constant proportion of the animal's wing span (to ensure a constant wing flapping angle), then:

$h \propto m^{1/3}$ and

$h \propto (I/m)^2$

From which it follows that the required impulse to achieve the clearance height is proportional to length$^{7/2}$.

Now, the actual impulse (the impulse available) is the integral of force over time, so:

$I \propto Ft$

Using the Alexander (1985a) relationship for force:

$F/m = 20m^{-1/3}$

So $F \propto m^{2/3}$ and in consequence the impulse available $I \propto l^{5/2}$, which has a much lower exponent that the impulse required.

The only allometric "lever" available is the launch stroke length, since if this is increased then the actual duration of the launch impulse can be increased. Since the duration of the launch stroke will be the stroke length x velocity, it can be shown that the stroke must scale as length^2, a powerful negative allometry, confirming that the launch mechanics are likely to place a relatively sharp upper limit on size.

8.6 Summary

Muscle flight power, which has often been used to estimate limits to the size of flying vertebrates, does not appear to constrain pterosaurs to be less than 12m in wingspan. Wing bone strength is more than adequate at that size although the aerodynamic efficiency is slowly compromised due to the disproportionate increase in wing bone diameter, which may serve as a weak limit somewhere above 12m. Landing may possibly be an issue but landing speeds do remain relatively modest even up to 12m. However, any limit will be difficult to determine with precision as the calculations also need to consider the ability of the body structures to absorb kinetic energy, which requires a model of the strain energy characteristics of the musculoskeletal structures.

In contrast, launch does appear to be a strongly limiting factor. Assuming a forelimb muscle mass fraction of up to 40% appears to limit size to between 9m and 11m.

Even at 9m, giant pterosaurs are significantly larger than the largest recorded birds, which are thought to have had maximum wingspans of 6m to 7m (Campbell & Tonni 1983, Vizcaino & Farina 1999, Palmqvist & Vizcaino 2003, Ksepka 2014) and much larger than the largest extant birds.

What was it about pterosaurs that enabled them to reach so much greater sizes than birds?

Firstly, they were capable of relatively slow flight since their flexible, membrane wings enabled them to have high camber wing sections and consequently much higher maximum lift coefficients than birds. Since power is the product of drag and speed, their power requirements were correspondingly less for the same total body mass.

Secondly, they were able to use the same muscles for flight as for take-off, whereas birds have to separate these two functions. This means that pterosaurs are potentially able to recruit a larger fraction of total muscle mass for launch (since they did not need to split muscle mass between hind and fore limbs in the manner of birds), and consequently have significantly greater launch power available.

Lastly, by using the forelimbs for launch, they can potentially achieve a longer launch stroke and greater launch impulse than birds.

Summary and Conclusions

History of reconstructions

Ever since the first discoveries and recognition of pterosaur fossils in the late 18th century, attempts have been made to reconstruct their mode of life and flight style. At first they were likened to bats but gradually their reptilian origins became recognised and by the early 20th century reconstructions were looking much as they do today. The first detailed attempts to reconstruct pterosaur aerodynamics were made by Hankin & Watson (1914) and Short (1914) but it was not until the 1970s and 1980s that researchers such as Bramwell & Whitfield (1974), Stein (1975), Brower (1983), Sneyd (1984), Padian (1985), Pennycuick (1988) and Hazlehurst & Rayner (1992) started to make detailed analyses. Famously, in 1985, Dr Paul MacCready, an aerodynamics researcher, and his team built a successful full scale flying "replica" of *Quetzalcoatlus northropi*. More recently, attention has also turned to attempting to understand the wing membranes (Padian & Rayner 1993, Bennett 2000, *Elgin et al.* 2009 amongst others) as well as the myology (Bennett 2007, Prondvai & Hone 2008) and functional assessments of the skeletal morphology (Wilkinson 2006, 2008) and Witton & Habib (2010).

All these studies have been hampered and ultimately limited in their veracity by two key areas where information has been lacking - the aerodynamic performance of the wing sections and the structural capabilities of the wing spar. Without this information it is impossible to create reliable estimates of flight performance or of the potential effects of structural flexibility.

To address these deficiencies, two programs of data collection were undertaken. The first used wind tunnel testing to measure the aerodynamic performance of a wide range of possible pterosaur wing sections and the second was to measure wing bone morphology, including in particular the bone cross sections and internal structure, from which to estimate the bending stiffness.

Wind tunnel tests

The wind tunnel tests were conducted in a facility at University College, Dublin and evaluated the aerodynamic characteristics of sections representative of both proximal regions where the propatagium is present, and more distally where it is absent. The effect of different wing bones shapes, their positions relative to the membrane and the relative sizes of wing bone and membrane were quantified, providing a unique dataset from which reliable three dimensional wing performance could be predicted for the first time.

3D flight models

The three dimensional flight models were used to reconstruct the flight polars for gliding flight - the variation of descent (sink) speed with flight speed. The results showed that the flight efficiency of pterosaurs (as measured by the ratio of lift to drag) was inferior to all previous estimates. This was because the likely wing sections were inferior to the sections that had previously been assumed, which did not account for the presence of the leading edge wing bones. However, it also revealed that the flexibility and high curvature (camber) of the membrane sections resulted in higher maximum lift coefficients, which translated to improved low speed flight performance. The flight envelope was thus extended in the low speed regime, which reduced the power required for takeoff and improved the landing margins of safety.

Effects of wing shape and flexibility on flight performance

In addition to the wind tunnel testing and reconstruction of 3D flight performance from these results, the effect of overall wing morphology (planform and lift distribution along the wing) on induced drag was investigated using vortex lattice computational fluid dynamics. This also allowed the accurate calculation of the location of the aerodynamic centre of pressure, which must be coincident with the centre of mass in steady flight. In order to achieve this balance, it was found that the wings required considerable anterior sweep - much more than is commonly shown in reconstructions.

The basic morphology of the single supporting spar in the pterosaur wing dictates that the wing membrane must taper in width progressively from the proximal attachment to the wing tip, where it becomes extremely narrow. Conventional aerodynamics (Anderson 2007:420) suggests that this highly tapered planform is very inefficient due to elevated levels of induced drag (the drag due to lift.) However, if the wing tip is curved posteriorly, to create what is known as a "lunate" shape (familiar in nature from the tails of fast swimming fish for example) then the aerodynamic efficiency is greatly improved. The combination of membrane tension and distal wing bone flexibility (WP4 in particular) likely made such a shape possible, allowing the highly tapered membrane to create an aerodynamically efficient morphology.

The vortex-lattice analysis also informed an assessment of the pitch stability and suggested that the combination of anterior sweep and wing flexibility could, with the right dynamics, be a novel feature that confers static stability in pitch without the high induced drag penalty characteristic of conventional flying wings.

Wing bone morphology

The pterosaur literature contains very little information on the three dimensional wing bone geometry. Sources such as Wellnhofer (1985, 1991b) and Bennett (2000) provide outlines in orthogonal views, but very little information about the cross section shape. They are almost silent on the internal structure. To address this deficiency, a program of museum visits was undertaken, seeking out wing bones

that were broken or damaged, allowing the cross section to be seen. A series of thin sections prepared by Steel (2005) were also examined. At the time this work was being started, CT scanning of fossils was rapidly becoming accessible and the technique was therefore used to provide the main body of information required. High quality scans of the first three wing phalanges were obtained and combined with observations and thin sections (Steel 2005) of broken specimens of the more proximal bones and the fourth wing phalanx. This provided a definition of the external shape and cortical thickness of a representative 3m long wing spar. ImageJ software was then used to determine the cortical area and second moments of area of the cross sections at regular intervals along the wing bones.

Structural modelling

Two options were evaluated for the analysis of the wing spar structure, finite element analysis (FEA) and simple beam theory. To undertake an FEA analysis the wing bone cross section information would have needed to be converted into continuous three dimensional models in order to generate the FEA meshes. Whilst techniques exists to do this, the time required would have been out of all proportion to the remainder of this study. As an alternative, a simple beam theory model was constructed in Excel. It was validated against analytical solutions for tapered beams and simple FEA models and provided results that were within a few percent of these results. It allowed the dorsoventral and anteroposterior deflections to be evaluated but took no account of torsion.

Structural performance

The analysis of the cross section properties revealed a hitherto unknown feature of the wing structure: the proximal bones (distally to the metacarpal) were stiffer dorsoventrally than anteroposteriorly, by a ratio of 1.5 to 2 to 1. This changed abruptly at the first wing phalanx, were the ratio was reversed and was maintained at 2:1 in WP2 and WP3. The fourth wing phalanx was much thicker walled than the others with stiffness more or less the same in all axes. This pattern of stiffness distribution is interpreted as a response to the dual requirements of controlling the wing tip deflection whilst at the same time providing a structure that can support the levels of membrane tension required to suppress aeroelastic flutter.

The dorsoventral bending moment is directly related to the aerodynamic lift forces, which in turn depend on the total body mass. A range of lift distributions and body masses were investigated and the resulting tensile stresses along the wing spar calculated. Under the extreme assumptions (the use of Witton (2008) mass estimates and the most efficient lift distribution from the XFLR5 analyses) these stresses came close to the yield stress of high modulus bone, suggesting that the Witton (2008) mass is very close, if not beyond the upper practical limit. Under these conditions the tip deflection was around 0.7m.

Membrane tension and flutter limits

An allowable (tensile) strain approach was used to evaluate the structural performance of the wing spar in the anteroposterior plane, which provided an indication of the upper limit of membrane tension that was achievable. If the wing bones were strained to their practical limit they could resist a membrane tension of between 500N/m to 1,000N/m. An analysis of the flutter boundaries of tensioned membranes subject to air flows (Watanabe 2002) showed that tensions of this magnitude were sufficient to suppress membrane flutter over the likely flight speed range of the animal. However, the membrane must also retain its shape and not "balloon" excessively under load. In order to resist the required membrane tensions and the effects of the aerodynamic pressure loads without excessive stretch (less than a few percent) a high modulus material was indicated, with a tensile stiffness greatly in excess of the membranes of bats for example. In order to achieve the required modulus (and remain thin) the composition of the membrane was postulated to include a substantial fraction of nature's highest modulus (flexible) material, keratin, confirming Bennett's (2000) view of the composition of the reinforcing aktinofibrils.

Limits to size

There appears to be little doubt that pterosaurs the size of *Pteranodon* (around 7m wingspan) were capable fliers (Bennett 2000, Unwin 2006:194, Witton 2013:56-63 for example), but the flight abilities (or possible flightlessness) of the pterosaur giants, the azhdarchids are more contentious (Sato *et al.* 2009, Henderson 2010). The latest estimates (Witton & Habib 2010, Witton *et al.* 2010) suggest that these animals attained a wingspan of at least 10m and weighed as much as 250kg. When the limits to size of birds have been studied, the approach generally adopted has been to compare the power required with the power available. Since basic isometric scaling implies that the latter scales with a lower exponent of size, there must at some point be a cross over, which represents an upper limit to size. Investigation of this approached showed that in practice the location of the cross-over point depended very heavily on the underlying assumptions about the bird morphology and aerodynamic performance, to the extent that in some cases the answer could not be narrowed down to closer than between 1kg and 100kg, in others there was no convergence at all!

As an alternative approach, an allometrically scaled series of azhdarchid forms were modelled *in silico* with wingspans ranging from 6m to 12m. The results showed that the power (and structural strength) limit approaches did not limit size within this range and probably had cross-overs towards 15m wingspan or more. The dynamics of landing and takeoff were also investigated and these behaviours were found to be more limiting. Take off in particular proved very onerous and scaled with strong negative allometry, leading to the conclusion that the practical maximum size of an azhdarchid capable of unassisted take-off from level ground was in the range between 9m and 11m wingspan.

The pterosaur advantage

The largest extant birds have wingspans of around 3m and the giants of the fossil record do not appear to have exceeded 7m (Palmqvist *et al.* 2003, Ksepka 2014), significantly smaller than the largest pterosaurs. What was it about pterosaurs that enabled them to evolve to larger sizes than birds? First, the flexible wing membrane gave higher maximum lift coefficients, which allowed lower speed flight relative to size, with consequent reductions in power requirements and an expanded safe landing envelope. Secondly (assuming that pterosaurs did use the quadrupedal launch technique proposed by Habib 2008) they could recruit a larger proportion of muscle mass to power takeoff. Thirdly, because in this case the majority of the take-off force was developed in the forelimbs, the range of motion was potentially greater than for birds, resulting in a larger launch impulse.

Hypothesis testing

Against this background, I can now return to address the underlying hypothesis of the research, that:

Wing flexibility was a significant factor in defining the aerodynamic performance.

In a structural sense, flexibility does not appear to be a significant limiting factor. Fundamental scaling dictates that as flying creatures (or indeed man-made flying machines) become larger they must use progressively higher performance (specifically higher modulus, higher strength) materials to control deflection and provide adequate stress factors of safety. However, for pterosaurs of up to 12m wing span (or maybe more) it appears that nature's materials are adequate. The wing tip deflections due to aerodynamic lift of a 3m wing appear to be around 0.7m, which is only a little more than the unloaded ventral deflection that results from natural curvature in the wing bones. In other words, in gliding flight the wing tips could readily be held almost level with the glenoid. The factors of safety of the wing bone stresses are low, as is to be expected in a weigh sensitive flying animal, but adequate. In fact it is stress rather than deflection that drives the wing spar structure as size increases. The bone cross section scales with positive allometry, but with a small exponent that means the effects on aerodynamic performance and skeletal mass are small.

In an aeroelastic sense, flexibility is very significant. An analysis of the interaction between wing torsional deflection (twist) and static pitch stability suggests a mechanism whereby if the wing flexibility is correctly tuned, it might provide static stability in pitch. This is potentially advantageous in that other methods of achieving static pitch stability in flying wings carry a significant aerodynamic induced drag penalty.

The wing membrane itself is also clearly a flexible structure. This has advantages in that the resulting wing airfoils can generate high lift and have soft stall characteristics, which aid low speed flight

and control. Extending the flight envelope to low speeds reduces power requirements and assists in takeoff and landing, which appear to be one of the keys to gigantism in pterosaurs.

However, flexible membranes have the disadvantage that they are vulnerable to aerodynamic flutter, which has catastrophic effects on flight efficiency. The tendency to flutter depends to some extent on the weight, thickness and stiffness of the membrane (a lightweight, stiff material being best) but it is overwhelmingly a function of the tension in the membrane, which increases with the third power of the flight speed. Thus as pterosaurs became larger and consequently flew faster, the membrane tension had to increase very rapidly, requiring either a thicker (and consequently heavier) membrane or one with increasingly high tensile properties. This suggests strongly that the reinforcing aktinofibrils were made of a high modulus material such as keratin and that the wing membrane of pterosaurs was very different from that of bats. It may also be that this severe scaling is another factor that sets limits to size, due to the wing membrane having to become excessively stiff and heavy, but that is a study that will have to wait until another time.

So, yes, flexibility is an important factor in the aerodynamic and structural performance of pterosaurs, conferring both benefits and constraints. It may in part explain why they were able to grow so large, but also be a factor which influences the eventual upper limit to size.

Future work

This study has attempted to cover many aspects of the morphology and flight dynamics of large pterosaurs. As such some of the methods have been somewhat approximate, but suited to establishing baselines where none existed before. It would benefit from further development in the following ways.

Structural analysis

The wing spar structure was analysed using a simple quasi-static two-dimensional beam theory model, which broke the spar down into a number of individual sections, assumed to be rigidly connected elements characterised only by their second moments of area and section depth. Validation against known solutions showed that it gave reasonable results, but there is no doubt that a structural member subject to large deflection experiences non-linear effects that are not captured by this type of analysis. Also the dorsoventral and anteroposterior loads were treated separately, whereas in reality there will be coupling between them, creating torsional loading and complex deflections in three-dimensional space.

A problem such as this can only be fully captured by a finite element analysis, wherein the wing spar is modelled in fine detail and combined aerodynamic and membrane loads are applied. This is a PhD in itself. The membrane tension loading in particular is very complex and, as discussed, the development of the mesh required for the FEA analysis is a non-trivial endeavour. However, once such a model is developed, it has potential for more uses than simply determining the quasi-static response to loading. It could for example be extended to examine the structural performance in flapping flight or when manoeuvring.

Sweeping assumptions were made about the behaviour of the soft tissue on the wing spar, so a deeper analysis of the muscular-tendon anatomy of the wing bones would be beneficial, providing estimates of muscular anatomy and how the soft tissues influence deflection and load resistance.

Coupled FEA/CFD analysis

Another use for a FEA structural model would be to couple it with a CFD code (initially an unsteady panel code will probably be adequate) to fully simulate the flapping dynamics and determine the effects of differing levels of joint mobility. It could also provide more insight into the somewhat speculative suggestion that the combination of anterior sweep and wing flexibility provides static pitch stability.

Physical modelling

There is a time honoured alternative to this computational approach, namely the construction and testing of physical models. A pterosaur specific program of wind tunnel model testing could provide further information on the flutter characteristics of the membrane and large scale, or ideally full scale flying models could provide illuminating insights, if in a somewhat uncontrolled manner.

Limits to size and the quadrupedal launch

The parametric study described herein used very generalised and simplified calculations to start to investigate what factors may limit the size of giant pterosaurs. An area of particular interest is the almost unique quadrupedal mode of launch that pterosaurs are believed to have adopted. This was only assessed from the perspective of muscle power and simple forelimb geometry as it affects the length of the launch stroke. Clearly many other factors need to be considered before such a model can be considered to be reliable. This can only be achieved by musculoskeletal modelling using techniques such as OpenSIM.

A factor not considered in the search for the limits to size was the membrane tension. Potentially, this appears to scale with strong positive allometry, which may mean that it has powerful effects on the required bending stiffness in the wing spar and drive a requirement for a disproportionately thick (and heavy) membrane.

Glossary

Aerodynamic terminology

Aspect ratio (AR): a measure of the slenderness of a wing. Calculated as either the ratio of the mean chord to the wing span, or more generally as span^2/wing area. Larger values denote more slender wings.

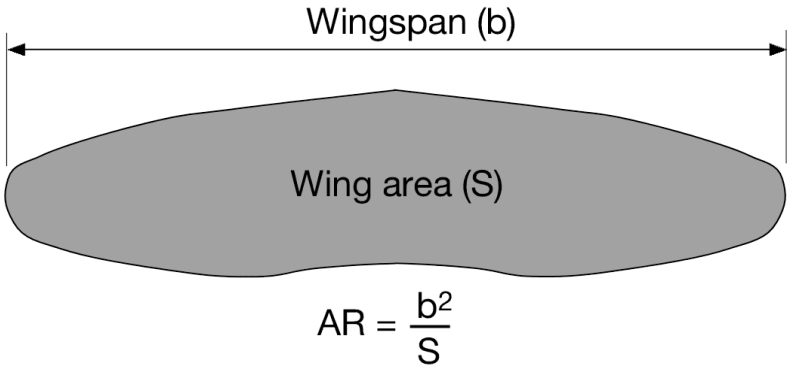

Dihedral: the upward angle from the horizontal of wings where they meet the body. In cases where the angle is downwards, the geometry is referred to as **anhedral**. Dihedral and anhedral influence the roll stability in flight.

Lift coefficient (C_L) and drag coefficient (C_D): non-dimensional values for aerodynamic lift and drag. Lift and drag are defined as the aerodynamic forces resolved normal and parallel to the incident airflow direction respectively. Lift coefficient is abbreviated to C_l where it applies to a local wing section and C_L to a three-dimensional structure such as an complete airplane (similarly C_d and C_D). They are calculated as:

$$C_L = \frac{L}{0.5 \rho S V^2}$$

Where:

L=lift force (N)

ρ=air density (kg/m^3)

S=wing projected surface area (m^2)

V=air speed (m/s)

For any given airfoil or complete flying body there will be a **maximum lift coefficient,** at which stall occurs. This is abbreviated to $C_{Lmax.}$

When a three dimensional wing produces lift, there is an increase in drag, the so called **drag due to lift or induced drag, C_{Di}**

Induced drag can be calculated from the following formula:

$$C_{D,i} = \frac{C_L^2}{\pi AR}$$

Where C_L and AR have the meanings defined above. This formulation is for a "perfect" wing and real wings often produce more induced drag, which is quantified by a constant "e" inserted as below:

$$C_{D,i} = \frac{C_L^2}{\pi ARe}$$

"e" depends on the lift distribution along the wing and is a measure of the deviation from an "perfect" elliptical shape. It is termed the **span efficiency.**

Oswald efficiency. The drag of a wing section comprises a frictional component and a pressure component, which are normally combined as the profile drag, giving the non-dimensional **profile drag coefficient C_{dpro}.**

In fact, the profile drag coefficient of a wing section varies with the lift coefficient, so the total three dimensional drag can be expressed as:

$$C_D = C_{D,0} + \frac{C_L^2}{\pi ARe}$$

Where C_{D0} is the drag at zero lift and e is the **Oswald efficiency,** which takes account of not only the induced drag as above but also the variation of the profile drag coefficient with C_L. Confusingly the Oswald efficiency is abbreviated to e, so it is important to distinguish between it and the span efficiency above. (See Spedding & McArthur 2010 for a very succinct explanation.)

Wing twist (wash-out and wash-in). For reasons of stability or minimising the induced drag, twist may be introduced along the length of a wing. When this twist is such that the more distal sections are rotated to be more "nose down" (with the leading edge ventral to the trailing edge) this twist is called wash-out. The opposite is wash-in. The total aerodynamic force (which is generally in a more or less vertical direction in normal flight) is assumed to act through a single point, the **Centre of Pressure, CP.** Similarly, the force due to gravity, the weight, is assumed to act through the **Centre of Mass, CM.** These points are illustrated in the adjacent sketch (taken from Figure 7.1).

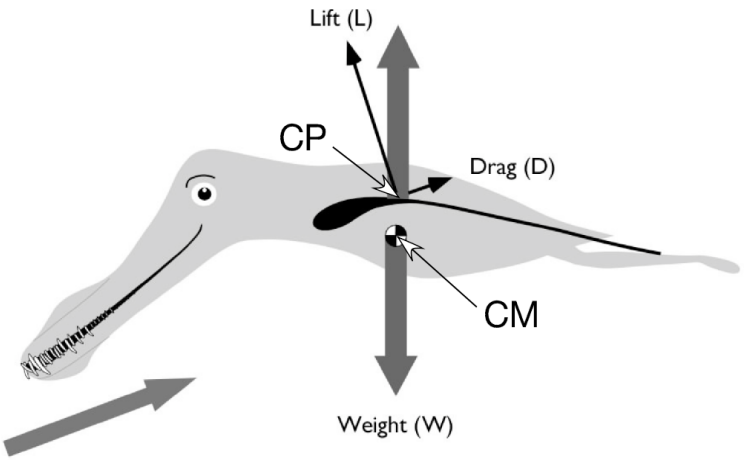

Reynolds number. The forces in a flowing fluid are a combination of frictional (viscous) and inertial, and the ratio of the two has profound effects on the flow characteristics. This ratio is captured by the Reynolds number

$$\mathrm{Re}=\frac{\rho \mathrm{VL}}{\mu}$$

Where:

L=a characteristic length (the wing chord for example) (m)

V=speed of fluid flow (m/s)

ρ=mass density of the fluid (kg/m^3)

μ=viscosity of the fluid (Pa.s)

Aerodynamic/biological dictionary

Inboard = proximal

Outboard = distal

Pitch = vertical (dorsoventral) rotation about the transverse axis.

Spanwise = mediolaterally along a wing

Chord=the local width (in anteroposterior direction) of a wing

Wingspan=the distance from one wing tip to the other

Leading edge = anterior margin of a wing

Trailing edge = posterior margin of a wing

Structural terminology

Young's modulus E. A measure of the stiffness of a material, defined as the ratio of stress to strain. So:

$$E=\varepsilon\sigma$$

Where:

ε=strain (non-dimensional)

σ=stress (Pa)

Section modulus I. The resistance of a beam section to bending (under simple beam theory) is determined by the product of the Young's modulus and the section modulus I, where I is the second moment of area of the cross section.

Beam theory equations. Under simple beam theory, the deflection of a beam is inversely proportional the EI. The stress distribution across the section is defined by:

$$\sigma = \frac{My}{I}$$

Where σ=stress (Pa),

M =bending moment (N.m)

y=distance from the neutral axis (m)

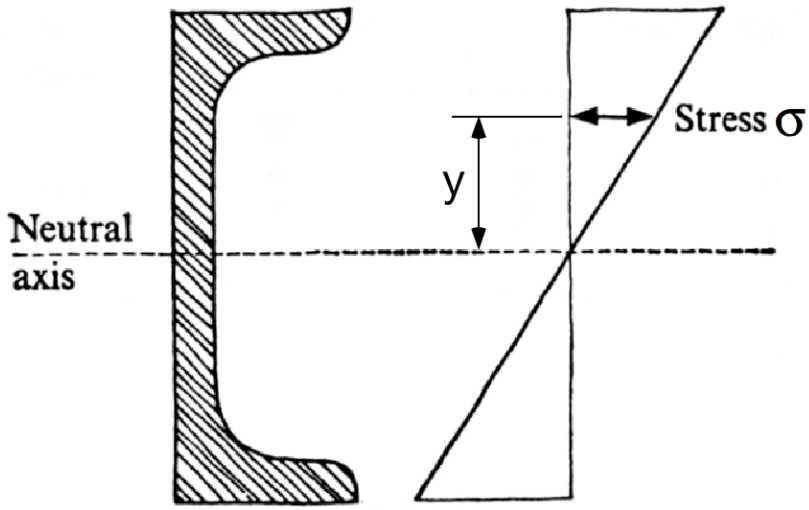

(Sketch modified from Gordon 1978)

References

Aditya, K. & Malolan, V. 2007. Investigation of Strouhal Number effect on flapping wing micro air vehicle. *AIAA 2007*:486.

Alerstam, T., Rosen, M., Backman, J., Ericson, P. G. & Hellgren, O. 2007. Flight speeds among bird species: allometric and phylogenetic effects. *PLoS Biol.* **5** e197.

Alexander, R. M. 1985. Body support, scaling and allometry. In *Functional Vertebrate Morphology.* Hildebrand, M., Bramble, D. M., Liem, K. F. & Wake, D. B. eds. Belknap Press, Cambridge, Mass. USA.

Alexander, R. M. 1998. All-time giants: the largest animals and their problems. *Palaeontology,* **41**(6): 1231-1245.

Alexander, R. M. 2003. *Principles of animal locomotion.* Princeton University Press, U.S.A.

Alexander, R. M. & Bennet-Clark, H. C. 1977. Storage of elastic strain energy in muscle and other tissue. Nature **256**:114-117

Anderson, J. D. 2007. *Fundamentals of aerodynamics.* London, UK: McGraw-Hill Int. Ed.

Ashby, M. F., Gibson L. J., Eegst U. & Olive R. 1995. The mechanical properties of natural materials. I. Material Property Charts. *Proceedings: Mathematical and Physical Sciences,* **450**:123-140.

Askew, G. N., Marsh, R. L. and Ellington, C. P. 2001. The mechanical power output of the flight muscles of blue-breasted quail (*Coturnix chinensis*) during take-off. *J. Exp. Biol.* **204**:3601–3619.

Azuma, A. 2006. *The biokinetics of flying and swimming,* 2nd edn. Reston, VA: AIAA Education Series.

Bedford, A. & Fowler, W. 2008. *Engineering mechanics: statics and dynamics.* Pearson Education Inc. Upper Saddle River, NJ. USA.

Bennett, S. C. 2000. Pterosaur flight: the role of actinofibrils in wing function. *Hist. Biol.* **14**:255–284.

Bennett, S. C. 2001. The osteology and functional morphology of the Late Cretaceous pterosaur *Pteranodon*. *Palaeontographica Abt*. A **260**:1-153.

Bennett, S. C. 2007. Articulation and function of the pteroid bone of pterosaurs. *J. Vert. Paleo.* **27**:881-891.

Berg, A. M. & Biewener, A. A. 2012. Muscle function during takeoff and landing flight in the pigeon (*Columba livia*). Journal of Experimental Biology **215**:4104-4114

Bertagnolio, F., Sorensen, N., Johansen, J. & Fuglsang, P. 2001. Wind turbine airfoil catalogue. Riso-R-1280(EN)

Biewener, A. A., Dial, K. P. and Goslow G. E. 1991. Pectoralis muscle force and power output during flight in the starling. *J. Exp. Biol.* **164**:1-18.

Biewener, A. A. 2005. Biomechanical consequences of scaling. *J. Exp. Biol.* **208**:1665–1676.

Bleischwitz, R., de Kat, R. & Ganapathisubramani, B. 2015. Aspect-ratio effects on aeromechanics of membrane wings at moderate Reynolds numbers. AIAA Journal **53**(3).

Bramwell, C. D. 1971. Aerodynamics of *Pteranodon*. *Biol. J. Linn. Soc.* **3**:313–328.

Bramwell, C. D. & Whitfield, G. R. 1970. Flying speed of the largest aerial vertebrate. *Nature.* **225**:660–661.

Bramwell, C. D. & Whitfield, G. R. 1974. Biomechanics of *Pteranodon*. *Phil. Trans. R. Soc. Lond.* B **267**:503–581.

Bramwell, C. D. & Whitfield, G. R. 1974. D. M. S. Watson's notes on pterosaurs. *Phil. Trans. R. Soc. Lond*. B **267**:587–589.

Brower, J. C. 1983. The aerodynamics of *Pteranodon* and *Nyctosaurus*, two large Pterosaurs from the Upper Cretaceous of Kansas. *J. Vert. Paleo.* **3**:84–124.

Brower, J. C. & Venius, J. 1981. Allometry in pterosaurs. *Univ. Kansas Paleontological Contributions* **105**:1–32.

Browning, L. 2007. *Modelling the flexible wings of a large pterosaur.* MSc Thesis, University of Bristol.

Buffetaut, E., Grigorescu, D. and Csiki, Z. 2003. Giant azhdarchid pterosaurs from the terminal Cretaceous of Transylvania (western Romania). *Geological Society, London, Special Publications* **217**:91-104.

Burkett, C. W. 1989. Reductions in induced drag by the use of aft swept wing tips. *Aeronautical J* **93**:400-405.

Butler, R. J., Barrett, P. M., Nowbath, S. & Upchurch, P. 2009. Estimating the effects of sampling biases on pterosaur diversity patterns: implications for hypotheses of bird/pterosaur competitive replacement. *Paleobiology* **35**:432–446.

Campbell, K. E. & Tonni, E. P. 1983. Size and locomotion in Teratorns (Aves: Teratornithidae). *The Auk* **100**:390-403.

Carruthers, A.C., Walker S.M & Taylor, G.K. 2009. Aerodynamics of aerofoil sections measured on a free-flying bird. *Proc. IMechE* **224**(G):855-864.

Chan, T. M., Gardener, L., Law, K. H. 2010. Structural design of elliptical hollow sections: a review. *Proc. Inst. Civil. Eng. Structures and Buildings* **163**:391-402.

Chapin, V. G., Jamme, S., Chassaing, P. 2005. Viscous computational fluid dynamics as a relevant decision-making tool for mast-sail aerodynamics. *Mar. Technol. Soc. J.* **42**(1):1-10.

Chatterjee, S. & Templin R. J. 2004. Posture, Locomotion, and Paleoecology of Pterosaurs. *Geological Society of America Special Paper 376.*

Chatterjee, C., Templin, R. J. & Campbell, K. E. 2007. The aerodynamics of *Argentavis*, the world's largest flying bird from the Miocene of Argentina. *PNAS* **104**:12398-12403.

Claessens, L. P. A. M., O'Connor, P. M. & Unwin, D. M. 2009. Respiratory evolution facilitated the origin of pterosaur flight and aerial gigantism. *PLoS ONE* **4**(2):e4497.

Collie, S. J., Jackson, P. S., Gerritsen M. and Fallow J. B. 2004. Two-dimensional CFD-based parametric analysis of down-wind sail design, *I. J. S. C. T. Part B1.*

Company, J., Ruiz-Omenaca, J. I. & Suberbiola, X. P. 1999. A long necked pterosaur (Pterodactyloidea, Azhdarchidae) from the Upper Cretaceous of Valencia, Spain. *Geologie en Mijnbouw* **78**: 319-333.

Cone, C. D. 1962. The theory of induced lift and minimum induced drag on nonplanar lifting systems. NASA TM R-139.

Corona, E., Lee, L. H and Kyriakides, S. 2006. Yield anisotropy effects on buckling of circular tubes under bending. *Int. J. of Solids and Structures* **43**:7099–7118.

Currey, J. D. 2004. Tensile yield in compact bone is determined by strain, post-yield behaviour by mineral content. *J Biomech.* **37**:549-556.

Currey, J. D. 2006. *Bones: Structure and Mechanics.* Princeton University Press, Princeton & Oxford.

Dalla Vecchia, F. M. 2013. Triassic pterosaurs. *Geological Society, London, Special Publications* **379**:119-155.

Den Hartog, J. P. 1949. *Strength of Materials.* Dover Publications, New York, USA.

Deperrois, A. 2011. Guidelines for XFLR5 v6.03 (http://sourceforge.net/projects/xflr5/files/xflr5%20v6.03%20Beta/).

DeYoung, J. 1976. Historical evolution of vortex-lattice methods. Washington, DC: *NASA SP-405, NASA Langley.*

Dial, K. P. & Biewener, A. A. 1993. Pectoralis muscle force and power output during different modes of flight in pigeons (*Columba livia*). *J. Exp. Biol.* **176**:31-54.

Dowlan, C. J. 1944. *An interim report on the stability and control of tailless airplanes.* NACA Report 796.

Drela, M, Giles, M. B. 1987. Viscous-inviscid analysis of transonic and low Reynolds number airfoils. *AIAA J.* **25**(10):1347-1355

Dumont, E. R. 2010. Bone density and the lightweight skeletons of birds. *Proc. R. Soc. B* **277**:2193-2198.

Earls, K. D. 2000. Kinematics and mechanics of ground take-off in the starling *Sturnis vulgaris* and the quail *Coturnix coturnix*. Journal of Experimental Biology **203**:725–739

Elgin, R., Hone, D. W. E. & Frey, E. 2010. The extent of the pterosaur flight membrane. *Acta Palaeontol. Pol.* **56**:99 – 111.

Eppler, R. 1979. Some new airfoils, In Science and technology of low speed and motorless flight, *NASA Conference Publication* **2085**:131-154.

Erickson, L. 1990. Panel Methods - An Introduction. NASA Technical Paper 2995

Falkner, V.M. 1946. The accuracy of calculations based on Vortex Lattice Theory. *Rep. No. 9621, British A.R.C.*

Frey, E., Buchy M.-C., Martill, D.M. 2003. Middle- and bottom-decker Cretaceous pterosaurs: unique designs in active flying vertebrates. *In Buffetaut, E. and Mazin,J-M. eds. Evolution and palaeobiology of pterosaurs. Geological Society of London, Special Publication* **217**, 267–274. London, UK.

Frey, E., Buchy, M.,-C., Stinnesbeck, W., González, A. G. & di Stefano, A. 2006. *Muzquizopteryx coahuilensis* n.g., n. sp., a nyctosaurid pterosaur with soft tissue preservation from the Coniacian (Late Cretaceous) of northeast Mexico (Coahuila). *Oryctos* **6**:19-40.

Frey, E., Tischlinger, H., Buchy, M.-C. & Martill, D. M. 2003. New specimens of Pterosauria (Reptilia) with soft parts with implications from pterosaurian anatomy and locomotion. *In Buffetaut, E. and Mazin,J-M. eds. Evolution and palaeobiology of pterosaurs. Geological Society of London, Special Publication* **217**, 233–266. London, UK.

Frey, E. & Martill, D. M. 1996. Preserved soft tissue in a specimen of *Pterodactylus kochi* (Wagner) from the Upper Jurassic of Germany. *J. Vert. Paleont.* **16**(3):35A.

Frey, E. & Riess, J. 1981. A new reconstruction of the pterosaur wing. *N. Jb. Geol. Paläont. Abh.* **161**:1–27.

Gordon, J. E. 1978. *Structures or why things don't fall down.* Penguin Books, London, UK.

Greenewalt, C. H. 1975. The flight of birds: the significant dimensions, their departures from the requirements for dimensional similarity, and the effect on flight aerodynamics of that departure. *Trans. Am. Phil. Soc.* **65**(4):1-67.

Habib, M. 2008. Comparative evidence for quadrupedal launch in pterosaurs. *Zitteliana* **B28**:159-166.

Haldane, J. B. S. 1926. *On being the right size.* Harper's Magazine.

Habib, M. 2009. Skeletal architecture, launch dynamics, and mechanical limits of flying vertebrates. *SVP 69th Annual Meeting*, Bristol, UK.

Hankin, E. H. & Watson, D. M. S. 1914. On the flight of pterodactyls. *Aero. J.* **18**:24–335.

Hazlehurst, G. 1991. *The morphometric and flight characteristics of the Pterosauria.* PhD Thesis, University of Bristol, UK.

Hazlehurst, G. & Rayner, J. M. V. 1992a. An unusual flight mechanism in the Pterosauria. *Palaeontology* **35**:927–941.

Hazlehurst, G. & Rayner, J. M. V. 1992b. Flight characteristics of Jurassic and Triassic Pterosauria: an appraisal based on wing shape. *Paleobiology* **18**:447–463.

Hedrick, T. L., Tobalske, B. W. & Biewener, A. A. 2003. How cockatiels (*Nymphicus hollandicus*) modulate pectoralis power output across flight speeds. Journal of Experimental Biology **206**:1363-1378

Henderson, D. M. 2010. Pterosaur body mass estimates from three-dimensional mathematical slicing. *J. Vert. Paleo.* **30**:768 – 785.

Henry, H. T., Ellerby, D. J. & Marsh, R. L. 2005. Performance of guinea fowl *Numida meleagris* during jumping requires storage and release of elastic energy. Journal of Experimental Biology **208**:3293-3302

Heptonstall, W. B. 1971. An analysis of the flight of the Cretaceous pterodactyl *Pteranodon ingens*. *Scott. J. Geol.* **7**:61–78.

Hoerner, S. F. 1965. *Fluid-Dynamic Drag.* Hoerner Fluid Dynamics, New Jersey.

Hoerner, S. F. 1985. *Fluid-Dynamic Lift.* Hoerner Fluid Dynamics, New Jersey.

Hoey, R. G. 1992. Research on the stability and control of soaring birds. *AIAA-92-4122-CP.*

Hooley, R. W., 1913. On the skeleton of *Ornithodesmus latidens.* An ornithosaur from the Wealden shales of Atherfield (Isle of Wight). *Quarterly Journal of the Geological Society,* **69**:372-421.

Howse, S. C. B., Milner, A.R., Martill, D.M. 2001. Pterosaurs. *In: Martill, D. M., Naish, D., eds. Dinosaurs of the Isle of Wight, Palaeontological Association, Field Guide to Fossils* **10**:324–335.

Jackson, P. S. & Christiet, G. W. 1986. Numerical analysis of three-dimensional elastic membrane wings. *AIAA J.* **25**:5.

Jackson, B. E. & Dial, K. P. 2011. Scaling of mechanical power output during burst escape flight in the Corvidae. *J. Exp. Biol.* **214**:452-461.

Jackson, B. E., Tobalske, B. W. & Dial, K. P. 2011. The broad range of contractile behaviour of the avian pectoralis: functional and evolutionary implications. *J. Exp. Biol.* **214**:2354-2361.

Karamanos, S. A. 2002. Bending instabilities of elastic tubes. *International Journal of Solids and Structures* **39**:2059–2085.

Karihaloo B. L. & Hemp W. S., 1987. Optimum sections for given torsional and flexural rigidity. *Proc. R. Soc. Lond. A* **409**, 67-77.

Karpouzian, G., Spedding, G. R. and Cheng, H. K., 1990. Lunate-tail swimming propulsion. Part 2. Performance analysis. *J. Fluid Mech.* **210**, 329-351.

Katz, J. & Plotkin, A., 2001. *Low-speed aerodynamics,* 2nd edn. Cambridge University Press. Cambridge, UK.

Kellner, A. W. A. 2003. Pterosaur phylogeny and comments on the evolutionary history of the group. *In Buffetaut, E. and Mazin, J-M. eds. Evolution and palaeobiology of pterosaurs. Geological Society of London, Special Publication* **217**:105-137.

Kellner A.W.A. & Tomida R. 2000. Description of a new species of Anhangueridae (Pterodactyloidea) with comments on the pterosaur fauna from the Santana Formation (Aptian–Albian), northeastern Brazil. *National Science Museum Tokyo, Monographs* **17**:1–135.

Kellner, A. W. A., Wang, X., Tischlinger, H., Campos, D., Hone, D.W.E., Meng, X. 2010. The soft tissue of *Jeholopterus* (Pterosauria, Anurognathidae, Batrachognathinae) and the structure of the pterosaur wing membrane. *Proc. R. Soc. B, doi:10.1098/ rspb.2009.0846*

Kellner, A. W. A., Campos, D. A., Sayao, J. M., Saraiva, A. A. F., Rodrigues, T., Oliveira, G. Cruz, L. A., Costa, F. R., Silva, H. P. & Ferreira, J. S. 2013. The largest lying reptile from Gondwana: a new specimen

of *Tropeognathus* cf. T. *mesembrinus* Wellnhofer, 1987 (Pterodactyloidea, Anhangueridae) and other large pterosaurs from the Romualdo Formation, Lower Cretaceous, Brazil. *Anais da Academia Brasileira de Ciências* **85**(1):113-135.

Kirkpatrick, S. J. 1994. Scale effects on the stresses and safety factors in the wing bones of birds and bats. *J. Exp. Biol.* **190**:195–215.

Kroo, I. M., 1981. Aerodynamics, aeroelasticity and stability of hang gliders – experimental results. *NASA TM 81269.*

Kroo, I. M. 2005. *Nonplanar wing concepts for increased aircraft efficiency.* VKI lecture series on Innovative Configurations and Advanced Concepts for Future Civil Aircraft. von Karman Institute, Belgium.

Krus, P. 1997 *Natural methods for flight stability in birds*. World Aviation Congress and Exposition, SAE AIAA. Anaheim, CA.

Ksepka, D. T. 2014. Flight performance of the largest volant bird. *P.N.A.S.* **111**(29):10624-10629.

Lawson, D. A. 1975,. Pterosaur from the latest Cretaceous of West Texas: discovery of the largest flying creature. *Science* **187**(4180):947-948.

Kuenn, A. D., 2009. Non-planar lifting-line theory for fixed and deformable geometries. MSc Thesis. Wichita State University, USA.

Lissaman, P. B. S. 1983. Low-Reynolds-number airfoils. *Annual Review of Fluid Mechanics* **15**:223-239.

Lissaman, P. B. S. 2005. Wind energy extraction by birds and flight vehicles. *AIAA paper 2005-241.*

Liu, T. 2006. Comparative scaling of flapping- and fixed-wing flyers. AIAA Journal. **44**(1):24-33

Liu, T. 2007. Time-area-averaged momentum stream tube model for flapping flight. J. Aircraft. **44**(2): 459-466

Marchaj, C. A. 1988. *Aero-hydrodynamics of Sailing.* Adlard Coles Nautical. London, UK.

Marchaj, C. A. 1996. *Sail performance: Theory and Practice*. Adlard Coles Nautical. London, UK.

Marden J. H. 1994. From damselflies to pterosaurs - how burst and sustainable flight performance scale with size. *American Journal of Physiology,* **266**(4):R1077-R1084.

Marden, J. H., 1987. Maximum lift production during takeoff in flying animals, *J. Exp. Biol.*, **130**:235-258.

Maughmer, M. D. 1979. A comparison of the aerodynamic characteristics of eight sailwing airfoil sections. *in Science and Technology of Low Speed and Motorless Flight. NASA Conference Publication* **2085**:155-175.

Maynard Smith, J. 1952. The importance of the nervous system in the evolution of animal flight. *Evolution* **6**:127–129.

McMasters, J. and M. L. Henderson. 1979. Low-speed single-element airfoil synthesis. *in Science and Technology of Low Speed and Motorless Flight. NASA Conference Publication* **2085**:1-32.

Middleton, K.M. & English, L.T. 2014. Challenges and advances in the study of pterosaur flight. Can. J. Zool. **92**:1–15

Milgram, J. H., 1971. Section data for thin, highly cambered airfoils in incompressible flow. *NASA CR-1767*.

Molnar, J. 2009. *How giant reptiles flew: visualising quadrupedal launch in pterosaurs.* MA Thesis. University of Maryland, Baltimore, USA.

Morris, C. R. & Askew, G. N. 2010. Comparison between mechanical power requirements of flight estimated using an aerodynamic model and in vitro muscle performance in the cockatiel (*Nymphicus hollandicus*). Journal of Experimental Biology **213**:2781-2787

Morris-Thomas, M. T. & Steen, S. 2009. Experiments on the stability and drag of a flexible sheet under in-plane tension in uniform flow. *J. Fluids Struct.* **25**:815-830.

Mueller, T. J. & Batill, S. M. 1980 Experimental studies of the laminar separation bubble on a two-dimensional airfoil at low Reynolds numbers. *AIAA*:**80**-1440.

NACA 1921. Aerodynamic characteristics of aerofoils. *NACA-TR-93*.

Norberg, U. M. L. 1972. Bat wing structures important for aerodynamics and rigidity (Mammalia, Chiroptera). *Z. Morph.* **73**:45-61.

Norberg, U. M. L & Norberg, R. A. 2012. Scaling of wingbeat frequency with body mass in bats and limits to maximum bat size. *J. Exp. Biol.* **215**:711-722.

Nudds, R. L., Taylor G. K. & Thomas, L. R. 2004. Tuning of Strouhal number for high propulsive efficiency accurately predicts how wingbeat frequency and stroke amplitude relate and scale with size and flight speed in birds. *Proc. R. Soc. Lond. B* **271**:2071-2076.

Padian, K. 1985 The origins and aerodynamics of flight in extinct vertebrates. *Palaeontology* **28**(3):413-433.

Padian, K. & Rayner, J. M. V. 1991 Structural fibers of the pterosaur wing: anatomy and aerodynamics. *J. Vert. Paleontol.* **11**(3), 49A.

Padian, K. & Rayner, J. M. V. 1993. The wings of pterosaurs. *American Journal of Science* **293**:91–166.

Palmer, C. 2010. Flight in slow motion: aerodynamics of the pterosaur wing. *Proc. R. Soc. B* **277**:1881–1885.

Palmer, C. & Dyke, G. J. 2009. Biomechanics of the unique pterosaur pteroid. *Proc. R. Soc. B* **277**(1684): 1121-1127.

Palmer, C. & Dyke, G. J. 2010. Moving on from Kirkpatrick (1994): estimating 'safety factors' for flying vertebrates. *J. Exp. Biol.* **213**(12):2174.

Palmqvist, p. & Vizcaíno, S. F. 2003. Ecological and reproductive constraints of body size in the gigantic *Argentavis magnificens* (Aves, Theratornithidae) from the Miocene of Argentina. *Ameghiniana* **40**(3):379–385.

Parslew, B. & Crowther, W. J. 2010. Simulating avian wingbeat kinematics. *J. Biomechanics* **43**:3191-3198.

Parslew, B. 2014. Predicting power-optimal kinetics of avian wings. *J. R. Soc. Interface* **12**:20140953.

Paton, J. S. & Morvan, H. P. 2007. The effect of mast rotation and shape on the performance of sails. *Int J. Mar. Eng. DOI:10.3940/rina.ijme.2007.a2.10307.B* **277**:1121– 1127.

Paul, G. S. 1990. A re-evaluation of the mass and flight of giant pterosaurs. *J. Vert. Paleont.* **10**(3)37A.

Pennycuick, C. J. 1968. A wind tunnel study of gliding flight in the pigeon *Colomba livia*. *J. Exp. Biol.* **49**:509-526.

Pennycuick, C. J. 1971a. Gliding flight of the white-backed vulture *Gyps africanus*. *J. Exp. Biol.* **55**:13-38.

Pennycuick, C. J. 1971b. Gliding flight of the dog-faced bat *Rousettus aegyptiacus* observed in a wind tunnel. *J. Exp. Biol.* **55**:833-845.

Pennycuick, C. J. 1983. Thermal soaring compared in three dissimilar tropical bird species, *Fregata magnificens, Pelecanus occidentalis* and *Coragyps atratus*. *J. Exp. Biol.* **102**:307-325.

Pennycuick, C. J. 1990. Predicting wingbeat frequency and wavelength of birds. *J. Exp. Biol.* **159**:171-185.

Pennycuick, C. J. 1996. Stress and strain in the flight muscles as constraints ion the evolution of flying animals. *J. Biomechanics.* **29**(5):577-581.

Pennycuick, C. J. 1988. On the reconstruction of pterosaurs and their manner of flight, with notes on vortex wakes. *Biol. Rev.* **63**:209–231.

Pennycuick, C. J. 1990. Stripes on a pterosaur wing. *Nature*. **346**:116.

Pennycuick, C. J. 2008. *Modelling the flying bird.* Theoretical Ecology Series, Academic Press, Elsevier Inc.

Polhamus, E. C. & Naeseth R. L. 1963. Experimental and theoretical studies of the effects of camber and twist on the aerodynamic characteristics of parawings having nominal aspects ratios of 3 and 6. *NASA TN D-972.*

Prange, H. D., Anderson, J. F. & Rahn, H. 1979. Scaling of skeletal mass to body mass in birds and mammals. American Naturalist, **113**(1):103-122

Prandtl, L. 1921. Applications of modern hydrodynamics to aeronautics. *NACA TR 116.*

Prentice, K. C., Ruta, M. & Benton M. J. 2011. Evolution of morphological disparity in pterosaurs. *J. Systematic Palaeontology.* **9**(3):337-353.

Prondvai, E. & Hone, D. W. E. 2008. New models for the wing extension in pterosaurs. *Hist. Biol.* **20**(4): 237-254.

Prondvai, E., Tanács, T. & Frey, E. 2008. Mass estimate of pterosaurs: A case study on *Rhamphorhynchus* and the problems of finding the best method. *6th Meeting of the European Association of Vertebrate Palaeontology, Spišská Nová. Ves. Abstracts.*

Rayner, J. M. V. 1988. Form and function in avian flight. *Curr. Ornithol.* **5**:1–66.

Reich, T. & Gefen, A. 2006. Effect of trabecular bone loss on cortical strain rate during impact in an in vitro model of avian femur. *BioMedical Engineering OnLine* **5**:45.

Reddy, B. D. 1979. An experimental study of the plastic buckling of circular cylinders in pure bending. *Int. J. Solids Structures* **15**:669-683.

Rogers, R. R. & LaBarbera, M. 1992. Contribution of internal bony trabeculae to the mechanical properties of the humerus of the pigeon (*Columba livia*). *J. Zool., Lond.* **230**, 433-441.

Rohr, J. J. & Fish, F. E. 2004. Strouhal numbers and optimisation of swimming by odontocete cetaceans. *J. Exp. Biol.* **207**:1633–1642.

Rupin, F., Saied, A., Dalmas, D., Peyrin, F., Haupert, S., Barthel, E., Boivin, G. and Laugier, P. 2008. Experimental determination of Young modulus and Poisson ratio in cortical bone tissue using high resolution scanning acoustic microscopy and nanoindentation. *J. Acoust. Soc. Am.* **123**:3785.

Sachs, G. 2015. Aerodynamic cost of flapping. *J. Bioninc Eng.* **12**:61-69.

Salehipour, H & Willis, D. J. 2013. A coupled kinematics–energetics model for predicting energy efficient flapping flight. Journal of Theoretical Biology **318**:173–196

Sander, P. M., Christian, A., Clauss, M., Fechner, R., Gee, C. T., Eva-Maria Griebeler, E-M., Gunga, H-C., Hummel, J., Mallison, H., Perry, S. F., Preuschoft, H., Rauhut, O. W. M., Remes, K., Tutken, T., Wings, O. & Witzel, U. 2011. Biology of the sauropod dinosaurs: the evolution of gigantism. Biol. Rev. **86**:117–155

Sato, K., Sakamoto, K. Q., Watanuki, Y., Takahashi, A., Katsumata, N., 2009. Scaling of soaring seabirds and implications for flight abilities of giant pterosaurs. *PLoS ONE B(4): e5400. doi:10.1371/ journal.pone.0005400.*

Schmidt Nielsen, K. 1984. *Scaling: why is animal size so important?* CUP, Cambridge, UK.

Selig, M. S. & Gulielmo, J. J. 1977. High-lift low Reynolds number airfoil design. *J. Air.* **34**(1):72-79.

Shahar, R., Zaslansky, P., Barak, M., Friesem, A. A., Currey, J. D., and Weiner, S. 2007. Anisotropic Poisson's ratio and compression modulus of cortical bone determined by speckle interferometry. *J. Biomechanics,* **40** (2):252-264.

Short, G. H., 1914. Wing adjustments of pterodactyls. *Aeronautic J.* **18**:336–343.

Shyy, W., Lian, Y., Tang, J., Viieru, D. & Liu, H. 2008. *Aerodynamics of Low Reynolds Number Flyers.* Cambridge University Press.

Smith, R., & Shyy, W. 1996. Computation of aerodynamic coefficients for a flexible membrane airfoil in turbulent flow: A comparison with classical theory. *Physics of Fluids,* **8**(12):3346-3353.

Sneyd, A. D., Bundock, M. S. & Reid, D. 1982. Possible effects of wing flexibility on the aerodynamics of *Pteranodon*. *Am. Nat.* **120**:455–477.

Sneyd, A. D. 1984. Aerodynamic coefficients and longitudinal stability of sail aerofoils. *J. Fluid Mech.*, **149**:127-146.

Steel, L., 2005. *Studies of pterosaur bone histology.* Unpublished Ph.D. Thesis. Portsmouth: University of Portsmouth.

Steel, L., 2009. The palaeohistology of pterosaur bone: an overview. *Zitteliana* **B28**:109-125.

Stein, R. S. 1975. Dynamic analysis of *Pteranodon ingens:* a reptilian adaptation for flight. *J. Paleont.* **49**:534–548.

Strang, K., Kroo, I., Gerritsen, M. & Delp, S., 2009. Efficient flight of pterosaurs - an unsteady aerodynamic approach. *AIAA 2009-1301.*

Swartz, S. M., Groves, M. S., Kim, H. D. & Walsh, W. R., 1996. Mechanical properties of bat wing membrane skin. *J. Zool. Soc. London* **239**:357-378.

Taylor, G. K. & Thomas, A. L. R. 2014. *Evolutionary biomechanics.* OUP, Oxford, UK.

Taylor, G. K., Nudds, R. L. & Thomas, A. L. R. 2003. Flying and swimming animals cruise at a Strouhal number tuned for high power efficiency. *Nature* **425**:707-711.

Tennekes, H., 1997. *The Simple Science of Flight:From Insects to Jumbo Jets.* ISBN0-262-20105-4, MIT Press, Cambridge, MA.

Thomas, A. L. R. & Taylor, G. K. 2001. Animal flight dynamics. I. Stability in gliding flight. *J Theor Biol* **212**:399–424.

Tobalske, B. W. 2007. Biomechanics of flight. *J. Exp. Biol.* **210**:3135-3146.

Tucker, V. A. & Parrott, G. C., 1970. Aerodynamics of gliding flight in a falcon and other birds. *J. Exp. Biol.* **52**:345 -367.

Tucker, V. A. & Heine, C. 1990. Aerodynamics of gliding flight in a Harris' hawk, *Parbuteo unicinctus*. *J. Exp. Biol.* **149**:345 -367.

Unwin D. M., 2005. *The pterosaurs: from deep time.* New York: Pi Press.

Unwin, D. M. & Bakhurina, N. N. 1994. *Sordes pilosus* and the nature of the pterosaur flight apparatus. *Nature* **371**:62–64.

Unwin, D. M., Martill, D. M. & Bakhurina, N. N. 1993. The structure of the wing membrane in pterosaurs. *J. Vert. Paleont.* **13**(3)61A.

Van Dam, C. P. 1987. Efficiency characteristics of crescent-shaped wings and caudal fins. *Nature*, **325**:435-7.

van den Berg, C & Rayner, J. M. V. 1995. The moment of inertia of bird wings and the inertial power requirement for flapping flight. Journal of Experimental Biology **198**:1655-1664

Videler, J. J. 2005. *Avian Flight.* ISBN0198566034, Oxford University Press, USA.

Vizcaino, S. F. & Farina, R. A. 1999. On the flight capabilities and distribution of the giant Miocene bird *Argentavis magnificens* (Teratornithidae). Lethaia, **32**:271-278

Vogel, S. 1994. *Life in Moving Fluids: The Physical Biology of Flow.* Princeton University Press, Princeton.

Wadee, M. K., Wadee, A. A., Bassom, A.P and Aigner, A. A. 2006. Longitudinally inhomogeneous deformation patterns in isotropic tubes under pure bending. *Proc. R. Soc. A.* **462**:817–838.

Wang, X., Kellner, A. W. A., Jiang, S., Cheng, X & Rodrigues, T. 2010. New long-tailed pterosaurs (Wukongopteridae) from western Liaoning, China. *Anais da Academia Brasileira de Ciências* **82**(4):1045-1062.

Watanabe, Y., Suzuki, S., Sugihara M. & Sueoka Y. 2002 An experimental study of paper flutter. *Journal of Fluids and Structures* **16**(4):529–542.

Weis-Fogh, T., 1977. Dimensional analysis of hovering flight, *Scale Effects in Animal Locomotion*,:405–420. Pedley, T. J. Ed. Academic Press, New York.

Wellnhofer, P., 1985. Neue pterosaurier aus der Santana- Formation (Apt) der Chapada do Araripe, Brasilien. *Palaeontographica* A **187**:105–182.

Wellnhofer, P., 1988. Terrestrial locomotion in pterosaurs. *Hist. Biol.* **1**:3-16.

Wellnhofer, P., 1991a. *The illustrated encyclopedia of pterosaurs.* Salamander Books. London. UK.

Wellnhofer, P., 1991b. Weitere Pterosaurierfunde aus der Santana-Formation (Apt) der Chapada do Araripe, Brasilien. *Palaeontographica A* **215**:43–101.

Williamson, M. R., Dial, K. P. & Biewener, A. A. 2001. Pectoralis muscle performance during ascending and slow level flight in mallards (*Anas platyrhynchos*). Journal of Experimental Biology **204**:495–507

Wilkinson, S. 1984. *Partially Separated Flows Around 2D Masts and Sails*. Ph.D. thesis, University of Southampton, UK.

Wilkinson, M. T., 2003. *Flight of the ornithocheirid pterosaurs.* Ph.D. thesis, University of Cambridge. UK.

Wilkinson, M. T., 2007. Sailing the skies: the improbable aeronautical success of the pterosaurs. *J. Exp. Biol.* **210**:1663-1671.

Wilkinson, M. T., 2008. Three-dimensional geometry of a pterosaur wing skeleton, and its implications for aerial and terrestrial locomotion. *Zool. J. Linn. Soc.* **154**:27–69.

Wilkinson, M. T., Unwin, D. M. & Ellington, C. P., 2006. High lift function of the pteroid bone and forewing of pterosaurs. *Proc. Royal Soc. B* **273**:119-126.

Windte, J., Scholz U. & Radespiel, R. 2006 Validation of the RANS-simulation of laminar separation bubbles on airfoils. *Aerospace Science and Technology* **10**:484-494.

Witton, M. T. 2009. A new approach to determining pterosaur body mass and its implications for pterosaur flight. *Zitteliana* **B28**:143-159.

Witton, M. 2013. *Pterosaurs: Natural history, Evolution, Anatomy.* Princeton University Press. New Jersey, USA.

Witton, M.P.; Habib, M.B. 2010. On the size and flight diversity of giant pterosaurs, the use of birds as pterosaur analogues and comments on pterosaur flightlessness. *PLoS ONE* **5**(11): e13982.

Witton, M.P., Martill, D.M. and Loveridge, R.F. 2010. Clipping the Wings of Giant Pterosaurs: Comments on Wingspan Estimations and Diversity. *Acta Geoscientica Sinica,* **31** Supp.1:79-81.

Woodward, F. A. 1968 Analysis and design of wing-body combinations at subsonic and supersonic speeds. Journal of Aircraft, **5**(6):528-534.

XFOIL 6.9.4 An open-source panel code, website http://web.mit.edu/drela/Public/web/xfoil/

Young, W. C. & Budynas, R. G. 2002. *Roark's Formulas for Stress and Strain.* McGraw-Hill.

Annex 1

Materials and Methods

Wind tunnel testing

Wing bone sections and wing reconstruction

The wing phalanx sections were based upon measurements taken from a detailed specimen description Wellnhofer (1985) and from measurements of specimens in the collections at Karlsruhe Museum (three dimensionally preserved Brazilian material: *C. robustus* (SMNK 1133); Ornithocheiridae indet. (SMNK 1134PAL, SMNK 1135PAL)), the Natural History Museum in London, specimens labeled 'ornithocheirid sp.' in the collections of three-dimensionally preserved specimens from the Greensand in the Sedgwick (Cambridge UK) and York (York, UK) museums. Wing size assumptions (required to estimate the wing section chord) were based on published reconstructions of *Pteranodon* (Bramwell & Whitfield, 1974, Bennett 2007) and *Anhanguera sp*. (Wilkinson 2008).

Models

The wing section models were made in both rigid and flexible forms. The rigid sections were made by laminating fibre reinforced composite over a male mould, with hand finishing. The mould was made by arching a stiff piece of plastic sheet, secured to a firm base by wooden blocks. The laminate comprised a thin 50g scrim of finely woven glass fibres followed by three layers of 2x2 twill weave carbon fibre, with the inner layer laid on the bias. Another thin scrim was placed on top. The fibres were impregnated by hand with SP 106 multipurpose epoxy resin, consolidated by stippling with a stiff brush. When cured the upper surface was given a thin coat of filled epoxy resin (West System 407 low density filler) and hand finished to a smooth surface, finishing off with 600grit paper.

The leading edge spar sections were carved by hand from fine grained softwood and attached with countersunk screws. The joints and screws were faired with plasticine.

The flexible wing membrane were made by laminating a sheet of latex rubber (Latex Dipping Rubber), embedding within the laminate threads of black sewing cotton.

Model tests

The wind tunnel used was a Plint TE 44 Subsonic open jet wind tunnel with a working cross section of 457 mm x 457 mm. The mean turbulence level is less than 0.7% r.m.s. and velocity variation

less than +/- 1.0% outside the boundary layer. Forces were measured with a Plint three component balance.

Computer models and calculations

Two proprietary pieces of aerodynamic software were used:

XFLR5 (http://www.xflr5.com/xflr5.htm) for three dimensional wing analysis. XFLR5 has wing design and analysis capabilities based on the lifting line theory, the vortex lattice method (VLM) and on a 3D panel method. It also includes XFOIL so allowing wing sections to be incorporated. The VLM option was used since tests showed that the 3D panel method gave identical results but was computationally more demanding.

XFOIL (http://web.mit.edu/drela/Public/web/xfoil/), an interactive program for the design and analysis of subsonic isolated airfoils in viscous (or inviscid) flow regimes.

Three Excel based codes were specially developed for the project:

Beam theory model for the analysis of the wing spar. *Portsmouth moments XFLR lift distribution.xlsx*

Time stepping model for analysis of landing dynamics. *Flight path.xlsx*

Time stepping model for analysis of take-off dynamics. This model was developed in consultation with Mike Habib. *Take off power 6 Sep 2015.xlsx*

Annex 2

Co-authorship letter: G Dyke

UNIVERSITY OF Southampton

CONFIRMATION OF CO-AUTHORSHIP

Colin Palmer,

The Old Barn, Shalfleet, Isle of Wight

21st September 2015

Dear Colin,
I am writing in regard to our two co-authored publications that appeared in 2012 and 2010 as I understand you are planning to refer to them in your PhD Thesis (University of Bristol):

Palmer, Colin and Dyke, Gareth (2012) Constraints on the wing morphology of pterosaurs. Proceedings of the Royal Society of London B, 279, (1731), 1218-1224 . (doi:10.1098/rspb.2011.1529).

Palmer, Colin and Dyke, Gareth J. (2010) Biomechanics of the unique pterosaur pteroid. Proceedings of The Royal Society B Biological Sciences, 277, (1684), 1121-1127. (doi:10.1098/rspb.2009.1899).

I would like to confirm that you came up with the ideas for both these papers, performed all analyses and wrote much of the initial text. My input (at the time you were at a much earlier stage of your research career) was to assist with writing, editing and focussing these manuscripts for publication.

Yours sincerely

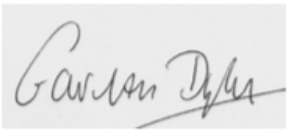

Gareth Dyke
Associate Professor

Telephone: 023 8059 3110

Email: gareth.dyke@soton.ac.uk

Papers

Figures